Estimation of vertical load on a tire from contact patch length and its use in vehicle stability control

Deepak Dhasarathy

Thesis submitted to the faculty of the
Virginia Polytechnic Institute and State University
in partial fulfillment of the requirements for the degree of

Master of Science
In
Electrical Engineering

Saied Taheri, Chair
Daniel J. Stilwell, Co-chair
William T. Baumann

June 1, 2010
Blacksburg, VA

Keywords: Intelligent tire, contact patch length, normal load, vehicle stability control

Estimation of vertical load on a tire from contact patch length and its use in vehicle stability control

Deepak Dhasarathy

ABSTRACT

The vertical load on a moving tire was estimated by using accelerometers attached to the inner liner of a tire. The acceleration signal was processed to obtain the contact patch length created by the tire on the road surface. Then an appropriate equation relating the patch length to the vertical load is used to calculate the load. In order to obtain the needed data, tests were performed on a flat-track test machine at the Goodyear Innovation Center in Akron, Ohio; tests were also conducted on the road using a trailer setup at the Intelligent Transportation Laboratory in Danville, Virginia. During the tests, a number of different loads were applied; the tire-wheel setup was run at different speeds with the tire inflated to two different pressures. Tests were also conducted with a camber applied to the wheel. An algorithm was developed to estimate load using the collected data.

It was then shown how the estimated load could be used in a control algorithm that applies a suitable control input to maintain the yaw stability of a moving vehicle. A two degree of freedom bicycle model was used for developing the control strategy. A linear quadratic regulator (LQR) was designed for the purpose of controlling the yaw rate and maintaining vehicle stability.

ACKNOWLEDGEMENTS

I would like to thank Dr.Taheri for providing me the opportunity of working on this interesting and challenging research project. I thank him for the confidence he had in me to take me under his wing despite my limited knowledge in the area of tires and generally for being such a wonderful person. I would like to thank Dr.Stilwell for his valuable inputs during the course of the project and Dr.Baumann for his comments and suggestions. I would also like to thank the folks at Goodyear Tire and Rubber Company for funding the project and providing the facilities for testing.

I would like to thank the folks at the Intelligent Transportation Laboratory (ITL) in Danville who helped me with the testing procedure – Bryan Sides for machining the parts needed for testing and getting the test rig to work as required; Josh Caffee and Brad Hopkins for helping me mount the tire and helping with the data acquisition; Seth for helping me run errands around Danville; all of them for the many hours spent testing in the summer heat at the Danville Regional Airport. I appreciate the fact that folks at the airport let us use their facilities for our test runs. A special thanks to Gaurav Dongaonkar and Dr. Ding for letting me stay over during my visits to Danville.

I appreciate the help of the people at the Center for Vehicle Systems and Safety (CVeSS) – Michael Craft for providing me plenty of information and materials and answering all my questions; Nima Mahmoodi and Ben Duprey for helping me understand the working of the data acquisition system and setting it up; Hossein Tamaddoni for helping me understand the control algorithm; Sue Teel for helping me place orders for all the required parts.

Finally, I would like to thank my parents. For everything that they have done.

All photographs by the author, 2010.

Table of Contents

List of Tables

List of Figures

1. Introduction

The study of tires is important to understanding the dynamics of a vehicle, as tires are the only means of contact between the road and the vehicle and they produce the forces needed to control the vehicle. One important component of operating vehicles is safety and the best place to start would be through the study of tire parameters that can be utilized in keeping passengers safe. Unfortunately, not many stability and safety features focus directly on the factors affecting tires. This thesis aims to present a method by which some of these factors can be predicted and utilized in improving safety.

The dynamic load being applied on a tire at the tire-road surface can be a useful parameter in stabilizing the vehicle. Vehicle stability is maintained by a number of technologies including electronic stability control (ESC), anti-lock braking systems (ABS), traction control systems (TCS) and electronic brakeforce distribution (EBD) systems. These systems have been quite effective in increasing passenger safety [1]. Incorporating data from tires will be an additional safety measure.

The first part of the research focuses on developing an algorithm that can estimate the dynamic load by first estimating the tire contact patch length. The second shows how this dynamically estimated load can be used in controlling a vehicle moving under a certain set of conditions.

1.1 Motivation

The problem presented to us was to develop an algorithm that would be able to estimate the dynamic load on a moving tire, by first estimating the length of the contact patch. Being able to estimate load and patch length will be an important tool in helping maintain the vehicle on a desired course. Large changes in these parameters could signify unstable behavior, which could then be corrected using an appropriate control algorithm.

One of the places where this finds use is in controlling the yaw rate of a car performing a turn under conditions that may cause instability. The information available from the tire can be used

to calculate parameters such as lateral force and cornering stiffness, which can be used in a control algorithm to maintain a desired yaw rate.

1.2 Research Approach

For estimating load from patch length, accelerometers were attached to the inner liner of a tire to measure the radial acceleration produced inside the moving tire. A data acquisition system was set up to collect the data in real time. A tire test rig inside a trailer was used to load the tire and run on dry asphalt. The data obtained was used as a starting point for the development of a signal processing algorithm to obtain dynamic load from patch length.

Tests were then performed on a flat track at the Goodyear Innovation Center in Akron, Ohio. The flat track or rolling road is an indoor facility on which a tire can be run while being subjected to different forces, speeds, slip angles and camber, all controlled by a program. The data obtained from this second set of experiments was used to arrive at a version of the algorithm that is able to detect the required parameters favorably.

The algorithm thus developed was shown to be useful in designing a vehicle stability controller that can utilize the information from the intelligent tire. A two degree-of-freedom 'bicycle' vehicle model was used for this purpose. Matlab and Simulink were used to simulate the output of the controlled system.

1.3 Thesis Outline

Chapter 2 is a brief review of the literature available on intelligent tires, the research done in this area and the area of vehicle stability.

Chapter 3 explains the setting up of the equipment needed to capture data from the running tire. It includes a description of the tire-wheel assembly, the electrical connections and the data acquisition system.

Chapter 4 shows the testing carried out at the Intelligent Transportation Laboratory. This chapter details the initial work carried out in developing a signal processing algorithm that would aid in estimating the dynamic load on a tire.

Chapter 5 shows the tests carried out at the Goodyear Innovation Center in Akron, Ohio and the modifications to the algorithm developed in chapter 4 to fit the data obtained from flat track tests. The results of applying those modifications are shown as plots of estimated load against the rotations of the tire.

Chapter 6 explains how the estimates from chapter 5 can be used in developing a control strategy to keep the yaw rate of a vehicle at a desired value.

Chapter 7 contains a summary of the research and recommendations on how to improve the algorithm to work under practical conditions.

Chapter 8 contains future work that can be based on the work done in this research.

2. Literature Review

In this chapter, we take a brief look at the current safety features associated with tires and research in the field of equipping tires with sensors; an outline of how the existing literature provides a way to incorporate these ideas into the project is provided. We finally take a look at vehicle stability and its relation to factors affecting a tire.

2.1 Intelligent Tires

Intelligent tires are tires equipped with sensors that measure quantities like pressure, acceleration, temperature, friction et al [2]. From model year 2008, due to the NHTSA requirements [3], all passenger cars and light trucks in the U.S.A. have tire pressure monitoring systems (TPMS), which provide information to the driver in case the tire is dangerously underinflated; these became especially important since tire recalls in the year 2000 by a leading tire manufacturing company after a number of deaths due to rollovers. These systems use direct or indirect TPMS [4]. Other sensors used in tires include surface acoustic wave (SAW) sensors [5] and strain gauges [6]. All of these aim to provide information regarding conditions of tires that may be potentially dangerous.

Research is being conducted in the area of using sensor information from tires directly in controlling the motion of a vehicle, and not just as a driver aid. A study conducted previously [7] involved different kinds of sensors (single axis and triaxial accelerometers, triaxial optical sensor and piezo strain sensor) placed inside a tire to measure acceleration; this was used to find the patch length of the tire as it moves. Accelerometers and other sensors like piezoresistive elastomers have also been used in other studies [8-12] of tire behavior when it is moving. These studies showed that accelerometers produce a characteristic waveform (figure 2.1) that can be used to find contact patch length, as will be explained soon. This thesis details the experiment that used accelerometers, aiming to reproduce the scenario in [7] and [8] and further build on it by estimating the dynamic load on the tire by appropriate signal processing.

As stated in [7], the patch length can be calculated as the product of the time spent by the accelerometer inside the patch and the speed of the vehicle. The accelerometer experiences a

radial acceleration when outside the contact patch due to a centrifugal force. On either side of the contact patch, the acceleration shoots up as the accelerometer is entering and leaving the patch. Inside the patch, the acceleration falls (ideally to zero) because there is only linear motion, as shown in [7-8] and [11-12]. Figure 2.1 shows an example of what the acceleration signal might look like for one cycle of rotation of the tire.

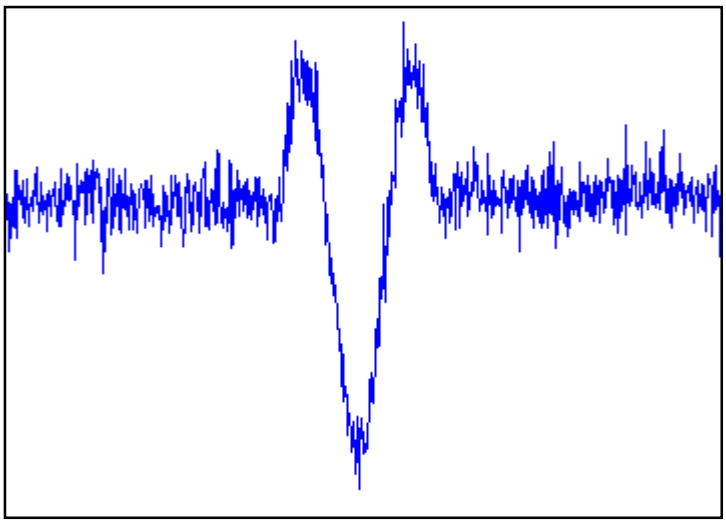

Figure 2.1. Typical acceleration profile for one rotation of the tire

The patch length, according to [7], can be calculated as

$$\text{Patch length} = \text{peak to peak time} \times \text{linear speed} \tag{2.1}$$

However, it would be more appropriate to take the patch length from halfway up the slope on one side to halfway on the other side, as this is where the accelerometer is actually entering or leaving the patch. The linear speed of the vehicle is taken because in the contact patch, the accelerometer moves linearly along the ground along with the patch.

Two different equations have been investigated for their suitability in calculating load. The patch length can be substituted in these equations to estimate the load on the tire. Both equations are for a static tire. A suitable multiplicative factor dependent on the speed and inflation pressure would have to be introduced in dynamic conditions i.e. when the tire is in motion. In the

following equations (2.2 and 2.3), the load is expressed in terms of its ratio to vertical stiffness of the tire. The vertical stiffness is a measure of the resistance offered by the tire to a vertical load and is expressed in newton per meter.

The relation between patch length and load according to [13] is

$$\text{Patch length } L = 2ad\sqrt{\frac{\delta}{d} - \left(\frac{\delta}{d}\right)^2} \tag{2.2}$$

where a is a multiplication factor that was found to be 0.65 for the tire under test in static condition, d is the diameter of the tire and δ is the ratio of the normal load to the vertical stiffness at a particular inflation pressure.

According to [14], the relation between patch length and load is

$$\text{Patch length } L = 0.7ar_f\left(\frac{\delta}{r_f} + 2.25\sqrt{\frac{\delta}{r_f}}\right) \tag{2.3}$$

where r_f is the radius of the unloaded tire. The multiplicative factor a in this case has a different value from that in equation 2.2. It is 1 for a static tire.

2.2 The Pacejka Model

Before reviewing the control strategy, it would be necessary to explain certain parameters related to the tire. It is necessary to know the forces acting on a tire before developing a control strategy for the vehicle. The Pacejka Magic Formula tire model [15] can be utilized in stabilizing a vehicle.

We are interested in the normal force (F_z), the lateral force (F_y), the slip angle (α) and camber angle (γ) for use in the Pacejka Magic Formula tire model. The camber angle is the inclination of the tire from its vertical position and the slip angle is the difference in the directions in which the wheel is traveling and that in which it is actually pointing. Figure 2.2 outlines the important forces acting on the tire and the angles of interest.

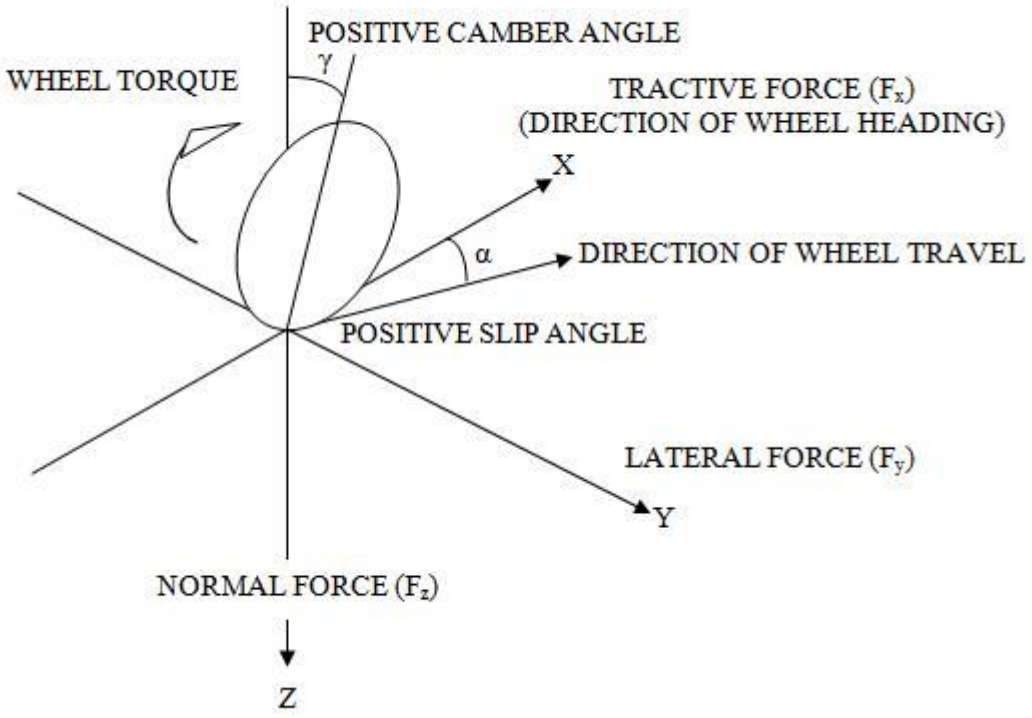

Figure 2.2. Forces acting on a tire

The Pacejka Magic Formula Tire model, a semi-empirical model developed by Hans Pacejka at TU Delft in Holland, was studied so that the load that can be calculated from equations 2.2 or 2.3 can be utilized in the control algorithm development for the vehicle. The formula is used to calculate steady state tire force and moments. As stated in [15], it is

$$Y = Dsin\left\{C \arctan\left[B(x + S_H) - E\left[B(x + S_H) - arctan\left(B(x + S_H)\right)\right]\right]\right\} + S_V \quad (2.4)$$

Y is the force or moment on the tire. We are interested in calculating the lateral force F_y. So in our case, Y will be the lateral force to be calculated from the normal load F_z. x is the slip angle. The coefficients B, C, D, E, S_H and S_V (called main coefficients) are dependent on the Pacejka coefficients [15] for the tire under test, the camber angle and the normal load F_z. The Pacejka coefficients are determined by appropriate curve fitting techniques based on tests conducted on the tire with different loads, slip angles and camber angles.

The equations for slip angle at the front and rear [16] are as follows.

Front:
$$\alpha_f = \delta_f - \theta_{vf} = \delta_f - \beta - \frac{l_f r}{V_x} \tag{2.5}$$

Rear:
$$\alpha_r = -\theta_{vr} = -\beta + \frac{l_r r}{V_x} \tag{2.6}$$

β is the vehicle slip angle [16], and is given by

$$\beta = \tan^{-1}\left(\frac{l_f \tan\delta_r + l_r \tan\delta_f}{l_f + l_r}\right) \tag{2.7}$$

l_f and l_r are, respectively, the distance of the front and rear axles from the center of gravity of the vehicle. δ_f and δ_r are, respectively, the front and rear steering angles at the wheels. Typically, δ_r is assumed to be zero; that is, the rear wheels are aligned along the direction of the vehicle.

The cornering stiffness [16], the ratio of the lateral force to the slip angle, for the front and rear tires are given as

Front:
$$C_{\alpha f} = \frac{F_{yf}}{\alpha_f} \tag{2.8}$$

Rear:
$$C_{\alpha r} = \frac{F_{yr}}{\alpha_r} \tag{2.9}$$

The cornering stiffness values thus calculated can be used in the dynamical equations of a system (as will be seen in the section 2.3) to estimate a feedback that will stabilize the system in case of instability.

2.3 Vehicle Model and Control

A two degree of freedom bicycle model is commonly used to model vehicles [16-17]. In such a model, each pair of front and back wheels is represented by a single wheel. The dynamic equations of the system are written in terms of the lateral velocity of the vehicle and the yaw rate as the state variables.

The system dynamic equation is

$$\begin{bmatrix} m & 0 \\ 0 & I_z \end{bmatrix} \begin{pmatrix} \dot{v} \\ \dot{r} \end{pmatrix} - \begin{bmatrix} -\frac{C_{\alpha f} + C_{\alpha r}}{u} & -mu + \frac{l_r C_{\alpha f} - l_f C_{\alpha r}}{u} \\ \frac{l_r C_{\alpha r} + l_f C_{\alpha f}}{u} & -\frac{{l_r}^2 C_{\alpha r} + {l_f}^2 C_{\alpha r}}{u} \end{bmatrix} \begin{pmatrix} v \\ r \end{pmatrix} - \begin{bmatrix} C_{\alpha f} \\ l_f C_{\alpha f} \end{bmatrix} (\delta_f) = 0 \qquad (2.10)$$

where

v = vehicle lateral velocity

r = yaw rate

m = mass of the vehicle

I_z = moment of inertia

$C_{\alpha f}$ = cornering stiffness of front tires

$C_{\alpha r}$ = cornering stiffness of rear tires

u = longitudinal speed of the vehicle

l_f = distance from center of gravity of the vehicle to the front axle

l_r = distance from center of gravity of the vehicle to the rear axle

δ_f = steering input at wheels

As shown in [17] (and as will be seen in chapter 6), the application of a steering input to this system results in the yaw rate shooting up to a high value, if the system is uncontrolled. This may cause the vehicle to topple over because the yaw rate increases to the large value in a short time.

Typically, control systems are designed so that the yaw rate r follows a desired yaw rate. When the driver uses a steering wheel to apply an input (i.e. rotates the wheel), an input is applied at the wheels of the vehicle, through a ratio called the steering ratio. The driver input is represented as δ, whereas the corresponding input at the wheels is represented as δ_f. A desired yaw rate [17] is calculated from the steering angle δ_f, given by the relation

$$r_d = \frac{u\delta_f}{(l_f + l_r)\left(1 + \frac{u^2}{V_{char}}\right)} \qquad (2.11)$$

V_{char} is the characteristic speed of the vehicle [18].

To control the yaw rate and bring it down to the desired value, a number of techniques are available. In [17], the author shows the use of a Lyapunov function to generate the control algorithm. In [16], the author shows a simple state feedback design to bring the yaw rate error to zero. Since the system is linear, a simple linear quadratic regulator (LQR) may be designed to follow a desired yaw rate. This method is applicable when the slip angle versus lateral force [15] curve is in the linear region. The control strategy is discussed in detail in chapter 6.

2.4 Summary

From the review of the literature, we can conclude that the signal obtained from an accelerometer attached to the inner liner of a tire can be used to estimate the patch length. The ascending front and descending front in the signal provide an indication of when the accelerometer enters and leaves the contact patch, thus leading to an estimate of the patch length.

The relation between patch length and load can be given by suitable equations. These equations can help estimate the load corresponding to the patch length, for a cycle of rotation of the tire. However, the load-patch length relation is only for a static tire, and suitable adjustments would have to be made for a moving tire.

The Pacejka Magic Formula Tire model was examined and its relation to the dynamic load explained. The use of this model can help predict the actual cornering stiffness from the load and slip angle; it can then be used directly in a vehicle model to stabilize it and maintain a desired yaw rate.

3. Test Setup

This chapter explains the setting up of the equipment required for performing the tests detailed in chapters 4 and 5, including the creation of the instrumented tire (i.e. the tire containing the accelerometers) and the necessary electrical connections. We begin with a short description of the tire used in testing.

3.1 The Tire and Wheel

Goodyear Fortera P245/65R17 tires were used to carry out the tests. These are radial tires with an unloaded radius of 14.82 inches. The rated load of the tires is 2039 pounds at an inflation pressure of 35psi. The tires were tested at two different inflation pressures, 35 psi and 32 psi, for different loads and different speeds. The vertical stiffness (equations 2.2 and 2.3) of the tire at these two inflation pressures was calculated from existing load-patch length data provided by the manufacturer. A wheel of diameter 17 inches and radius 8 inches was used to mount the tire.

3.2 Accelerometers

The accelerometers used were

1. Dytran 3225F (uniaxial) with a 500g peak measurement range.
2. Dytran 3023A5 (triaxial) with a 5000g peak measurement range.

The uniaxial accelerometers measure only the radial acceleration. The triaxial accelerometers can measure radial, lateral and tangential acceleration. These accelerometers were chosen for their range and high sensitivity, as the tire would be subject to large forces during testing. The accelerometers were glued to the inner liner of the tire using cyanoacrylate adhesive. The inner liner was cleaned with a water-based cleaner to remove dirt particles and allowed to dry before attaching the accelerometers. For on-road tests, the uniaxial accelerometers were directly glued to the inner liner. But examination of the accelerometers after testing revealed that some had come loose due to the forces experienced by the tire as it is moves on the road.

For testing on the flat track, the accelerometers were enclosed in latex (rubber) and the latex part was glued to the inner liner. This formed a stronger bond with the tire and reduced the chances of

the accelerometer coming loose when the tire is rotated. In addition, duct tape (in combination with cyanoacrylate adhesive) was used to secure the wires of the accelerometers inside the tire. The idea is to prevent the wires pulling on the accelerometers and yanking them out during rotation. Figure 3.1 (a) and (b) show how this was carried out.

(a) **(b)**

Figure 3.1. Accelerometer **(a)** enclosed in latex and **(b)** glued to the inner liner

3.3 Electrical Connections

The accelerometers were placed inside the tire-wheel assembly with electrical connections going to the power supply outside using an electrical bulkhead connector fixed in the rim of the wheel. There are two separate connecting pieces – one inner and one outer- that attach to the bulkhead connector, as shown in figure 3.2.

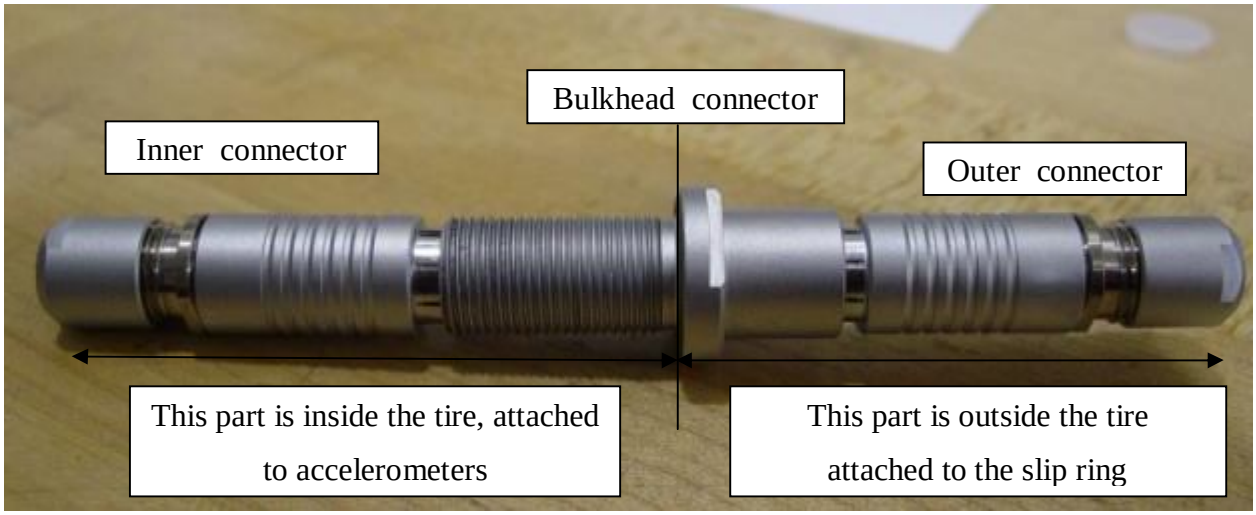

Figure 3.2. Bulkhead connector with the inner and outer connecting pieces attached

Each of these connector pieces has electrical soldering contact points. The accelerometer wires were soldered to the inner connecting piece. Wires from a slip ring were soldered to the outer connecting piece. The placement of the bulkhead connector on the rim is shown in figure 3.3.

Figure 3.3. Wheel with connector fixed on rim

3.4 Slip Ring

A slip ring assembly, placed at the center of the wheel, is required to allow the free rotations of the tire-wheel assembly without having the wires entangled in it or in other testing equipment.

Two different types of slip rings were used.

1. Low speed slip ring (figure 3.4) – this was used for on-road testing where low speeds of up to about 35mph were reached. The slip ring was placed at the center of the wheel cap.

2. High speed slip ring (figure 3.5) – this was used for tests conducted on the flat-track where higher speeds of up to 65mph were reached. A metal plate was machined to be

bolted to the center of the wheel (where the wheel cap normally sits), and the slip ring was bolted to this metal plate.

(a) **(b)**

Figure 3.4. (a) Low speed slip ring and **(b)** its placement on the wheel cap

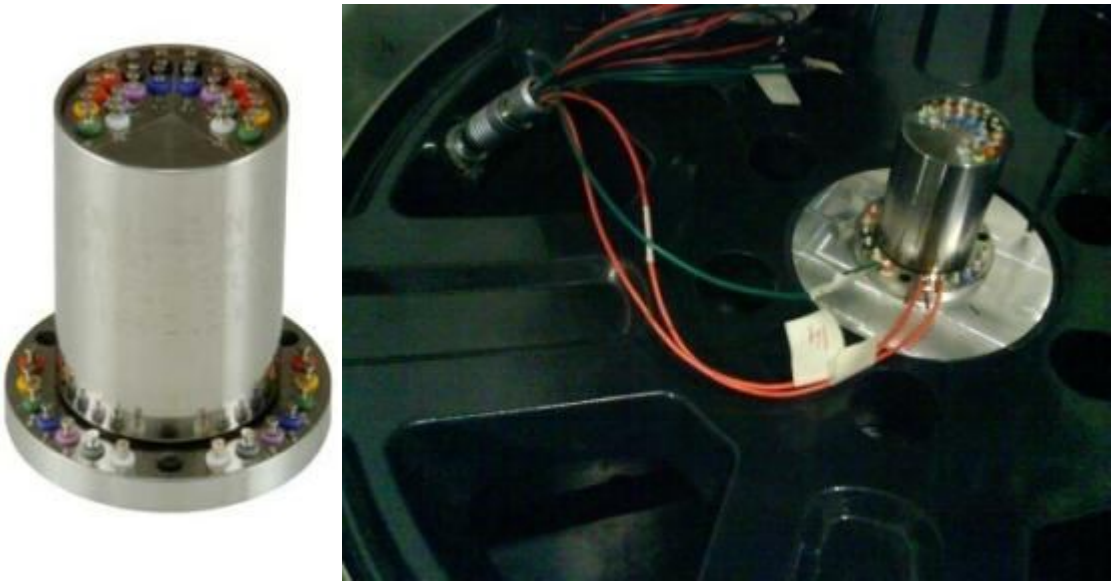

(a) **(b)**

Figure 3.5. (a) High speed slip ring and **(b)** its placement on a metal plate

One set of wires from the slip ring was soldered to the connector piece that attaches to the outside of the bulkhead connector (figure 3.5 (b)). The corresponding wires from the center of the slip ring were then connected to the wires carrying power to the accelerometer (the same

wires also carry acceleration signal from the accelerometer), and the ground wires. These wires were connected to the power supply for the accelerometers. The connection from the slip ring is shown in figure 3.6. The gray cables soldered to the slip ring wires attached to the wires that are carrying power to the accelerometers (each wire carrying the accelerometer signal and current has a 10-32 coaxial connector at the end and is shown with a yellow label in the figure below).

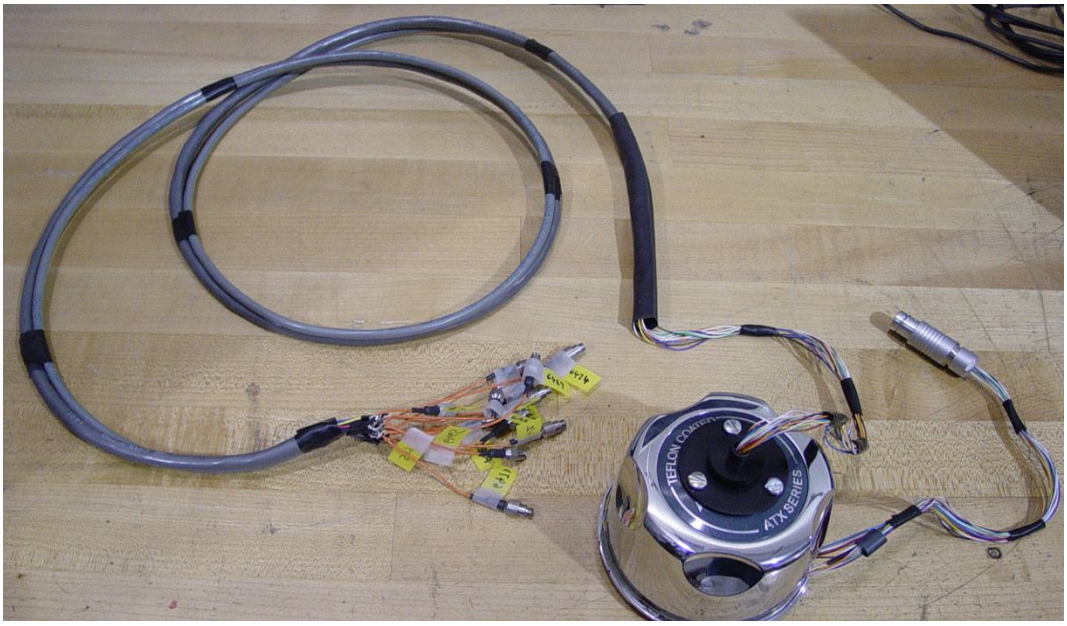

Figure 3.6. Connections to 10-32 coaxial cables from slip ring

Figure 3.7. Accelerometer power supply

The power supply also has terminals to which the data acquisition system can be connected through the use of BNC connectors. Each terminal carries the acceleration signal from a single accelerometer. The 16-channel power supply used to power the accelerometers is shown in figure 3.7.

3.5 Data Acquisition System

A dSpace 1401/1501 MicroAutoBox was used for collecting data from the accelerometers. A Simulink model was developed and linked to a project in ControlDesk, the software that captures data and allows it to be stored as a '.mat' file (Matlab data file) and hence allows easy analysis using Matlab.

3.6 Summary

The chapter started with a description of the tire used in testing and the wheel on which it was mounted. The procedure to install the accelerometers in the tire to facilitate testing is given. This included the method used in gluing the accelerometers to the inner liner of the tire and the electrical connections used to obtain data from inside the tire.

The installation of the connectors on the rim of the wheel was shown. The slip ring assembly and its connection to the connector on the rim were explained. Finally, a brief description of the data acquisition system was provided and it was explained how the data captured by the system could be easily analyzed.

4. Testing and Algorithm Development

The testing of the instrumented tire has been carried out at two locations.

a. The Intelligent Transportation Laboratory (ITL), a part of the Institute for Advanced Learning and Research (IALR) at Danville, Virginia. It also served as the base for putting together the instrumented tire and the associated electronics. A tire-test trailer was used for testing the instrumented tire on the tarmac.
b. Goodyear Innovation Center in Akron, Ohio. A flat-track test machine was used for testing the tire.

This chapter details the work done at the ITL.

4.1 Testing Equipment

Twelve Dytran 3225F (uniaxial) accelerometers were glued to the inner liner of the tire at equal intervals along the circumference. The setting up of the circuit to collect data was explained in chapter 3.

The tire was subject to static testing (figure 4.1) by suspending it using rubber chords as shown. The tire was hammered on different points on its surface, and the acceleration signal recorded and observed to test the working of the circuit. Once the set up was tested for proper functionality, on-road tests were performed.

Figure 4.1. Testing the set up with a free-hanging condition experiment

A tire-test rig was used to load up the tire (i.e. apply a normal load on it). The tire is attached to a hub that has a Kistler wheel force transducer for measuring the load. The load on the tire is varied by moving the rig up or down as per requirement. The rig is inside a trailer that can be towed by a truck (figures 4.2 and 4.3).

(a) **(b)**

Figure 4.2. (a) Tire test rig and **(b)** its placement in the trailer

The speed at which the tire is run is dependent on the speed at which the truck moves. The trailer was towed by a truck at different speeds and loads.

Figure 4.3. The trailer pulled by a truck

4.2 Sample Data

Samples of the acceleration experienced by the accelerometers inside the tire are shown in the following figures. Figure 4.4 shows the acceleration profile for data collected from a single accelerometer (the acceleration recorded by the other accelerometers in the tire follows the same characteristic pattern); figure 4.5 shows a magnified view for two cycles of rotation and figure 4.6 shows acceleration during a single rotation of the tire.

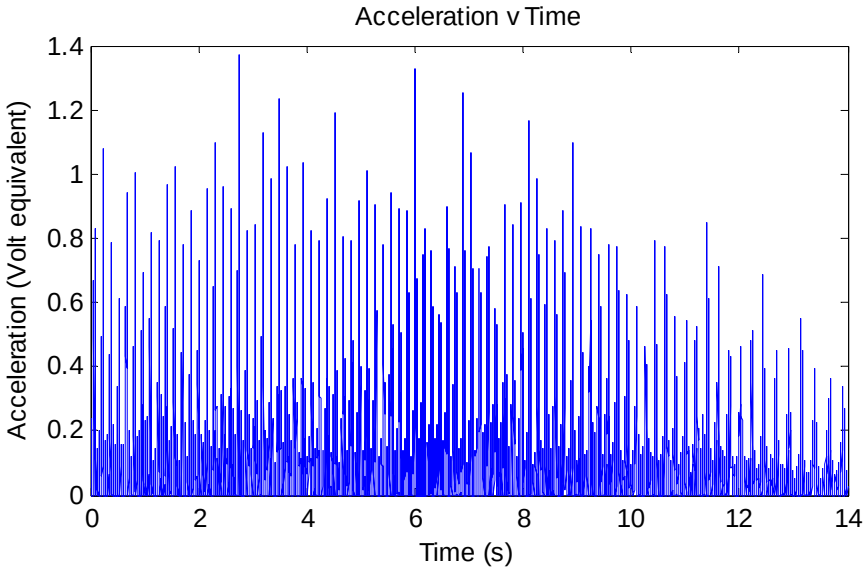

Figure 4.4. Sample of data from a single accelerometer for tire inflated to 35psi, initial load of about 1560 lbs

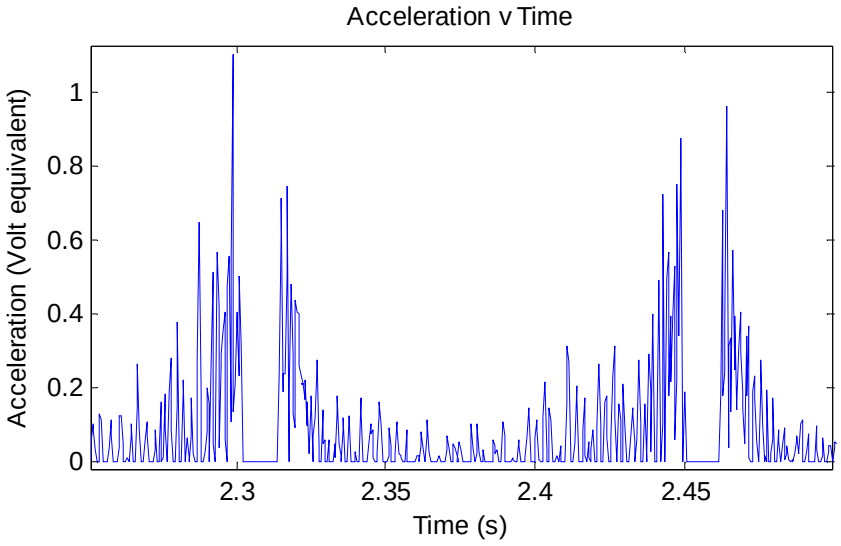

Figure 4.5. Magnification of the acceleration of figure 4.4

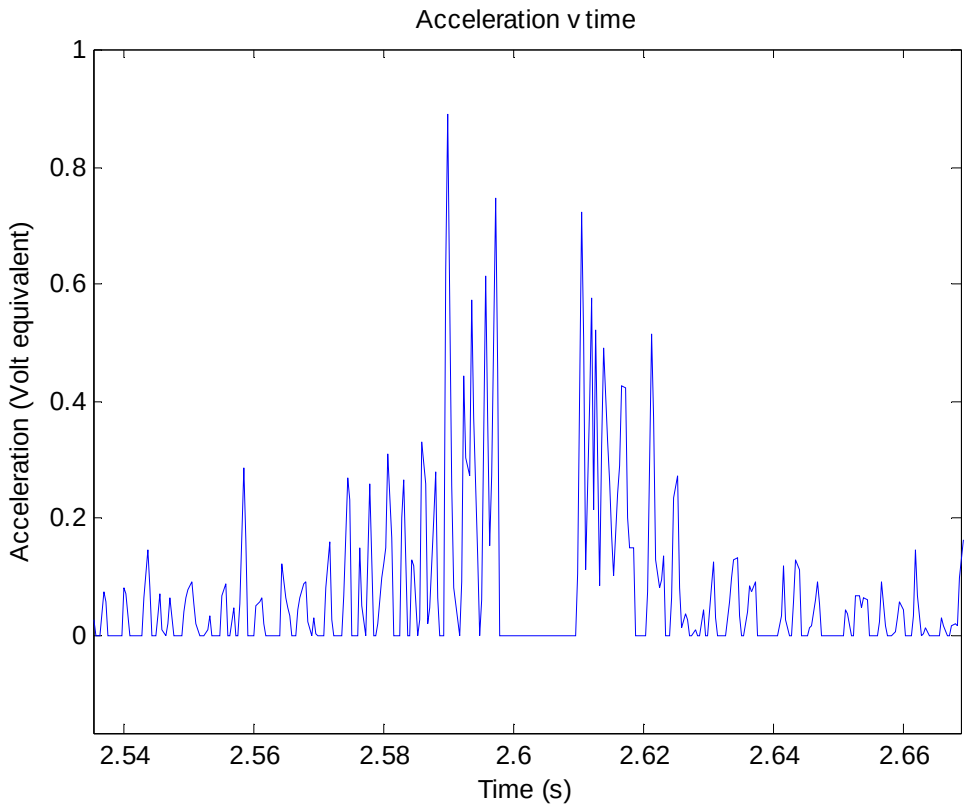

Figure 4.6. The acceleration profile for a single cycle of rotation of the tire

4.3 Description of the Data

As has been explained in section 2.1, when the accelerometer enters and leaves the contact patch, the acceleration shoots up. According to [8] there is a descending front corresponding to the entry of the accelerometer into the contact patch and the ascending front as it leaves the patch. In the set up for this research project, the acceleration recorded by the data acquisition system is only positive as the dynamic range of the accelerometers is only 0 to 5 Volts. Hence, the acceleration falls to zero (ideally) when the accelerometer is in the contact patch.

4.4 Signal Processing

The signal processing technique involves finding the 'flat spot' corresponding to the time spent by the accelerometer in the patch. The signal from a single accelerometer was considered for this purpose; the same procedure could be applied to other accelerometer data too. The general strategy is to find the peaks and process the data between the peaks to obtain the patch length.

A Butterworth filter [19] was used to filter the data before obtaining the peaks. To get the cut-off frequency for the filter, the Fourier Transform of the acceleration signal is taken for one cycle of rotation of the tire. The data for a particular cycle of rotation is multiplied by a Blackman window [19] prior to obtaining the Fourier Transform. From this, power plots in magnitude and decibel scales are constructed. Typical power plots in absolute magnitude and decibel scales are shown below.

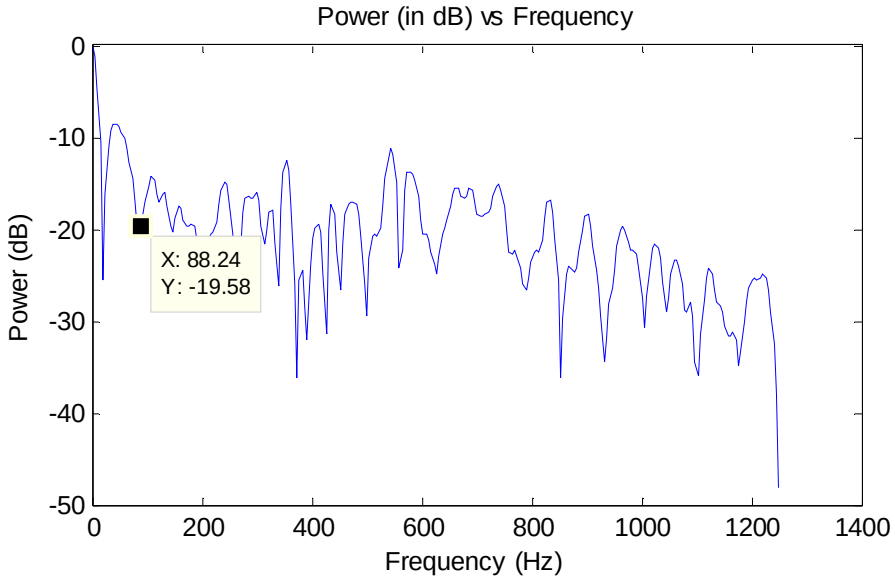

Figure 4.7. Power plot (dB scale) for a single cycle of rotation of the tire

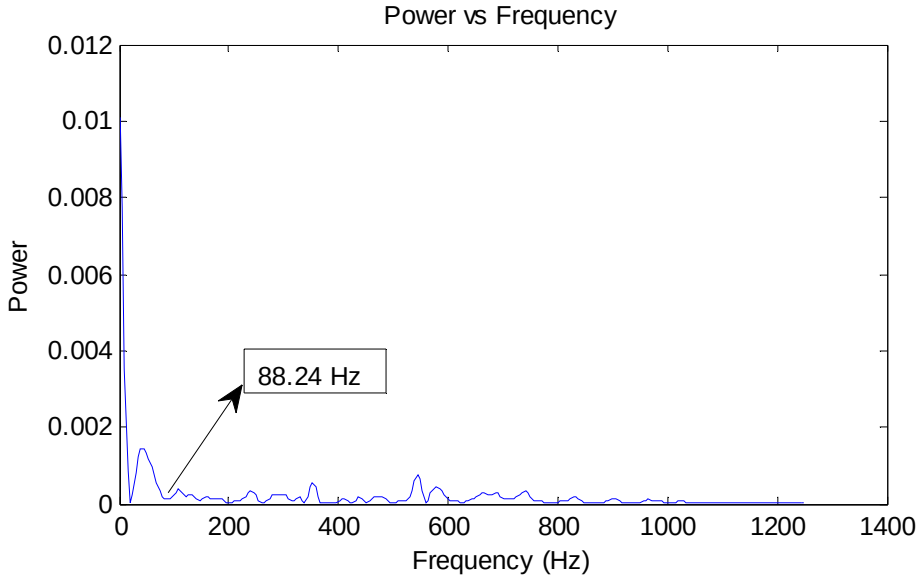

Figure 4.8. Power plot (absolute magnitude scale) for a single cycle of rotation of the tire

As can been seen in figures 4.7 and 4.8, the most significant component of power in the signal lies below the frequency indicated on each plot (in this particular case 88.24 Hz). This was taken as the approximate cut-off frequency of the Butterworth filter. A third order Butterworth filter was used to help attenuate the higher frequencies (that are treated as noise) better.

These plots were examined for multiple rotations of the tire for different operating speeds to see if a linear relation existed between the filter cut-off frequency and the speed at which the tire moved. This is explained in section 5.5. Result of filtering the signal is shown in the figure 4.9.

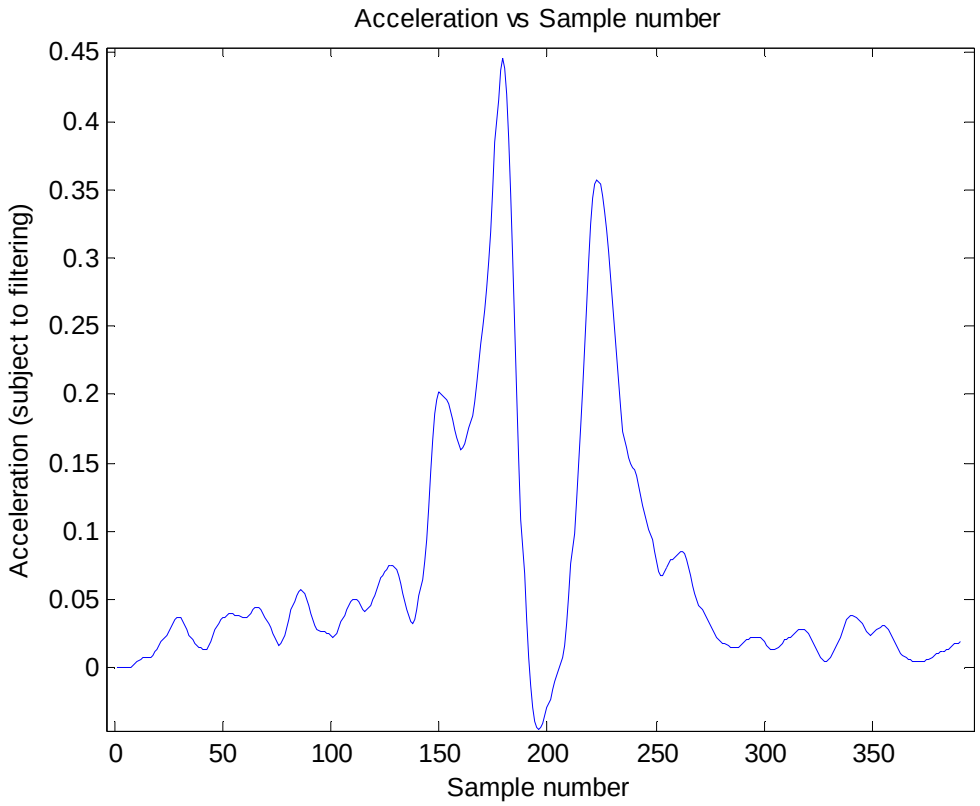

Figure 4.9. Low pass filtered version of the signal shown in figure 4.5

As a result of the filtering operation, multiple spikes observed in the raw data are reduced to a single ascending and a single descending front, similar to that seen in [8]. Please note that the filtered signal is represented as a function of the number of samples corresponding to that rotation of the tire and not as a function of time. The data acquisition system records the

acceleration data as a function of sample number; the sample numbers can then be converted to time by multiplying by the sampling period.

Once the filtered signal was obtained, the time instances at which the largest peaks occur were detected. Once we know where the peaks occur, in terms of their sample number, the original signal for the cycle of rotation under consideration is normalized and the best fit line subtracted (detrending operation, [8]) from it, resulting in a signal that had a zero crossing. A few samples before the first peak, a few samples after the second peak and all the data in between was taken from this modified signal. This signal between the peaks was then processed separately to find the zero crossing. In such a case, finding the zero-crossing of the (shortened) signal is approximated to be equal to finding the length of the flat spot (figure 4.10) that corresponds to the time spent by an accelerometer in the patch as the tire is moving.

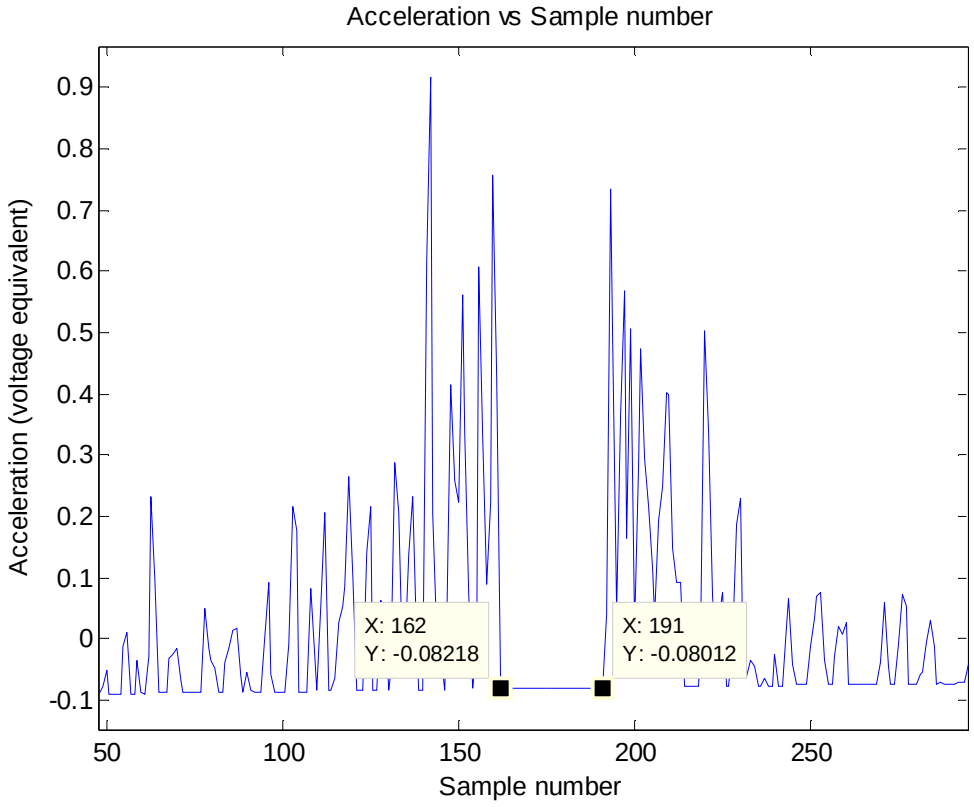

Figure 4.10. Normalized and detrended version of signal

A number of zero-crossings may be detected because the original acceleration signal (before detrending) varies constantly between zero and a finite value, except for when the accelerometer is in the contact patch. Usually, there are a number of zero crossings in the detrended signal, of which the longest zero crossing corresponds to the time spent by the accelerometer in the patch.

An immediate problem can be noticed here: what if there is a sudden spike in acceleration, corresponding to say, a pebble or irregularity that a tire may run over? In such a case, there may be a faulty detection in the patch length. This issue is addressed in section 5.5. However, this algorithm certainly works when data is assumed to be 'good', in the sense that there are no sudden jumps in acceleration when the accelerometer is going through the contact patch. It is assumed that, for now, the data is 'good'.

Once the samples corresponding to zero crossing are found, the difference between the higher sample number and the lower sample number gives the number of samples corresponding to the time spent by the accelerometer in the contact patch for that cycle of rotation. This sample length multiplied by the sampling time gives the actual time spent by the accelerometer in the patch.

To find the patch length, the time is multiplied by the speed of movement (which is the speed at which the trailer with the test rig is towed). Patch length is calculated as the product of number of samples (N) corresponding to flat region in the signal, the sample time (T) and speed (u).

$$\text{Patch length } L = NTu \tag{4.1}$$

Once the patch length was found, it was compared to the patch length calculated by observing the raw signal directly. The number of samples was comparable with very little to no difference between them, as shown in figure 4.11. The procedure was tested for a large number of cycles of rotation for different speeds. Figure 4.11 shows the comparison for twenty cycles of rotation for the conditions of load and speed that have been discussed so far (section 4.2).

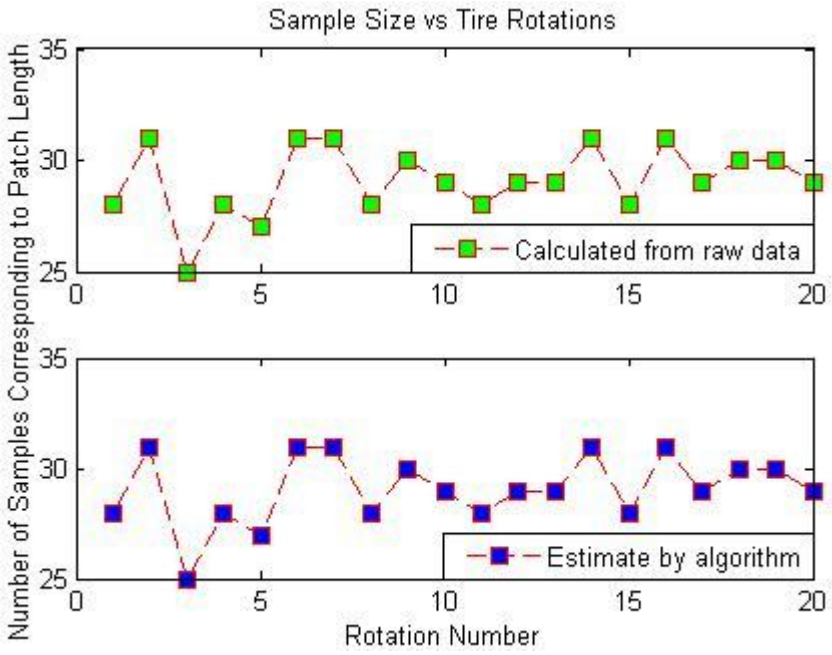

Figure 4.11. Actual versus algorithm-estimated patch length

As seen in the plot, the estimated patch length (in terms of number of samples) is the same for the two cases. The problem occurs when a scenario like the following plot (figure 4.12) arises. The acceleration shoots up in the middle of what is expected to be a region of zero acceleration.

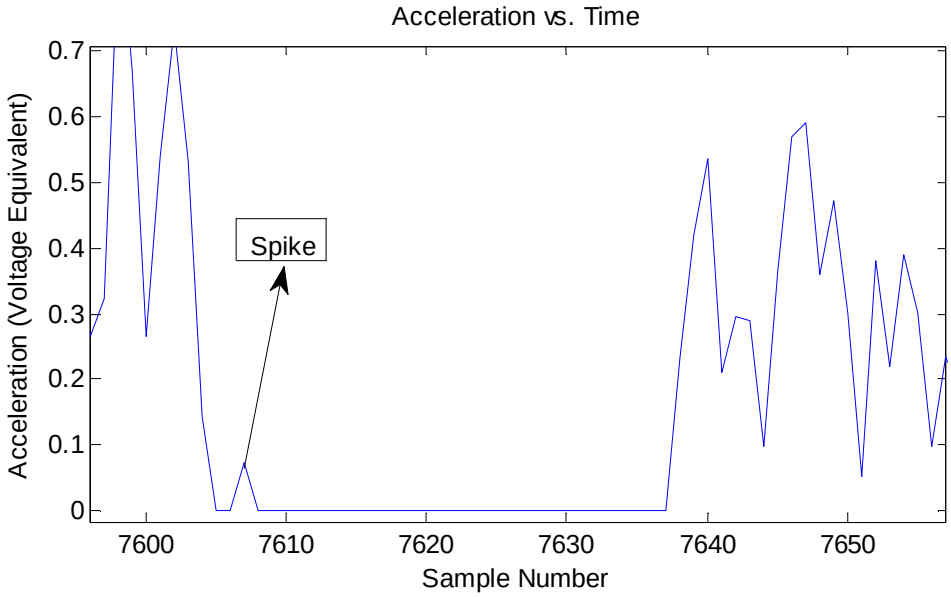

Figure 4.12. Possible cause of false detection – a spike in the middle of the patch

How should the number of samples be estimated? Is the data on either side of the spike considered as being part of the contact patch or is it only that after the spike occurs? Did the spike occur due to some imperfection in the road surface when the accelerometer is in the patch? What if the magnitude is much higher, and if the spike is in the middle of the flat region? In such cases, false detection of length of contact patch may occur. As will be seen in section 5.5, one solution is to use the filtered signal to calculate patch length.

4.5 Calculating Load

This section outlines the initial methodology used to estimate the load and does not represent the final solution.

As mentioned previously, the tire was attached to a hub that has a Kistler wheel force transducer for measuring the load. The hub can record samples of the vertical load; the load read from the hub was stored for comparison with the load estimated by the algorithm. The varying load was sampled at 10 Hz (on the hub) whereas the accelerometer data was sampled at 2500 Hz. Exact variation of load vs. patch length could not be found at that sample rate, but at certain points of synchrony, the calculated patch length was used to compare the expected load to the actual load.

The relation between the load and the patch length [13] is restated here.

$$\text{Patch length } L = 2ad\sqrt{\frac{\delta}{d} - \left(\frac{\delta}{d}\right)^2} \tag{4.2}$$

a = 0.65 for the tire under test in static conditions.

By substituting the calculated value of contact patch length (L) in the equation, the ratio (δ) of normal load to vertical stiffness can be found, which can be further used to calculate the normal load by knowing the value of tire vertical stiffness.

Table 4-1 shows the calculation of load from patch length for a tire inflated to 35 psi running at 35 mph with an initial load of 1560 pounds.

Table 4-1. Calculated and observed values of dynamic load for 3 different cycles of rotation, based on a single accelerometer

Calculated patch length (inches) (using algorithm)	Load calculated using formula (lbs)	Observed load (from Kistler hub) (lbs)	Expected patch length (inches) (from Goodyear provided data)
6.89	1580	1520	6.75
7.14	1700	1660	7
6.89	1580	1550	6.8

As can be seen in the table, the load was an average value (the measured load at the beginning of the experiment) and not the instantaneous load. To calculate the patch length instantaneously, the load also has to be sampled at the same rate as the acceleration.

Another round of testing was carried out with the load sampled at the same rate as the acceleration signal i.e. 2500 Hz to see if a correspondence could be established between the expected and actual load. Figures 4.13 and 4.14 show the variations of estimated load with tire rotation and actual load with time, respectively, for a tire moving at about 10 mph with an initial applied load of about 1550 lbs.

The estimated load does not match the applied load. The differences could possibly be because of variations in load in the time that the accelerometer is in the patch. The trailer bounced around during the test, causing an ever changing load to be applied on the tire.

The differences could also be because of the roughness of the surface over which the tire was tested as evidenced by a few points in the waveform where acceleration signals shoot up when zero acceleration is expected (figure 4.12). This could indicate that there were bumps/stones on the ground which caused the spikes. This would throw off the estimate of the patch length and the associated load.

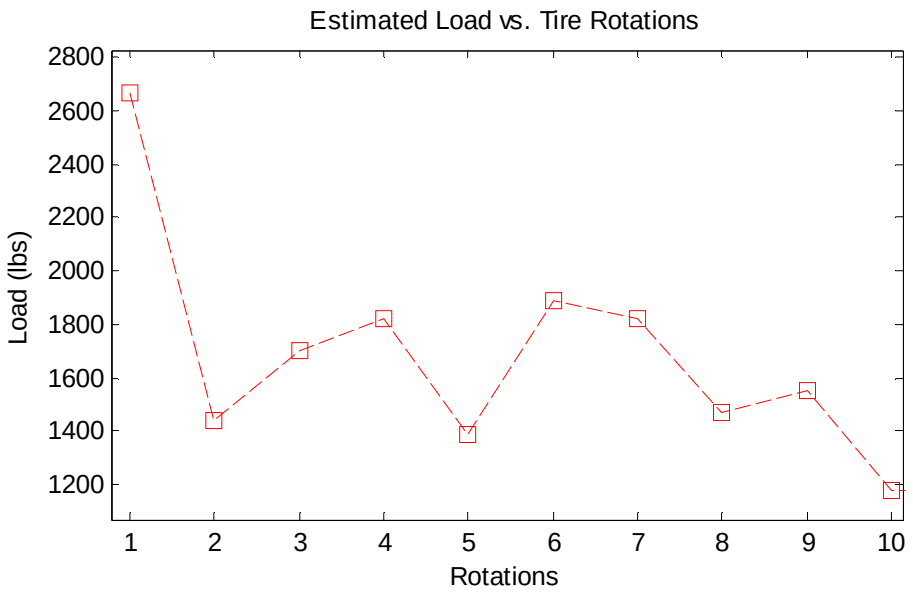

Figure 4.13. Estimated load

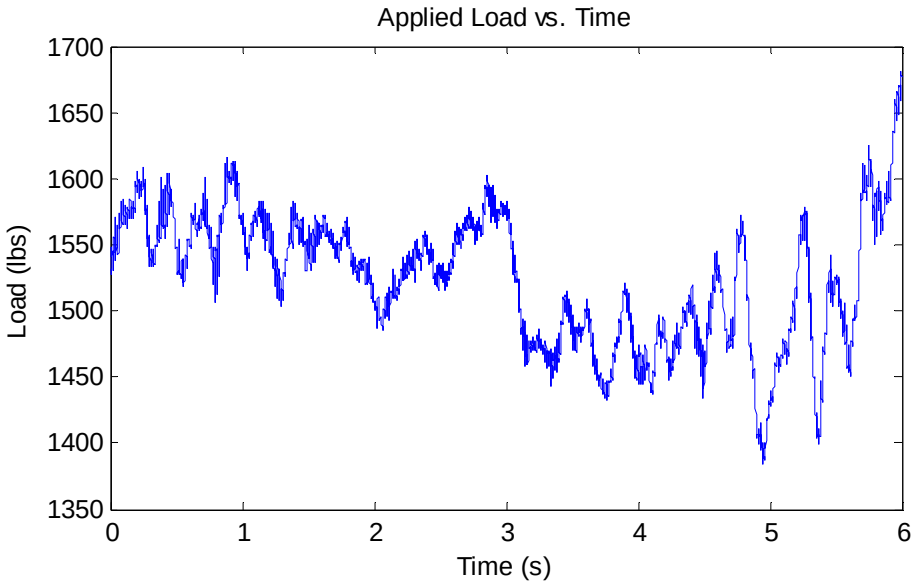

Figure 4.14. Load recorded by Kistler force hub

The multiplicative factor *a* would depend on the speed of movement and possibly the load. Without stable operating conditions, it was difficult to come up with an estimate for the multiplicative factor (a) for the particular set of conditions that would help in estimating the load.

The tests performed on the road were not conclusive enough and it was decided that the instrumented tire would be run on a stable flat surface, like a flat track machine. Also, it was clear that the estimation algorithm would work better if the load was constant or near constant during the period for which an accelerometer would be in the patch. This did not mean that the actual road surface would have to be smooth for the algorithm to work, but it would have to be tested for smooth surfaces before it can be developed to work for non-smooth roads. This leads to the next chapter on testing at the Goodyear Innovation Center in Akron, Ohio.

4.6 Summary

The methodology used to test the tire at the ITL in Danville was explained, including a brief description of the test rig. Samples of the data obtained from the tests were provided.

The sample for a single cycle of rotation of the tire was taken as an example to explain how the signal processing is carried out to estimate the patch length, which is (ideally) the region where acceleration falls to zero. It was shown that the estimates of the patch length could match up almost exactly with the expected values of patch length. The problem associated with this type of estimation was explained, wherein, without 'good' data, the estimates could fall short because of false detection.

The load on the tire was estimated based on the equation 2.2 relating patch length to load. It was shown that the estimates of the load varied because of the nature of the test set up, but that at certain instances, the estimates potentially matched up to the applied load. The results were inconclusive and led to the need for tests on a smooth surface to provide a usable working version of the algorithm.

5. Testing at the Goodyear Innovation Center, Ohio

This chapter details the tests done on a flat track machine at Goodyear's testing facility and the subsequent development of the algorithm to estimate load.

5.1 Flat Track Testing

Triaxial accelerometers were used in the testing to obtain data from lateral and longitudinal axes in addition to the yaw axis. This was done to see if any trends could be noticed in the data from the other axes that could help in estimating other tire parameters. However, the data from other axes was not used in load estimation. A flat track machine (figure 5.1) was used to carry out the tests for the tire at different pressures, speeds, loads, camber and varying slip angle.

Figure 5.1. Tire mounted on the flat track machine

The slip angle from the flat track machine's data acquisition system was used as a synchronizing signal between the accelerometer signal data acquisition and flat track machine data acquisition systems. The remaining set up for capturing the data was the same as that for tests conducted using the trailer.

A typical test involved a straight line run for 10 seconds and then a sweep maneuver, in which the tire is moved from side to side up to slip angles of 2 degrees on either side of the straight line, is applied for about 3 seconds.

A test matrix was created (table 5.1) that included the following information:

1. The speeds at which the tire would be run (10, 30, 45 and 65 mph)
2. The inflation pressures (35 and 32 psi)
3. The loads to which the tire is subjected (1300, 1500 and 1800 lbs at 35 psi and 1000, 1300 and 1500 lbs at 32 psi)
4. Slip angles (-2 to 2 degrees)
5. Camber (0 and 2 degrees)

Table 5-1. Test matrix for flat track testing

	Test Matrix for 8X4010C-6 and 8X4010C-7			
				Start at 0 deg 10 second dwell
	Zero degree camber			Go from 0 to -2 deg and sweep to +2 deg
	Pressure psi(kpa)	**Load lbs.(newtons)**	**Speed mph(kph)**	**Slip angle (degrees)**
1	35(241)	1300(5783)	10(16.1)	Sweep from -2° to 2° at 2 degrees/second
2	35(241)	1500(6672)	10(16.1)	Sweep from -2° to 2° at 2 degrees/second
3	35(241)	1800(8007)	10(16.1)	Sweep from -2° to 2° at 2 degrees/second
4	35(241)	1300(5783)	30(48.3)	Sweep from -2° to 2° at 2 degrees/second
5	35(241)	1500(6672)	30(48.3)	Sweep from -2° to 2° at 2 degrees/second
6	35(241)	1800(8007)	30(48.3)	Sweep from -2° to 2° at 2 degrees/second
7	35(241)	1300(5783)	45(72.4)	Sweep from -2° to 2° at 2 degrees/second
8	35(241)	1500(6672)	45(72.4)	Sweep from -2° to 2° at 2 degrees/second
9	35(241)	1800(8007)	45(72.4)	Sweep from -2° to 2° at 2 degrees/second
10	35(241)	1300(5783)	65(104.6)	Sweep from -2° to 2° at 2 degrees/second
11	35(241)	1500(6672)	65(104.6)	Sweep from -2° to 2° at 2 degrees/second

12	35(241)	1800(8007)	65(104.6)	Sweep from -2° to 2° at 2 degrees/second
13	32(221)	1000(4448)	10(16.1)	Sweep from -2° to 2° at 2 degrees/second
14	32(221)	1300(5783)	10(16.1)	Sweep from -2° to 2° at 2 degrees/second
15	32(221)	1500(6672)	10(16.1)	Sweep from -2° to 2° at 2 degrees/second
16	32(221)	1000(4448)	30(48.3)	Sweep from -2° to 2° at 2 degrees/second
17	32(221)	1300(5783)	30(48.3)	Sweep from -2° to 2° at 2 degrees/second
18	32(221)	1500(6672)	30(48.3)	Sweep from -2° to 2° at 2 degrees/second
19	32(221)	1000(4448)	45(72.4)	Sweep from -2° to 2° at 2 degrees/second
20	32(221)	1300(5783)	45(72.4)	Sweep from -2° to 2° at 2 degrees/second
21	32(221)	1500(6672)	45(72.4)	Sweep from -2° to 2° at 2 degrees/second
22	32(221)	1000(4448)	65(104.6)	Sweep from -2° to 2° at 2 degrees/second
23	32(221)	1300(5783)	65(104.6)	Sweep from -2° to 2° at 2 degrees/second
24	32(221)	1500(6672)	65(104.6)	Sweep from -2° to 2° at 2 degrees/second
	+2 degree camber			
	Pressure psi (kpa)	**Load Lbs.(Newtons)**	**Speed mph(kph)**	**Slip angle (degrees)**
25	35(241)	1300(5783)	45(72.4)	Sweep from -2° to 2° at 2 degrees/second
26	35(241)	1500(6672)	45(72.4)	Sweep from -2° to 2° at 2 degrees/second
27	35(241)	1800(8007)	45(72.4)	Sweep from -2° to 2° at 2 degrees/second
28	32(221)	1000(4448)	45(72.4)	Sweep from -2° to 2° at 2 degrees/second
29	32(221)	1300(5783)	45(72.4)	Sweep from -2° to 2° at 2 degrees/second
30	32(221)	1500(6672)	45(72.4)	Sweep from -2° to 2° at 2 degrees/second

5.2 Application of the Algorithm to the Collected Data

The algorithm developed earlier (section 4.4 and 4.5) was run on the data obtained from the flat track runs. Some of the results are documented here while the rest are documented in appendix A. Only the plots of the estimated load are shown as this is the main focus of the research project.

The algorithm was first tested with the value of the multiplicative factor *a* (equation 2.2) as 0.65, which is the value under static conditions; this led to unreasonably low estimates. Hence it was decided to test different values of *a* according to the speed. It was found that the following values of *a* for inflation pressure of 35 psi and 32 psi worked the best for the given speeds (table 5-2). The smaller values of *a* as compared to the static condition shows that the patch length is smaller under dynamic conditions. Also, the patch length seems to be increasing as speed increases, as the value of *a* increases with speed.

Table 5-2. Value of multiplicative factor *a* for different speeds

Speed (mph)	***a***
10	0.53
30	0.55
45	0.58
65	0.59

The following plots (figure 5.2 (a) – (d)) show how the estimated load varies with the cycles of rotation of the tire for different speeds, when the applied load is about 1800 lbs.

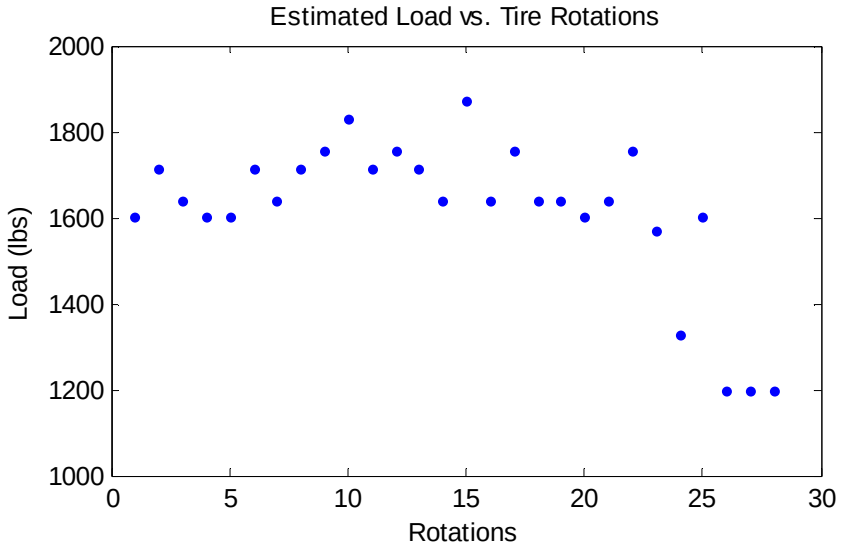

(a)

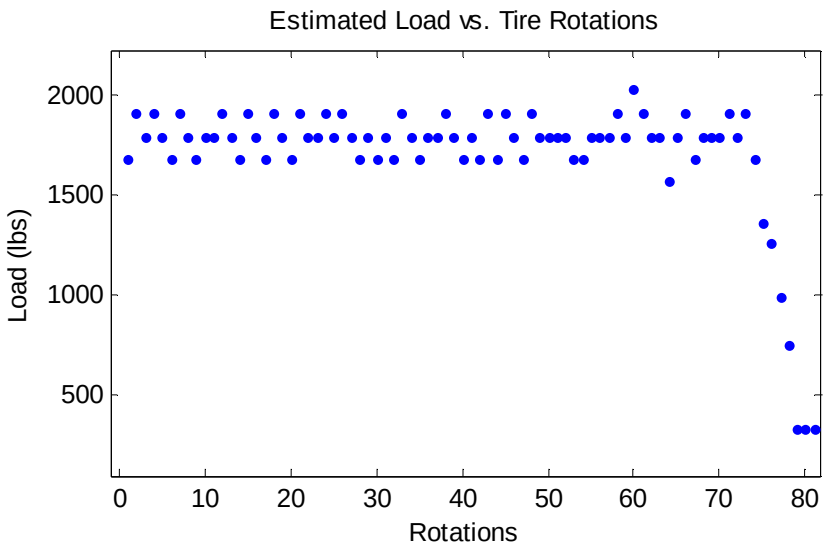
Estimated Load vs. Tire Rotations
Load (lbs)
2000
1500
1000
500
0
10
20
30
40
50
60
70
80
Rotations

(b)

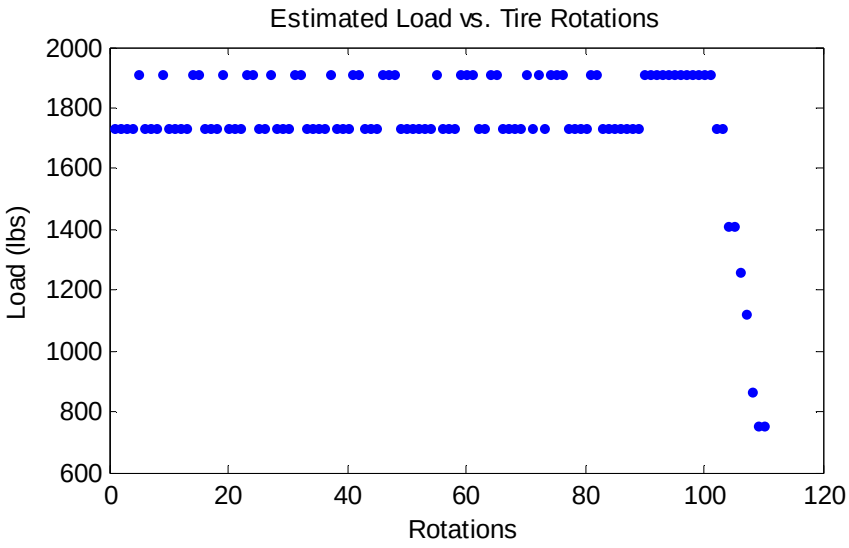
Estimated Load vs. Tire Rotations
Load (lbs)
2000
1800
1600
1400
1200
1000
800
600
0
20
40
60
80
100
120
Rotations

(c)

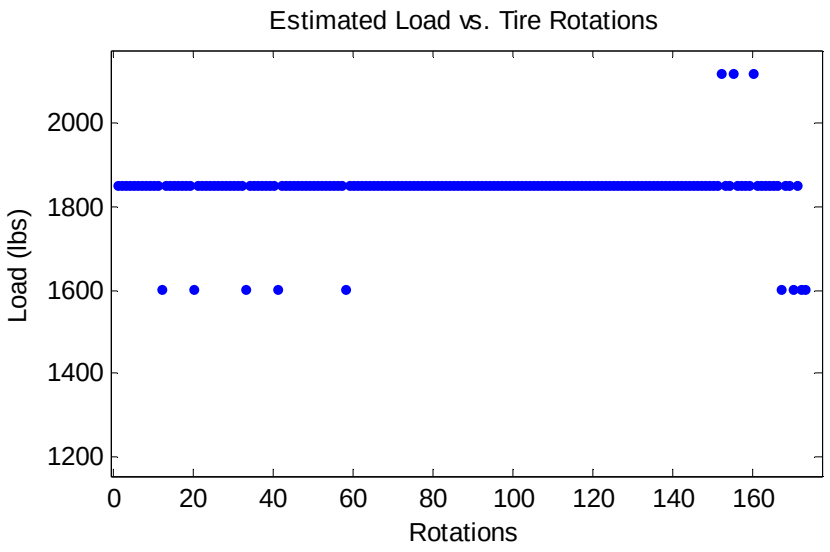

(d)

Figure 5.2. Variation of estimated load with rotation of tire with applied load of 1800 lbs at speeds of **(a)** 10 mph **(b)** 30 mph **(c)** 45 mph **(d)** 65 mph

It was observed that the same multiplicative factor (*a*) could be used across different loads when the tire is moving at a particular speed. The following plots show the estimated load for different applied loads at a speed of 65 mph, with an *a* value of 0.59.

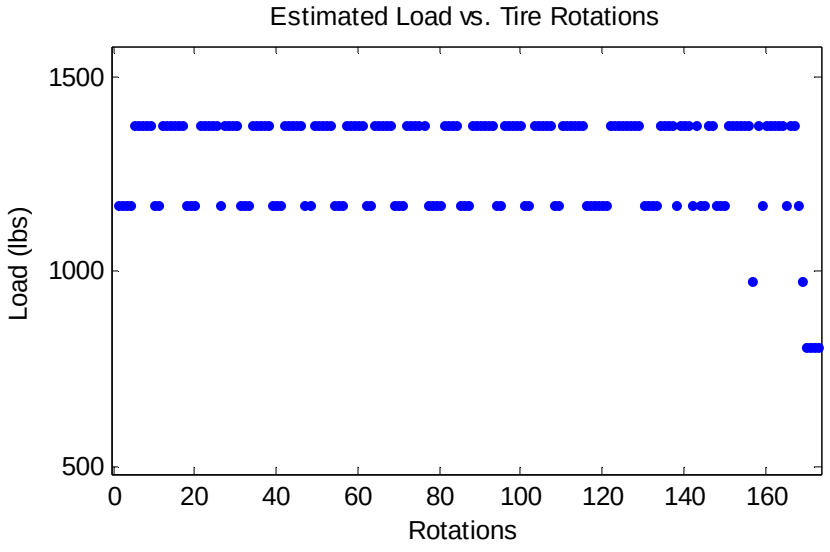

(a)

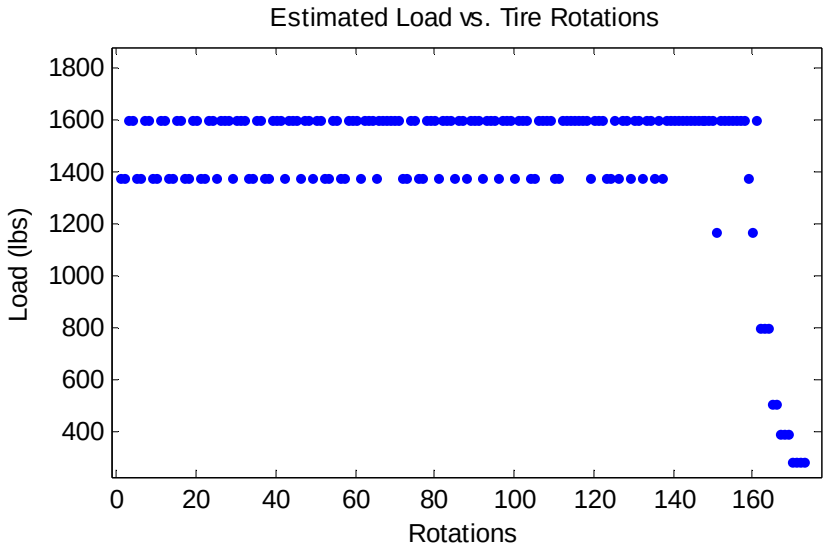

(b)

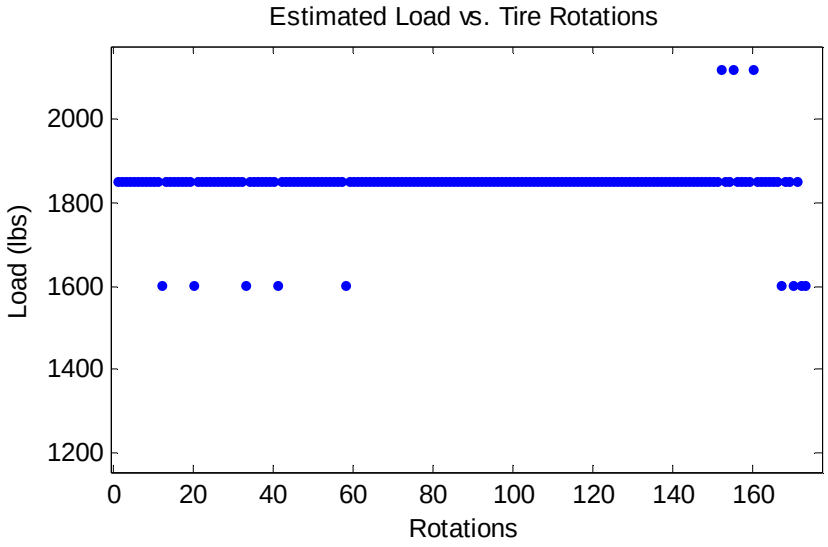

(c)

Figure 5.3. Variation of estimated load with tire rotation at 65 mph with applied loads of **(a)** 1300 lbs **(b)** 1500 lbs **(c)** 1800 lbs

The estimates of the load are clearly fluctuating too much and by large values (up to hundreds of pounds around the applied value) to prove useful. Some more results have been documented in

the appendix A, but as such they don't provide load estimates that can be used in control algorithms.

5.3 A Discussion on the Algorithm

As seen from the plots (figures 5.2 and 5.3), the estimated load is not consistent with the applied load. It was decided to alter the approach to calculate the patch length and the corresponding load. Most part of the algorithm explained in section 4.4 is still valid in detecting the patch length here, but with a few changes that will be explained in section 5.5.

One problem with the detection is that even a small change in the number of samples corresponding to the time spent by the accelerometer in the contact patch leads to a large change of up to 200 lbs in the estimated load (because of the change in estimated patch length).

Figure 5.4 is a typical plot of the applied load. The loads applied are not absolutely constant as can be seen below. The slightly higher loads near the end pertain to the application of a slip angle from -2 degrees to 2 degrees. Even though the variation in load is small (of the order of tens of ponds), it seems to throw off the data points by one or two samples.

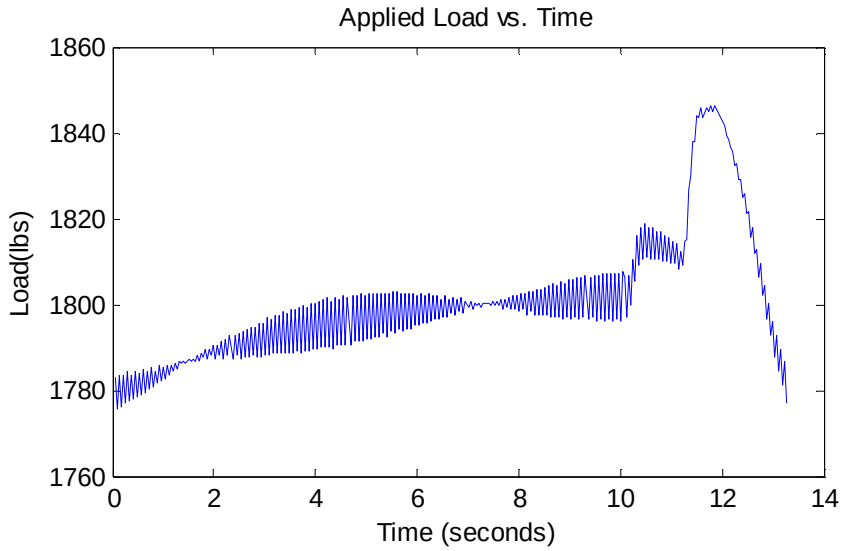

Figure 5.4. Typical applied load profile

Figure 5.5 shows the samples for two consecutive rotations at 65 mph and 1300 lbs load. In the first rotation, the number of samples is (3824 - 3813) = 11 and in the second, it is (4023 - 4011) = 12. We should add 1 sample to each; this is because the time to enter and leave the contact patch has not been counted. That would add half a sample on either side i.e. one more sample. So the actual number of samples would be 12 and 13, corresponding to the two rotations above.

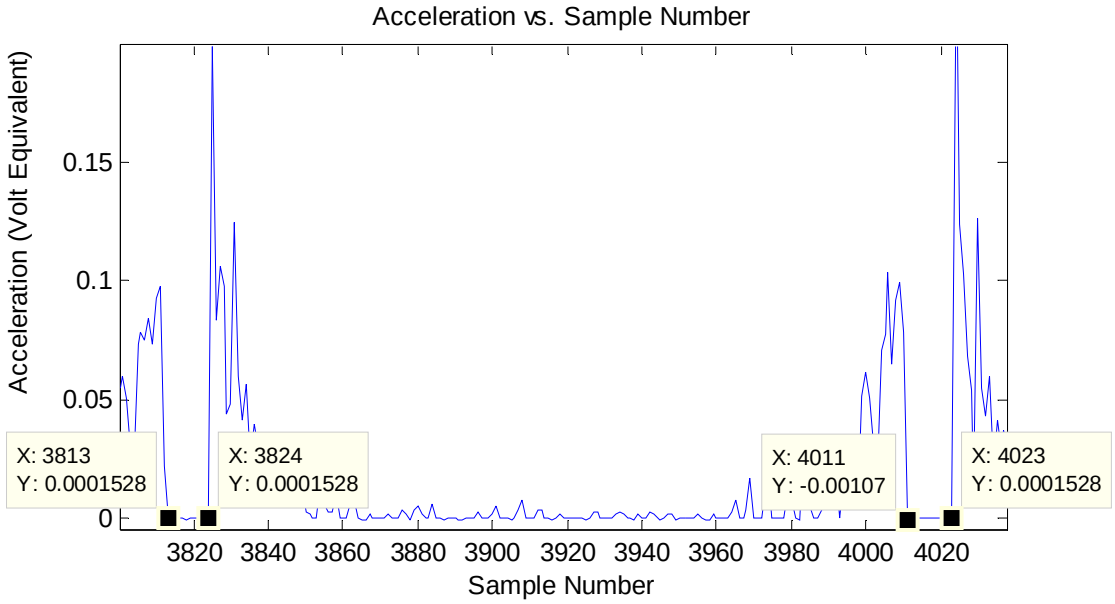

Figure 5.5. Comparison of samples corresponding to patch length for two consecutive cycles

The time spent in the patch is the product of number of samples corresponding to patch length and sampling period. In this case sampling period is 0.0004 seconds (sampling rate is 2500 Hz).

For first rotation: Patch length = speed in inches per second x time in the patch

$$= 65 \times 17.6 \times 12 \times .0004$$

$$= 5.4912 \text{ inches} \quad (5.1)$$

For second rotation: Patch length = 65 x 17.6 x 13 x .0004

$$= 5.9488 \text{ inches} \quad (5.2)$$

The factor 17.6 is the conversion from mph to inches per second.

This is only a 0.35 inch variation between cycles, which may seem like a small number. Converting these into the corresponding load values, however, we get 1507 lbs for the first rotation and 1780 lbs for the second. Thus, even a single point sample difference can lead to a large variation in load estimate, depending on the speed. The small variation in applied load may lead to this variation in estimated load; the actual load at the patch may be somewhere between these estimated load values but it cannot be accurately detected from the acceleration data. It may be possible to resolve this error using an even higher sampling rate, but that may not be a practical solution; such high sampling rates may only be possible with expensive data acquisition systems, which could be impractical if this has to be implemented in everyday cars.

The number of samples corresponding to the patch length need to be consistently close to each other for multiple cycles of rotation, when the load varies little around an average value. The multiplicative factor a in equation 2.2 (and in equation 2.3, which will be used in further calculations) can be suitably adjusted to estimate a load that is close to the applied load. This requires that the variations be smoothened out to get values that are consistent with the load.

Some the other important conclusions from applying the algorithm of sections 4.4 are as follows.

- The multiplicative factor (a) in equation 2.2 is speed dependent.
- An algorithm that would work for a certain inflation pressure could also be used for a different inflation pressure by selecting a suitable multiplicative factor in the load equation (section A.3).
- The algorithm so developed could possibly also be used on a cambered wheel (section A.2).
- The filter cut-offs needed to smooth the data seem to follow a linear relationship to the speed. This is shown in section 5.5.

5.4 Improvements in the Algorithm Using Kalman Filter

As seen in the previous sections, there is a large variation in the estimates of the patch length and hence the load. One way to smooth out these variations is to weight up or down the observation for a particular cycle of rotation by the value estimated in a previous cycle of rotation. This is done using a Kalman Filter [20].

The equations involved are as follows.

$$x(k) = A\,x(k-1) + B\,u(k) + w \tag{5.3}$$

$$z(k) = H\,x(k) + v \tag{5.4}$$

x(k) is the current state of the system, *x(k-1)* is the previous state of the system, *z(k)* is the observation vector, *u(k)* is the input, *A* is the state matrix, *B* is the input matrix, *H* is the observation model, *w* is the process noise and *v* is observation noise (with *w* and *v* being independent of each other).

For the current system, state matrix *A* is taken as unity, assuming that the patch length from one cycle of rotation to the next is consistent (which is reasonable, given that load varies very little and the surface over which the tire runs is smooth). There are no inputs to the system. Hence, the estimated state *x(k)* is the observation from the previous cycle, affected by a small process noise *w*, that is assumed to be zero mean, additive white Gaussian noise (AWGN) with a variance of 0.001. The observation vector *z(k)* is the estimate from the current cycle of rotation. The observation model *H* is taken as 1, assuming that the current observation *z(k)* is the same as the estimated state, with observation noise added. Observation noise (*v*), like process noise *w*, is taken as zero mean AWGN with a variance of 1.

In Matlab, the equations implemented are implemented as follows.

Kalman filter time update equations:

$$x(k) = A\,x(k-1) + B\,u(k-1) \tag{5.5}$$

$$P(k) = A\,P(k-1)\,A^T + Q \tag{5.6}$$

Kalman filter measurement updates equations:

$$K(k) = P(k)\,H^T(H\,P(k)H^T + R)^{-1} \tag{5.7}$$

$$x(k) = x(k) + K(k)(z(k) - H\,x(k)) \tag{5.8}$$

$$P(k) = P - K(k)\,H\,P(k) \tag{5.9}$$

P is the estimate covariance. This is assumed to be 1 at the start and is updated after each cycle until it reaches a steady value. *Q* is the process noise covariance, taken as 0.001. It was found that a noise variance of greater than about 0.001 did not fit the data appropriately; the variation in estimate became too high to prove useful. *R* is the measurement error covariance, taken as 1. *K* is a gain matrix that tries to minimize a posteriori (that which is known later) error covariance *P* and is calculated during each cycle of rotation.

Summarizing:

- $A = 1$, $H = 1$.
- No inputs to the system, $u(k) = 0$.
- $x(k-1)$ is the observation from previous cycle of rotation.
- $z(k)$ is the estimate from current cycle of rotation.
- w is assumed to be AWGN with variance $Q = 0.001$.
- v is assumed to be AWGN with variance $R = 1$.

During practical implementation, the steady state value of gain *K* is used in the load estimation as this will avoid the transient behavior, and hence greater fluctuations in load estimate, in which a constant value of *K* is reached after multiple iterations. The steady state value is K=0.0311, which is used in all test cases.

5.5 Additions and Changes to the Algorithm

There were some changes and additions made to the process of estimating the patch length and the vertical load.

1. A second order Butterworth filter has been used instead of a third order filter. When trying to implement the system in practice, this will help in bringing down the cost of the filter.

2. As in section 4.4, the power content of the acceleration signal as a function of frequency for each cycle of rotation was examined. The filter cut-off frequencies to be used in the Butterworth filter were determined by taking that frequency below which the most significant power content was available in the spectrum. The observations from this data lead to a near-

linear plot of filter-cut off frequency versus speed. For speeds between 10mph and 65mph (the lower and upper limits at which tests were conducted), the plot is as shown below. Note that this is for an inflation pressure of 35 psi.

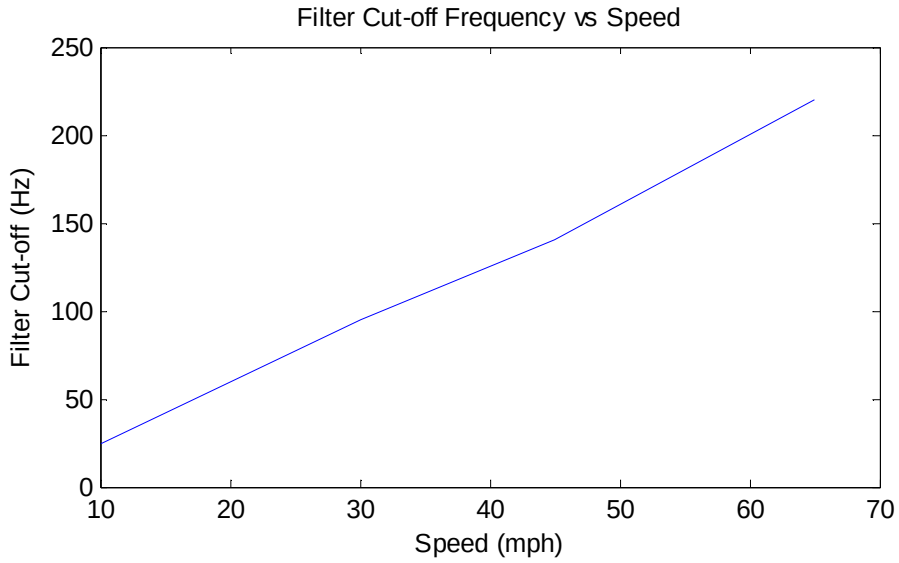

Figure 5.6. Plot of speed versus filter cut-off for tire inflated to 35 psi

Similarly, for an inflation pressure of 32 psi, the plot is as shown below.

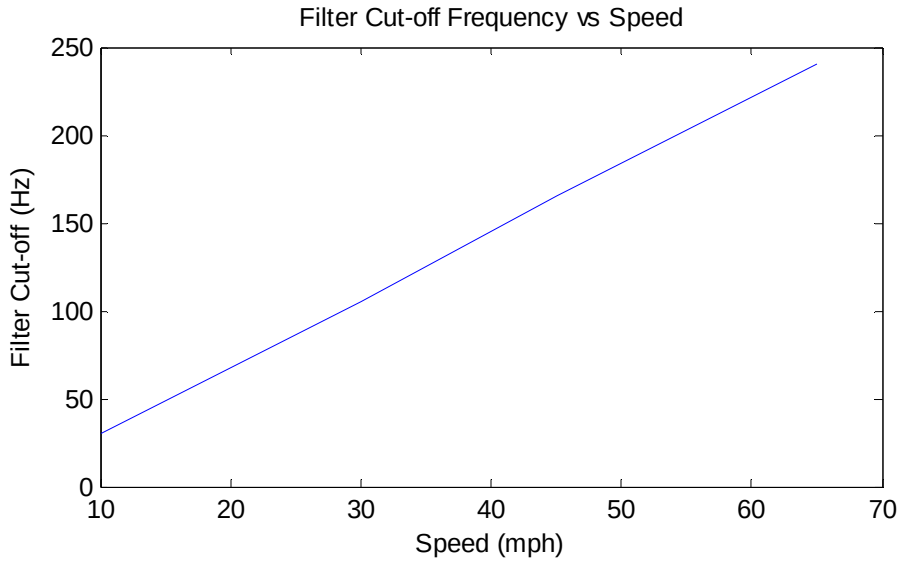

Figure 5.7. Plot of speed versus filter cut-off for tire inflated to 32 psi

The value of the cut-off frequency for any speeds between these limits of 10 and 65mph can be interpolated from the plot (this is done in the algorithm). For speeds outside the given range, more measurements can be taken at higher (greater than 65mph) and lower speeds (less than 10mph) to get a suitable curve that can be used for any speed.

3. As explained in section 4.4, there is the chance of false detection when working with the data as is. It was decided to test the low pass filtered version of the signal and subject it to the same procedure as the raw data. That is, after the peaks were detected, the normalization and detrending of the signal was carried out, followed by the zero-crossing detection of the signal between the peaks. Due to the smoothening of the waveform, there are obvious differences in the actual and filtered signal.

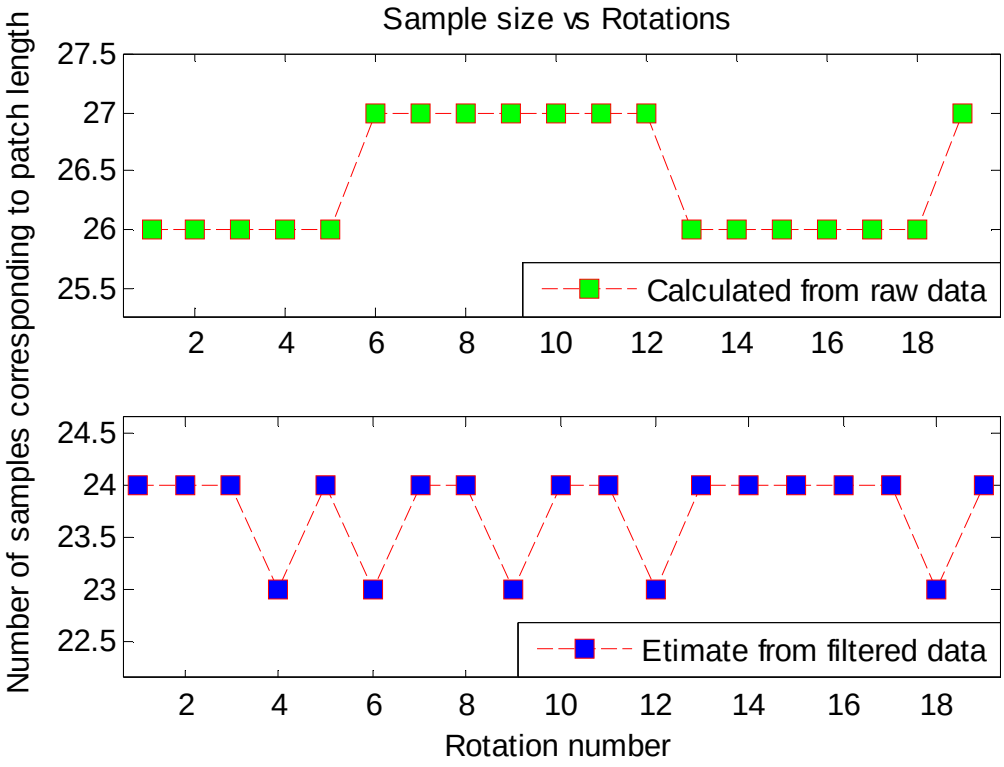

Figure 5.8. Actual versus estimated patch length (in terms of number of samples)

With the values of the number of samples oscillating between 26 and 27 for the raw data, those estimated from the filtered signal is varying between 23 and 24. Section 5.3 showed that even a one point difference in sample number can lead to a large variation in load. So

how can we justify using the algorithm that produces a difference of three or four sample points, even if the false detection problem is solved?

The use of the Kalman filter in combination with the multiplicative factor a in equation 2.3 can solve this problem. The Kalman filter causes smoothening of the variation in the estimate; suitable adjustments of the factor a results in estimates of load that are very near the expected load for each test case. This has been repeated for the thirty different test cases listed in table 5-1. This shows that using the filtered data can make the algorithm more robust.

This version of the algorithm is used for estimation of patch length in all further processing.

4. The equation to estimate load from patch length was changed to the more widely used formula shown below (equation 2.3 is restated here).

$$\text{Patch length } L = 0.7ar_f\left(\frac{\delta}{r_f} + 2.25\sqrt{\frac{\delta}{r_f}}\right) \tag{5.10}$$

r_f is the radius of the unloaded tire. a is 1 for a stationary tire. It was found that for a moving tire, a value of a from 0.81 to 0.83 at 35 psi and 0.84 to 0.85 at 32psi were sufficient to cover the entire range of speeds from 10mph to 65mph, instead of having a big variation based on the speed when equation 2.2 is used. Going forward, this formula is used for all the tests conducted on the flat track. For on-road testing, a may have to be recalculated as necessary, by further testing.

5.6 Results of Applying the Modified Algorithm

The results of applying the modified algorithm are shown in the form of the plots of estimated load against rotations of the tire (figures 5.09-5.38). For reference, the applied load as a function of time is also shown. It is to be noted that there is not a one-to-one correspondence between the plots of the applied and estimated load. However, the general trend can be observed in most cases shown below.

Note: All the results are for a sampling frequency of 2500Hz.

The following points can be noted from observing the plots.

1. The estimates of the load from patch length are comparable to the applied load, usually within 50 lbs of the applied value. This is a drastic improvement over the case when Kalman filtering was not used. The initial variation of the estimate from the applied may be quite high, but this settles down fairly fast, as attested by the plots.

2. The use of the steady state value of the gain *K* means that there is no transient portion, where there might be high fluctuations, in the estimates of the load.

3. The shape of the estimated load plot generally follows that of the applied load plot, i.e. it is generally increasing with a sharper increase where slip is applied. This is especially evident at higher speeds with more data points.

4. The values of *a*, the multiplicative factor used to estimate load are tabulated below.

Table 5-3. Value of multiplicative factor *a* for different speeds and inflation pressures

	Pressure = 35 psi	**Pressure = 32 psi**
Speed (mph)	***a***	***a***
10	0.81	0.83
30	0.82	0.835
45	0.83	0.835
65	0.84	0.86

As can be seen from the table, the general trend is an increasing value of *a* as the speed increases; however, the increase is not linear (unlike the case of the filter cut-off frequency). The variation of this factor with speed actually means the patch length is changing with speed; this variation has to be studied more carefully. For *a*, from a value of 1 at standstill to about 0.81 at 10 mph seems to indicate that patch length variation has be modeled before the algorithm can be actually implemented for speeds outside this range. This can be done by conducting more rigorous testing at higher and lower speeds.

5. The higher values of *a* at 32 psi inflation pressure as compared to 35 psi implies that the patch length is higher at lower inflation pressure, which is as expected.

6. The data acquisition could only capture data for 14 seconds at the sampling rate of 2500 Hz and had to be started and stopped manually based on approximate timing. Hence, in certain test cases, the complete maneuver (straight line run and application of a slip angle) may not have been performed before the data acquisition was completed. This is seen in some plots where the estimated load increases to a certain value, but does not drop according to the applied load plots. In some of the plots however, it can be seen that the load increases to a maximum value and then falls according to the applied load. This indicates that as each test was brought to an end, the load on the tire reduced, which is as expected (in actual flat track tests, the tire is lifted up from the track at the end of each test case, causing the drop in the applied load). Hence, it can be readily seen that the Kalman filter can help estimate the load, despite its varying nature.

Section 5.6.1 shows the variation of estimated load with rotations of the tire and applied load with time for an inflation pressure of 35 psi (cases 1-12 in table 5-1). Section 5.6.2 shows the same for an inflation pressure of 32 psi (cases 13-24 in table 5-1). Section 5.6.3 shows the same for the case when the wheel is cambered at 2 degrees.

5.6.1 Inflation Pressure of 35 psi

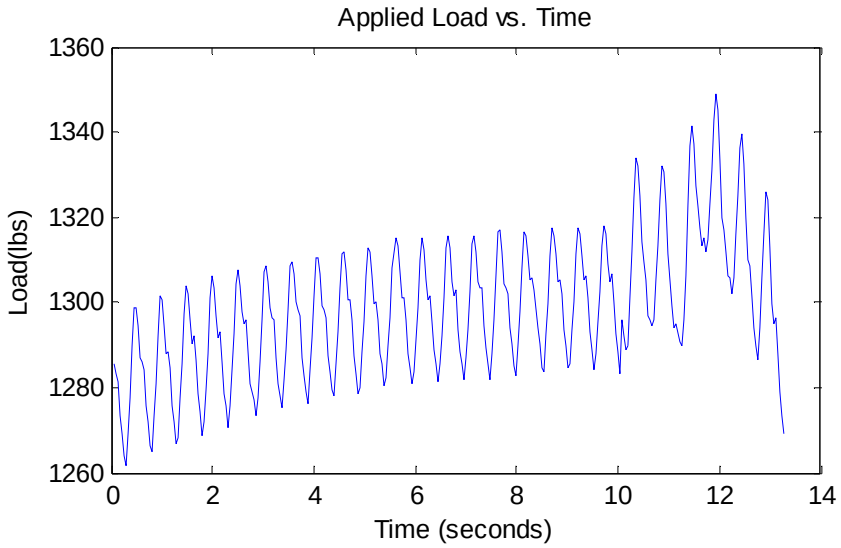

(a)

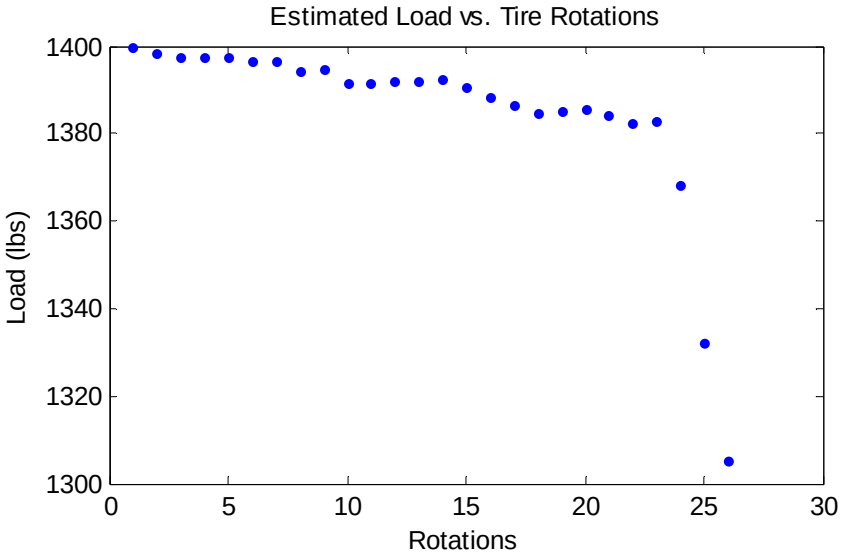

(b)

Figure 5.9. (a) Applied and **(b)** estimated loads at 35 psi inflation pressure for average applied load of about 1300 lbs and speed of 10 mph.

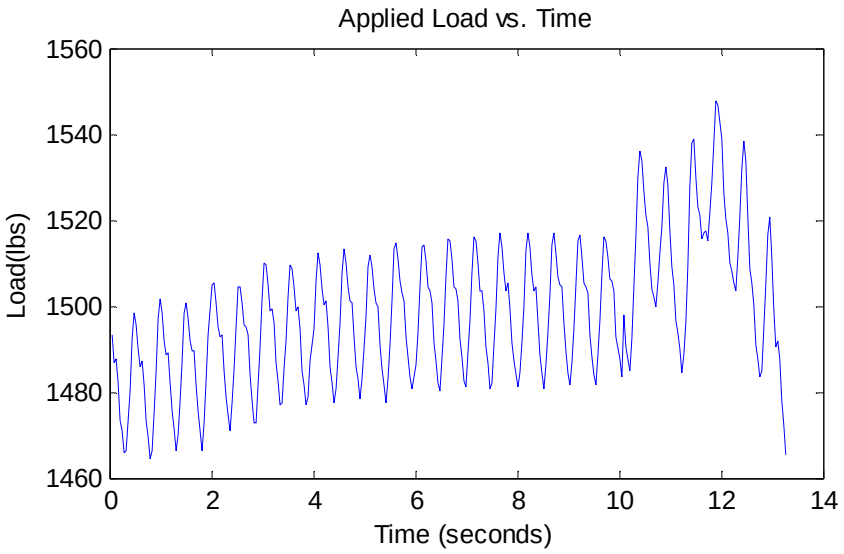

(a)

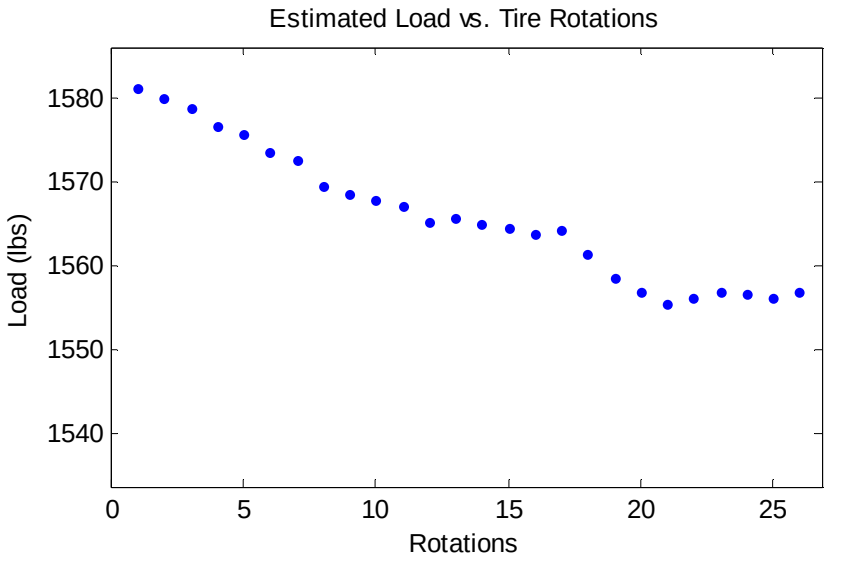

(b)

Figure 5.10. (a) Applied and **(b)** estimated loads at 35 psi inflation pressure for average applied load of about 1500 lbs and speed of 10 mph.

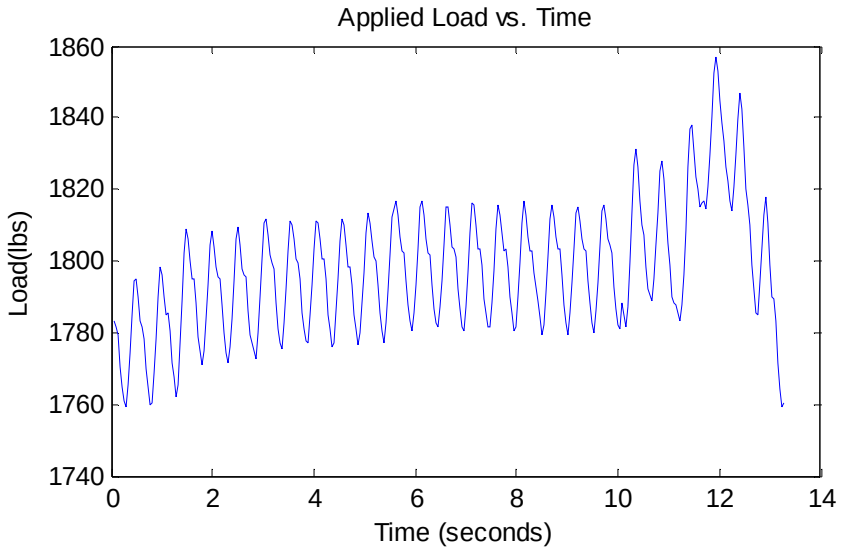

(a)

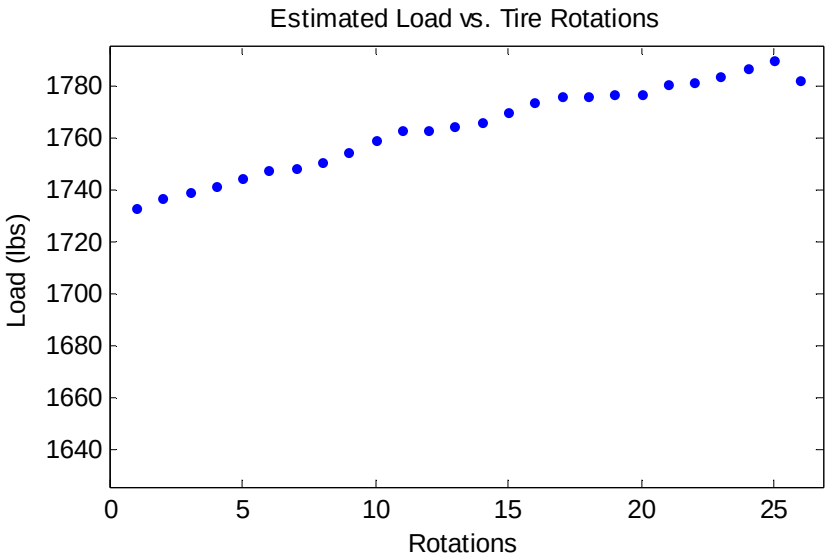

(b)

Figure 5.11. (a) Applied and **(b)** estimated loads at 35 psi inflation pressure for average applied load of about 1800 lbs and speed of 10 mph.

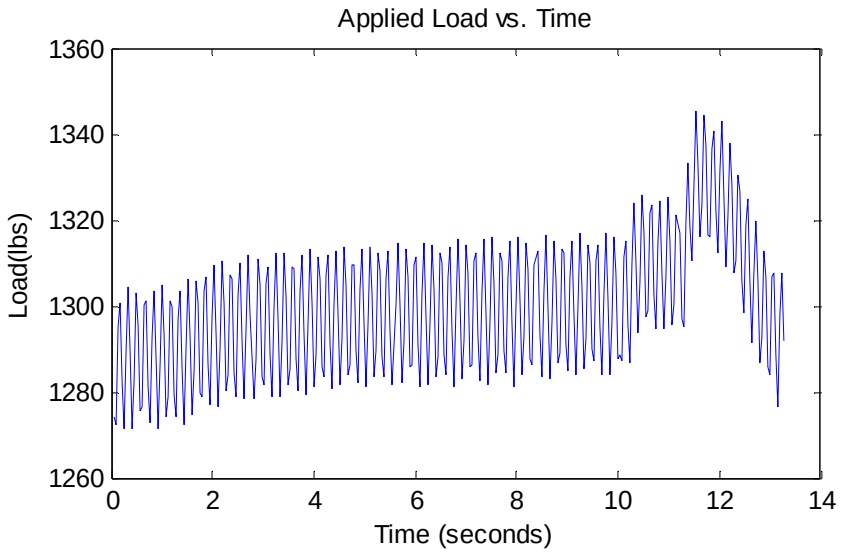

(a)

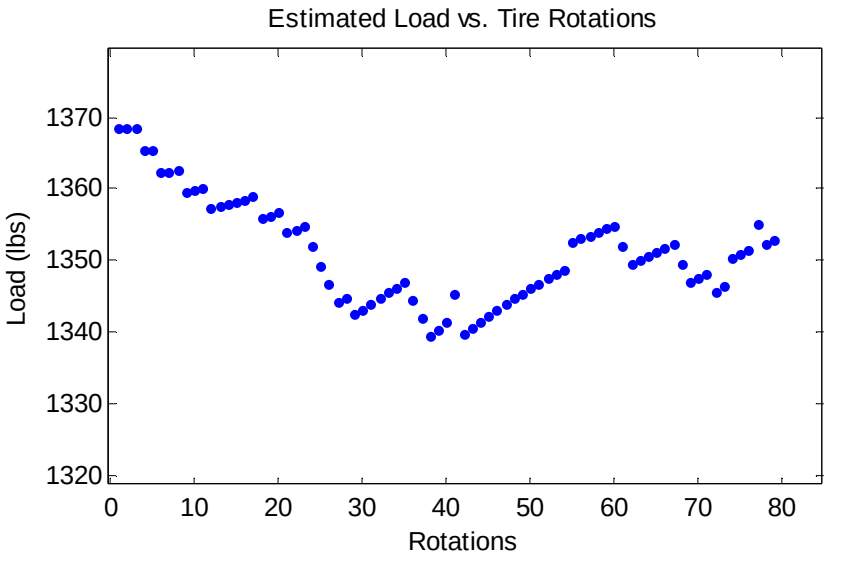

(b)

Figure 5.12. (a) Applied and **(b)** estimated loads at 35 psi inflation pressure for average applied load of about 1300 lbs and speed of 30 mph

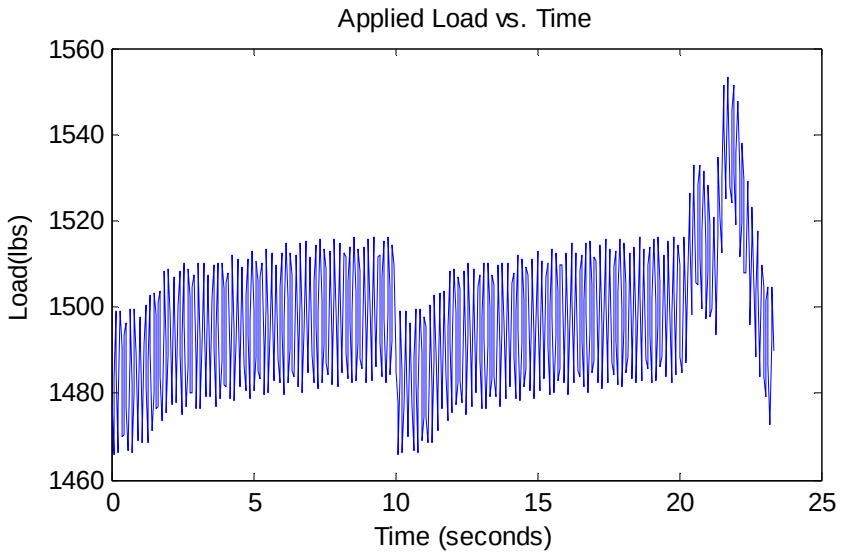

(a)

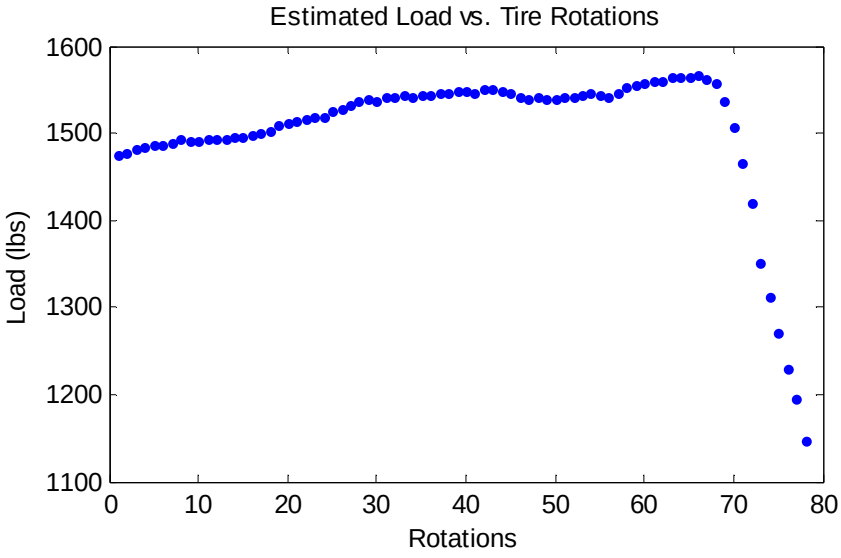

(b)

Figure 5.13. (a) Applied and **(b)** estimated loads at 35 psi inflation pressure for average applied load of about 1500 lbs and speed of 30 mph

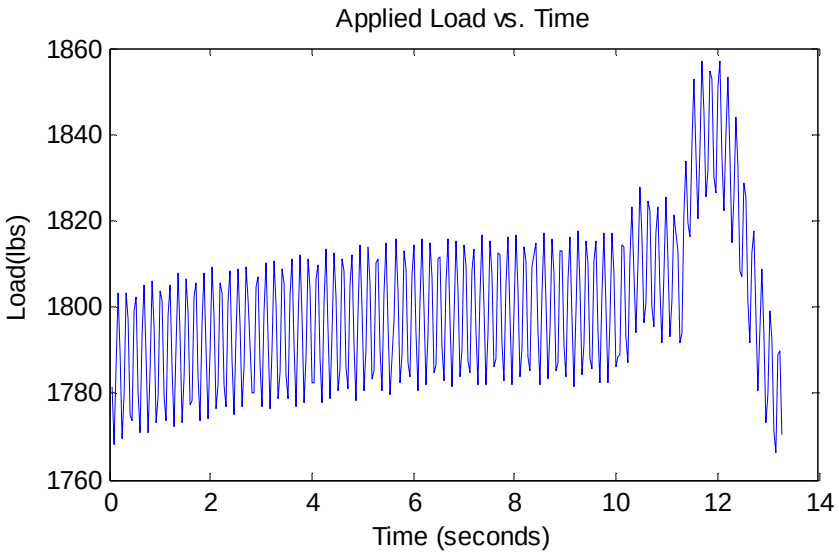

(a)

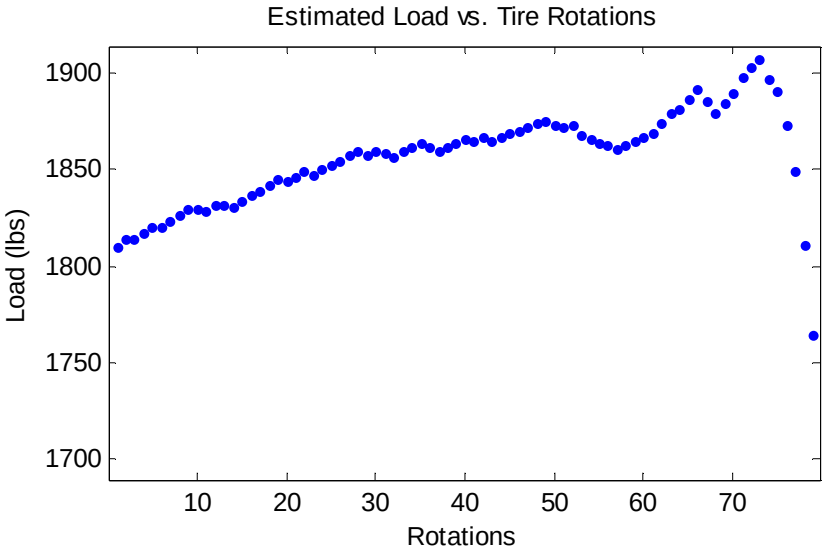

(b)

Figure 5.14. (a) Applied and **(b)** estimated loads at 35 psi inflation pressure for average applied load of about 1800 lbs and speed of 30 mph

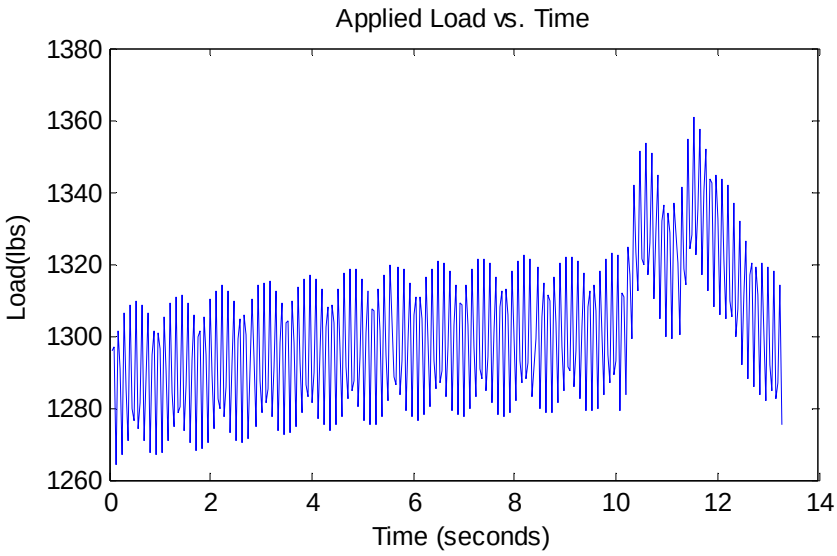

(a)

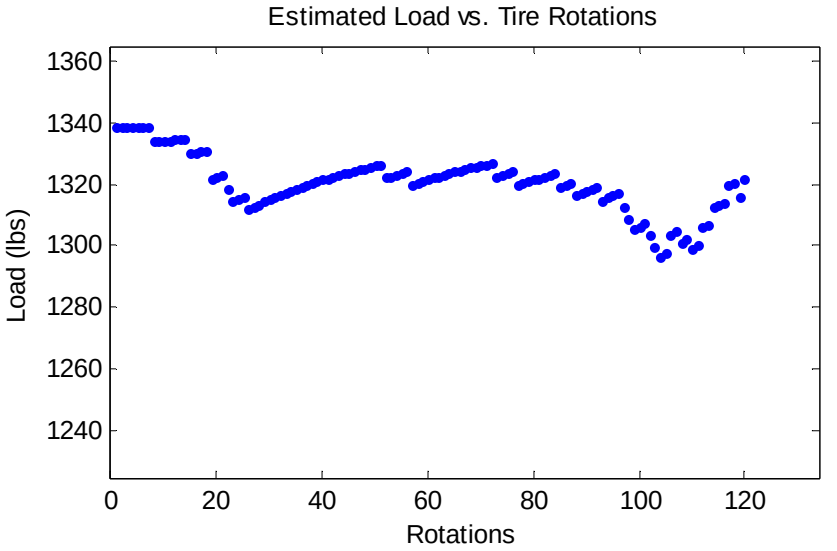

(b)

Figure 5.15. (a) Applied and **(b)** estimated loads at 35 psi inflation pressure for average applied load of about 1300 lbs and speed of 45 mph

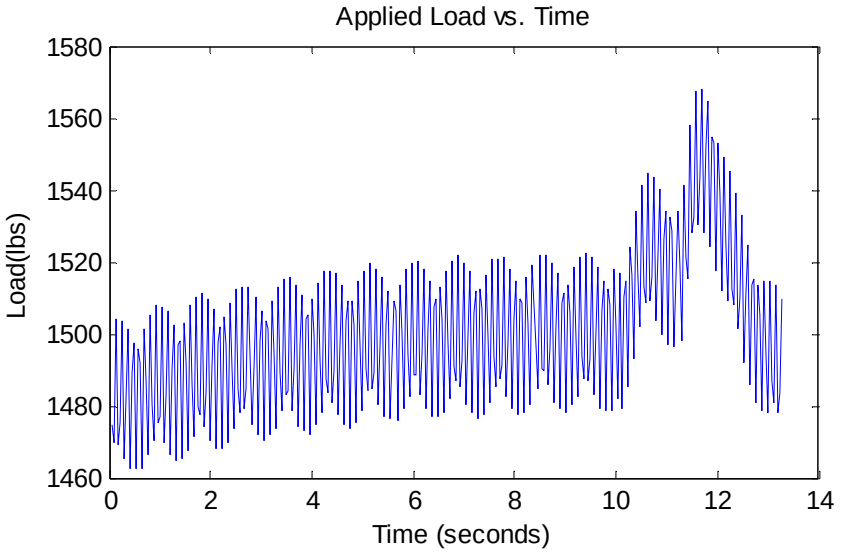

(a)

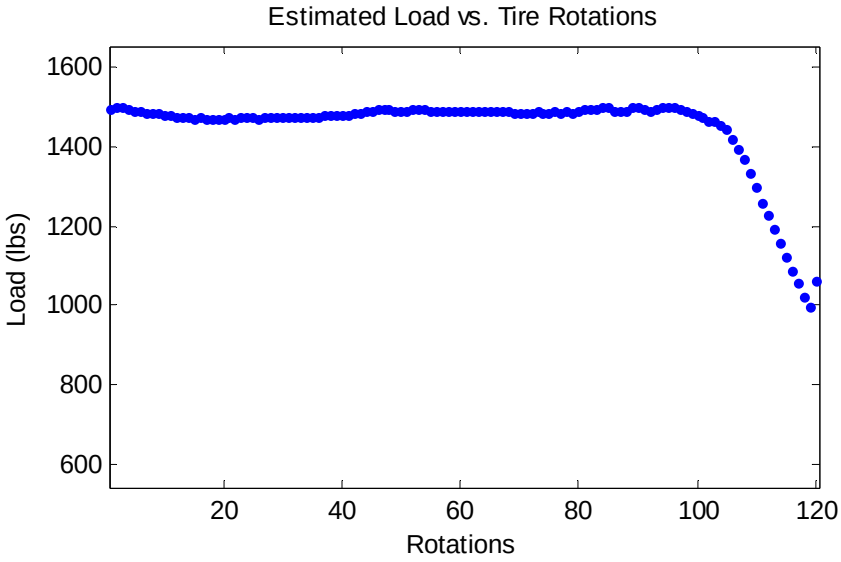

(b)

Figure 5.16. (a) Applied and **(b)** estimated loads at 35 psi inflation pressure for average applied load of about 1500 lbs and speed of 45 mph

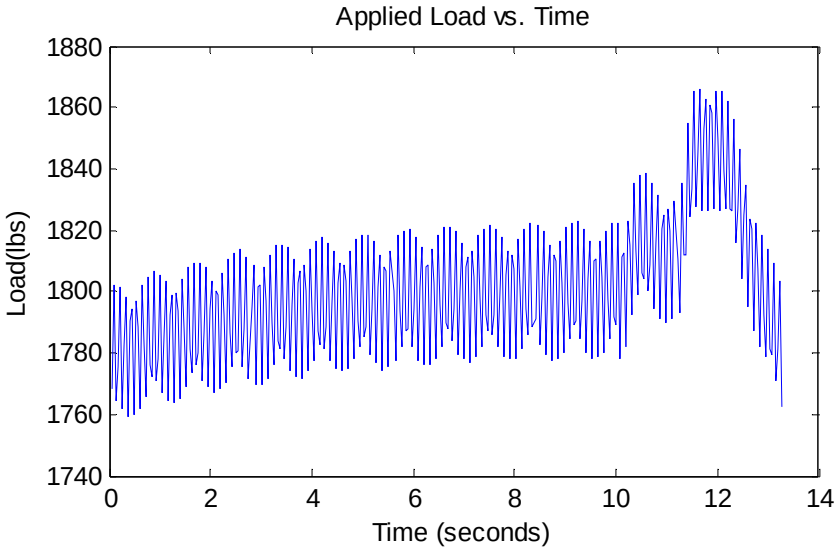

(a)

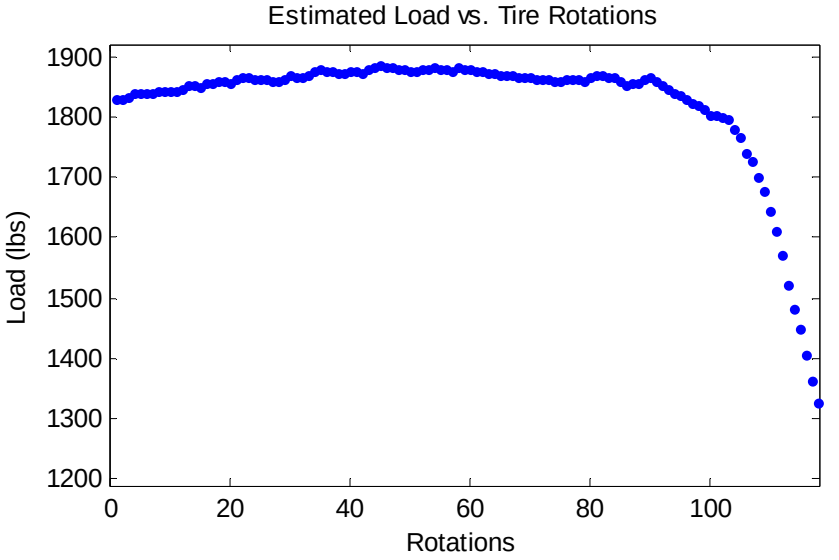

(b)

Figure 5.17. (a) Applied and **(b)** estimated loads at 35 psi inflation pressure for average applied load of about 1800 lbs and speed of 45 mph

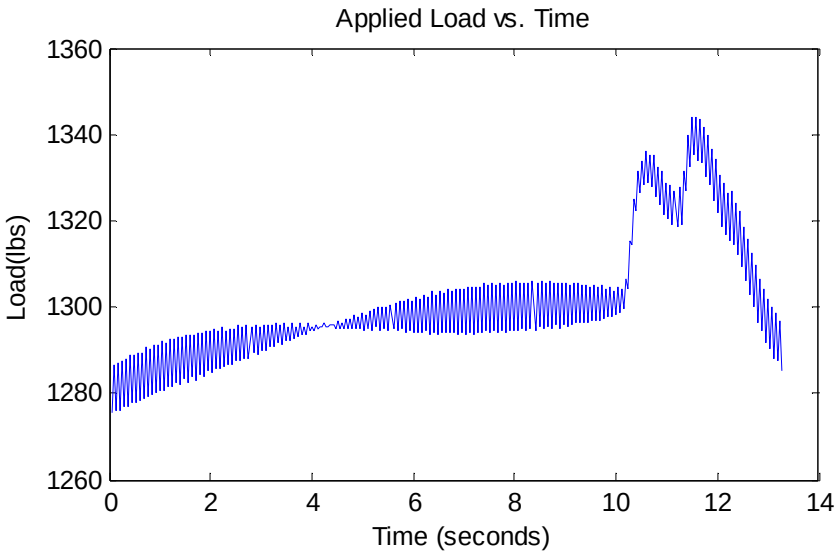

(a)

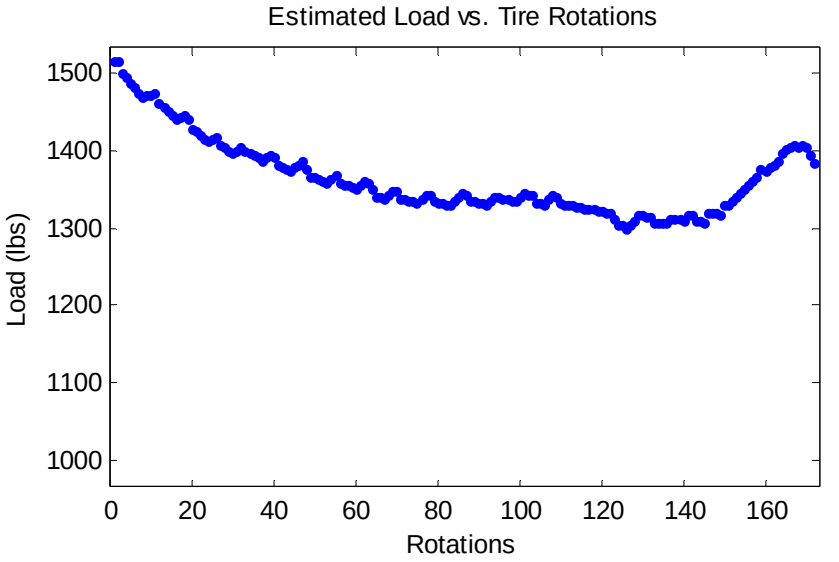

(b)

Figure 5.18. (a) Applied and **(b)** estimated loads at 35 psi inflation pressure for average applied load of about 1300 lbs and speed of 65 mph

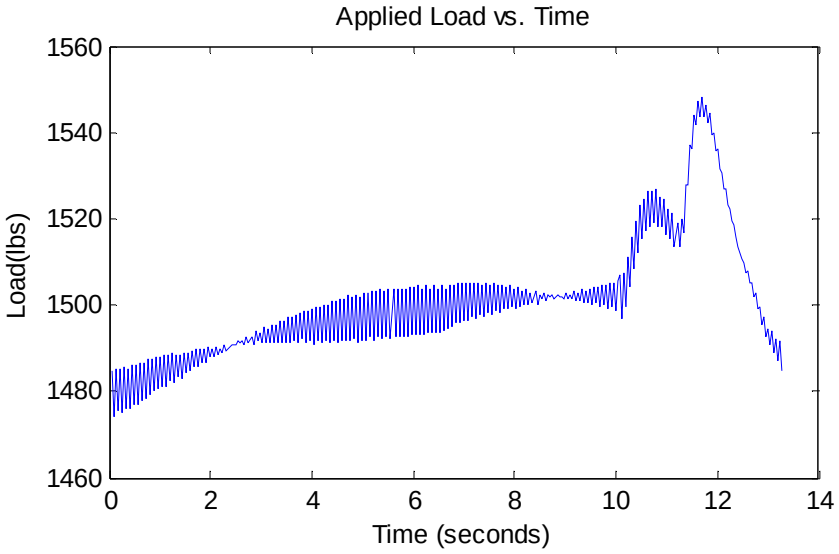

(a)

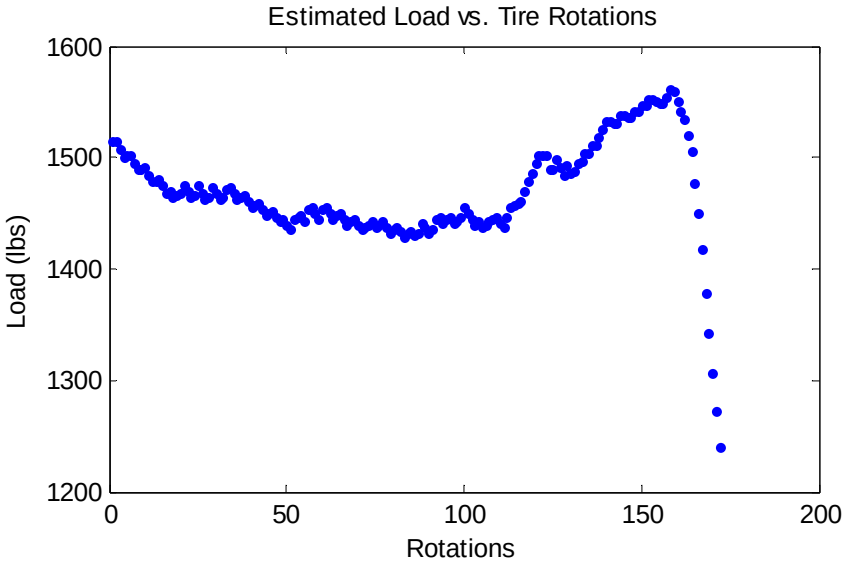

(b)

Figure 5.19. (a) Applied and **(b)** estimated loads at 35 psi inflation pressure for average applied load of about 1500 lbs and speed of 65 mph

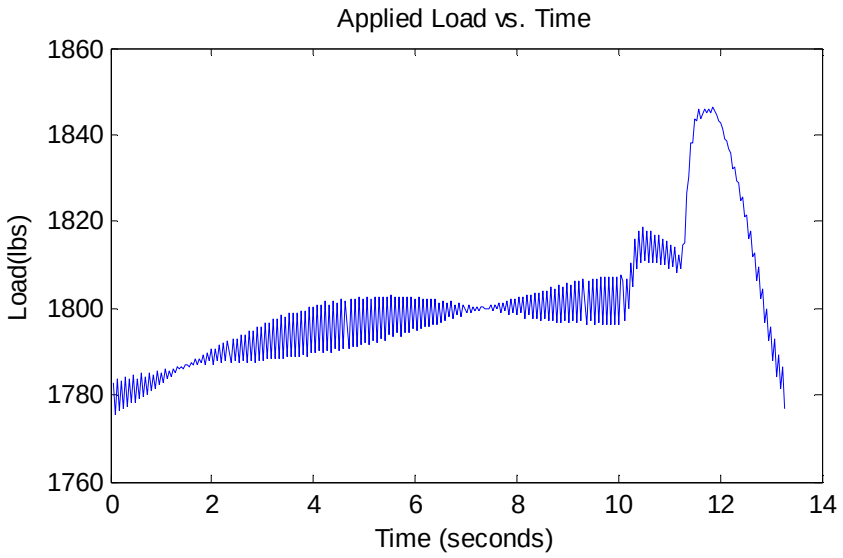

(a)

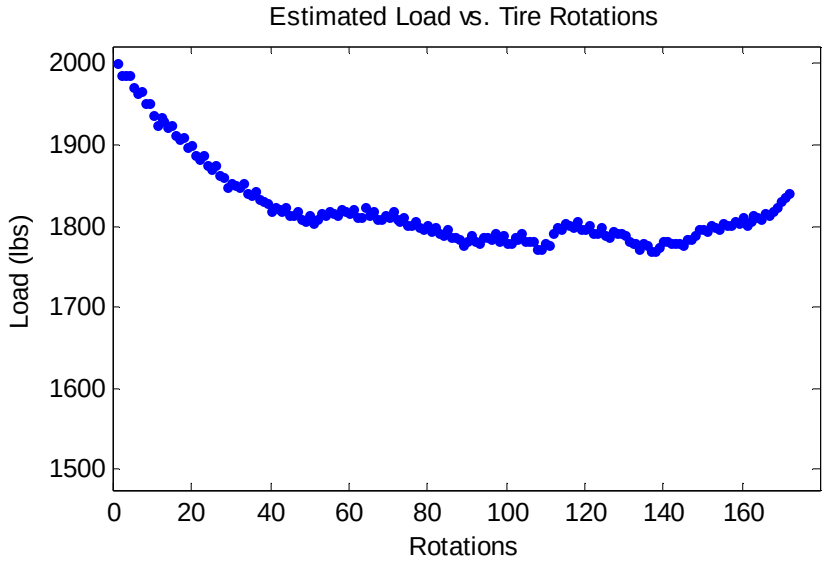

(b)

Figure 5.20. (a) Applied and **(b)** estimated loads at 35 psi inflation pressure for average applied load of about 1800 lbs and speed of 65 mph

5.6.2 Inflation Pressure of 32 psi

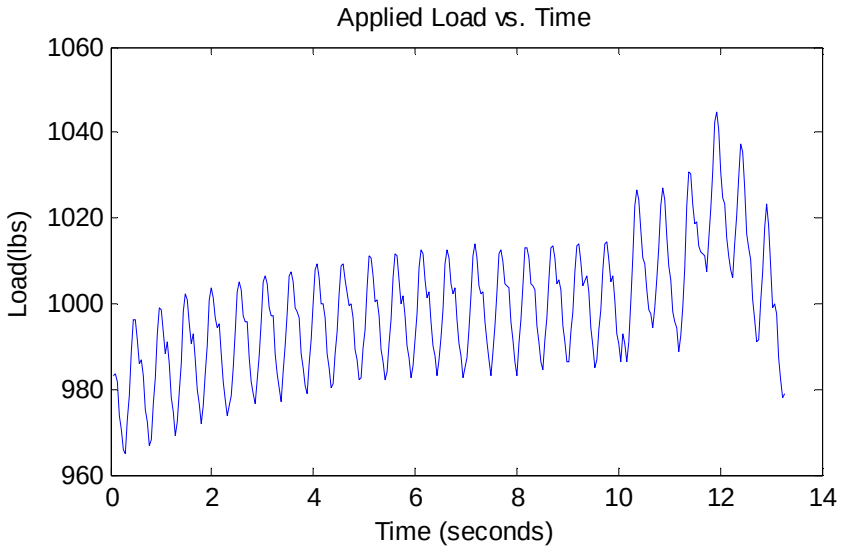

(a)

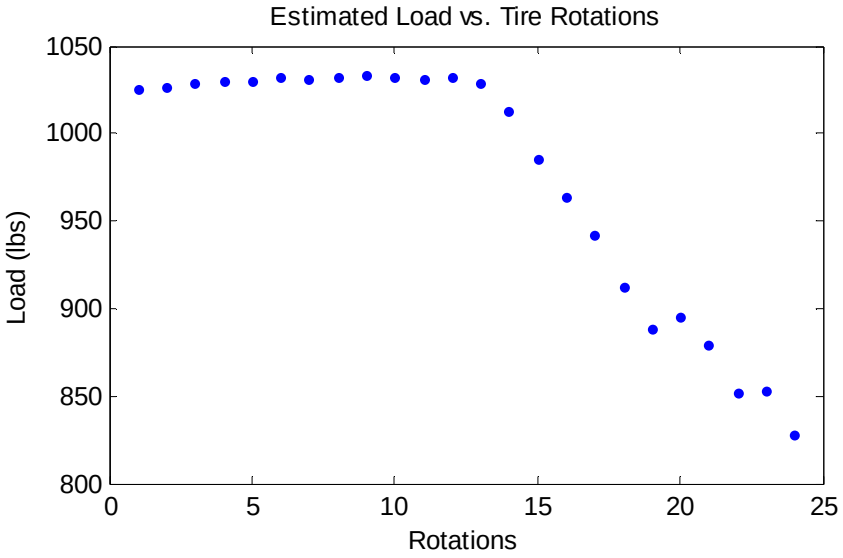

(b)

Figure 5.21. (a) Applied and **(b)** estimated loads at 32 psi inflation pressure for average applied load of about 1000 lbs and speed of 10 mph

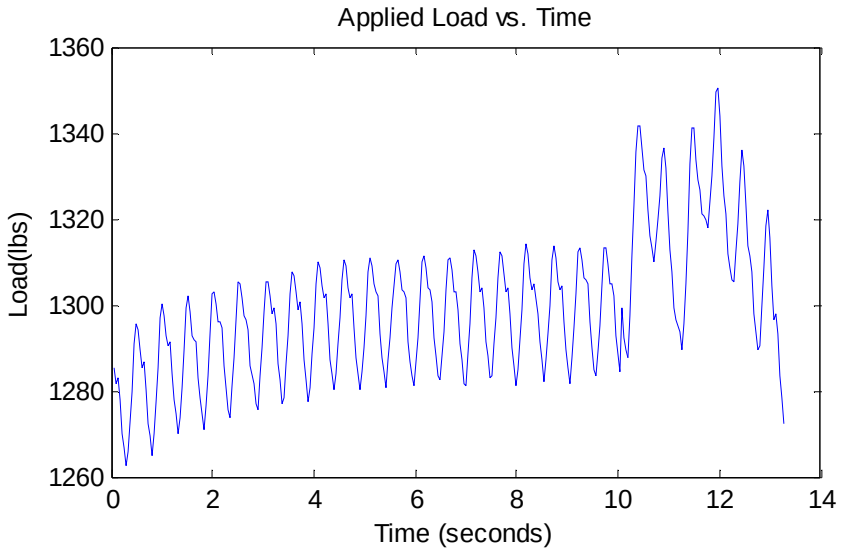

(a)

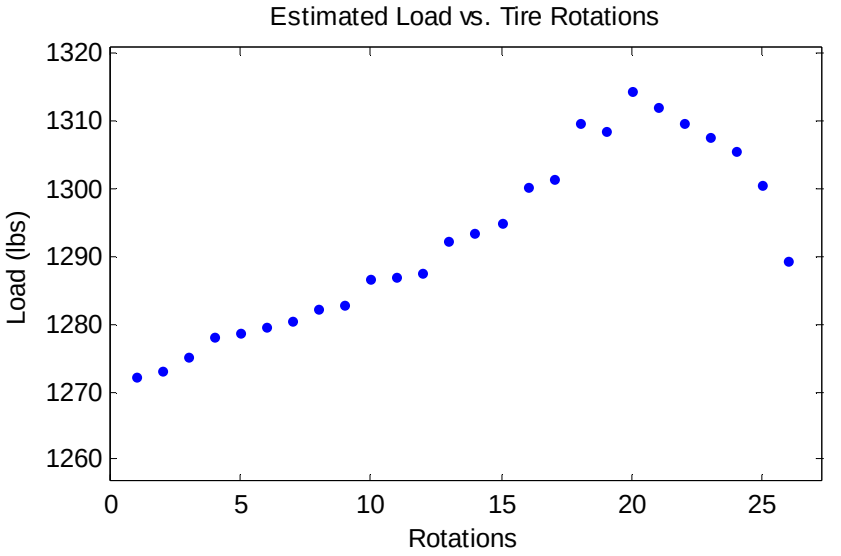

(b)

Figure 5.22. (a) Applied and **(b)** estimated loads at 32 psi inflation pressure for average applied load of about 1300 lbs and speed of 10 mph

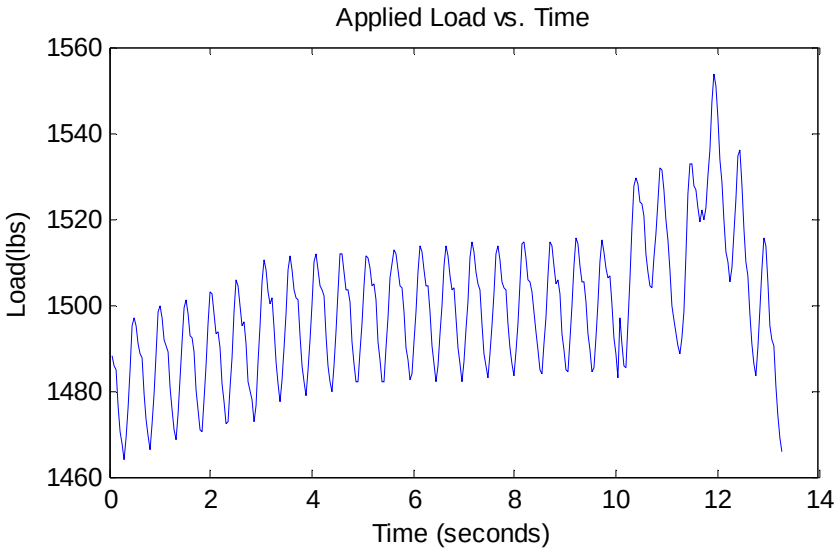

(a)

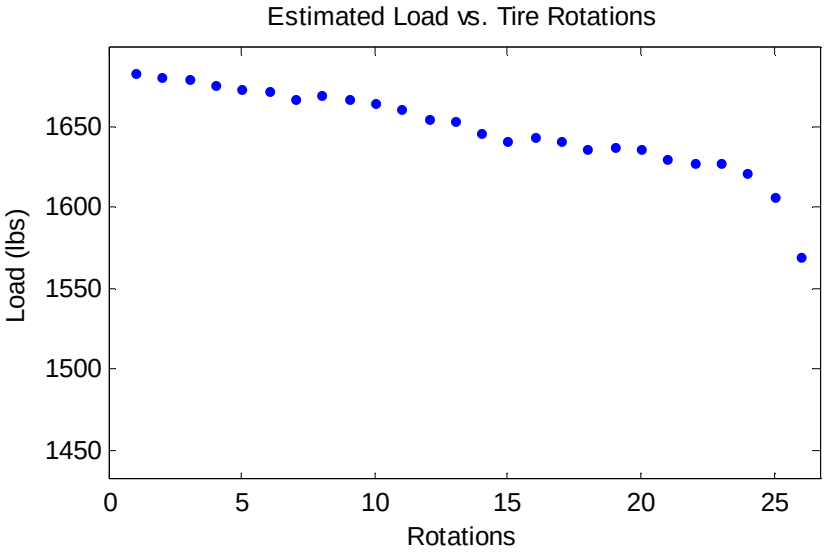

(b)

Figure 5.23. (a) Applied and **(b)** estimated loads at 32 psi inflation pressure for average applied load of about 1500 lbs and speed of 10 mph

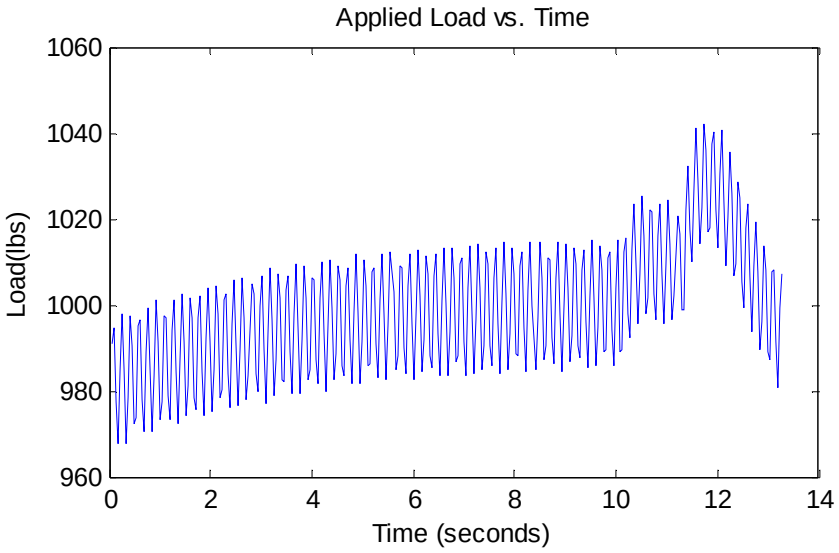

(a)

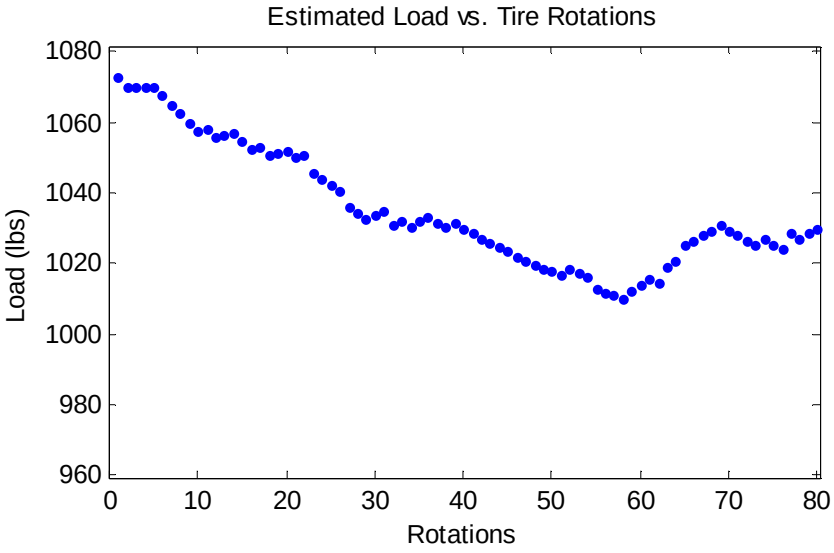

(b)

Figure 5.24. (a) Applied and **(b)** estimated loads at 32 psi inflation pressure for average applied load of about 1000 lbs and speed of 30 mph

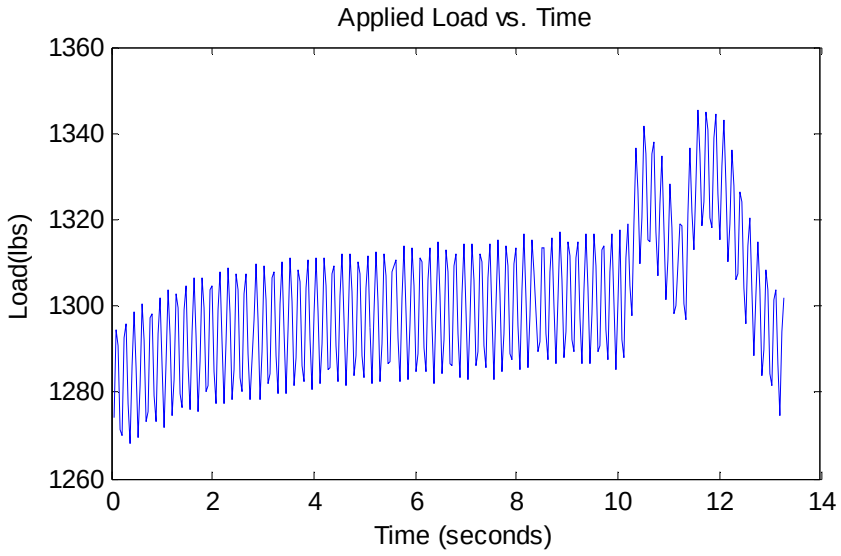

(a)

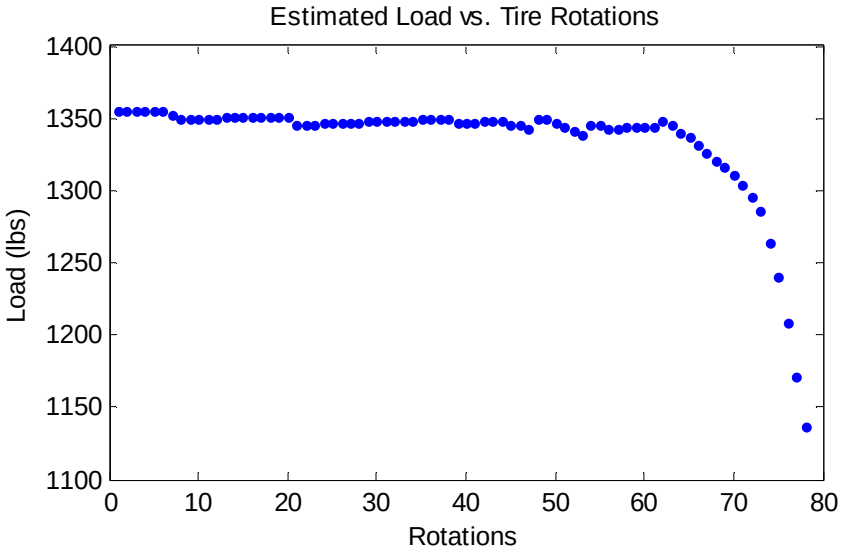

(b)

Figure 5.25. (a) Applied and **(b)** estimated loads at 32 psi inflation pressure for average applied load of about 1300 lbs and speed of 30 mph

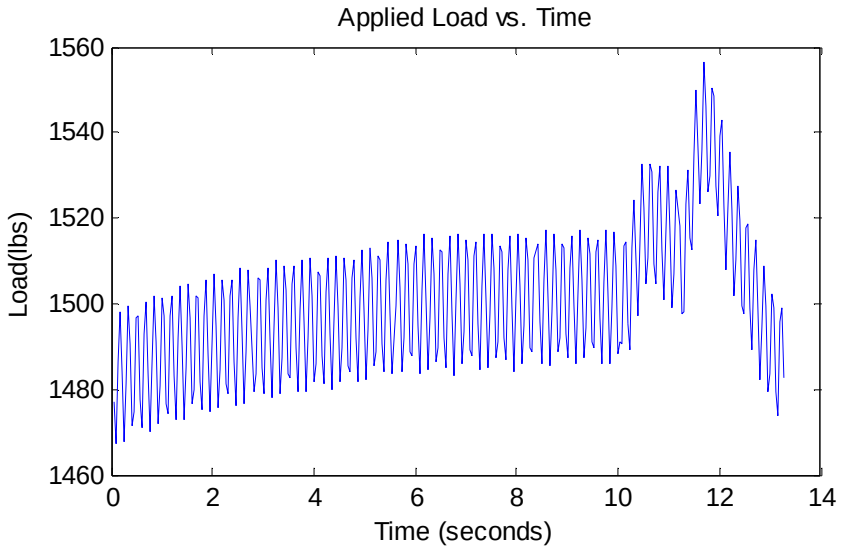

(a)

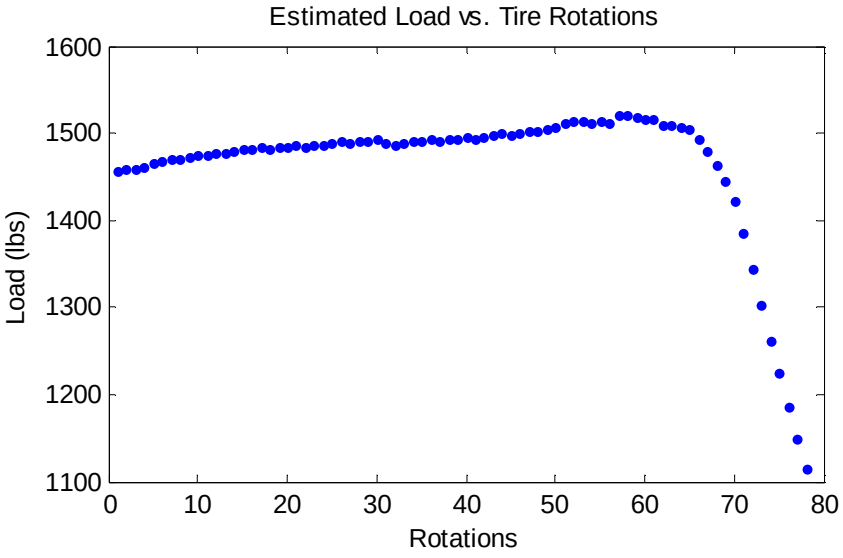

(b)

Figure 5.26. (a) Applied and **(b)** estimated loads at 32 psi inflation pressure for average applied load of about 1500 lbs and speed of 30 mph

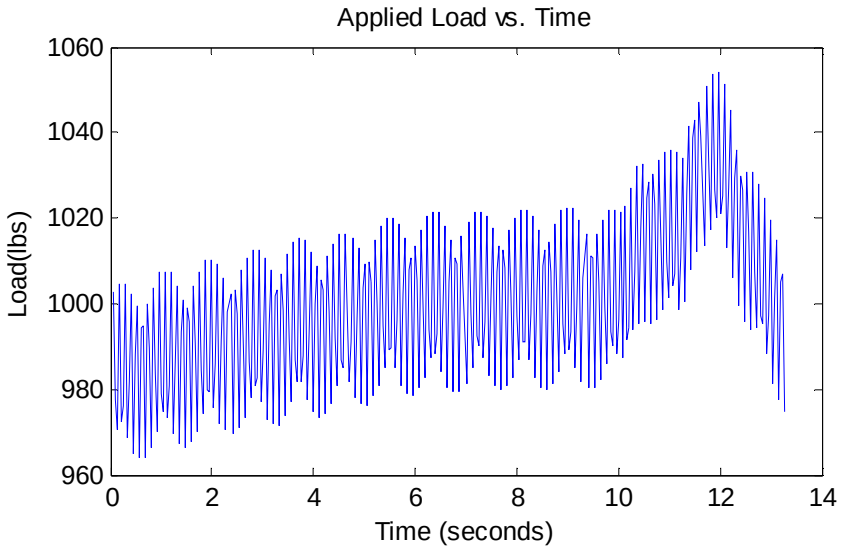

(a)

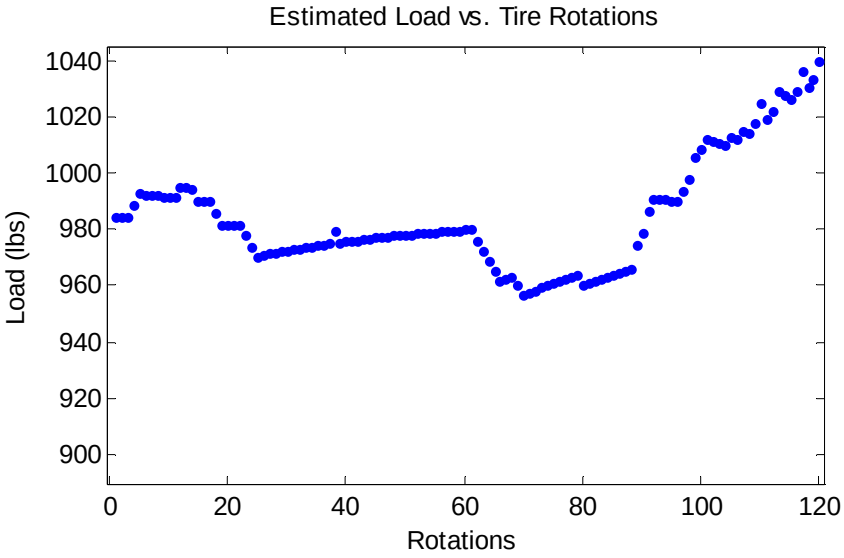

(b)

Figure 5.27. (a) Applied and **(b)** estimated loads at 32 psi inflation pressure for average applied load of about 1000 lbs and speed of 45 mph

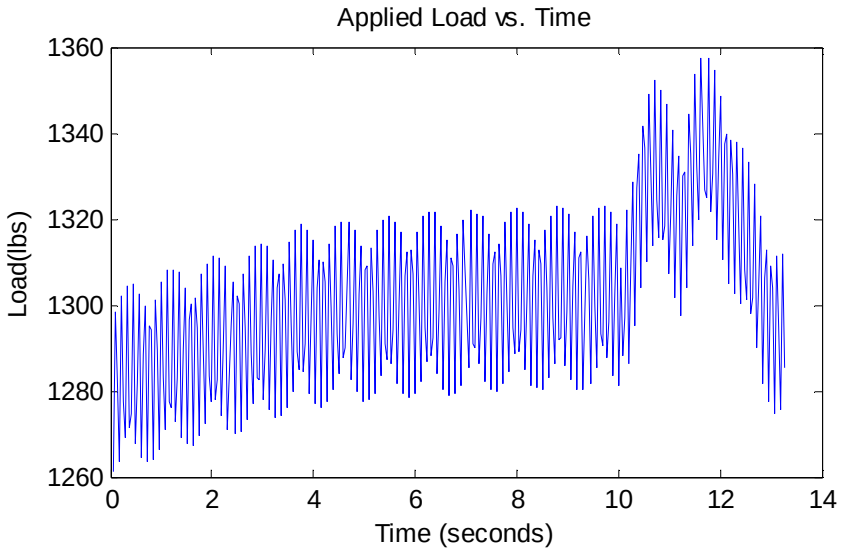

(a)

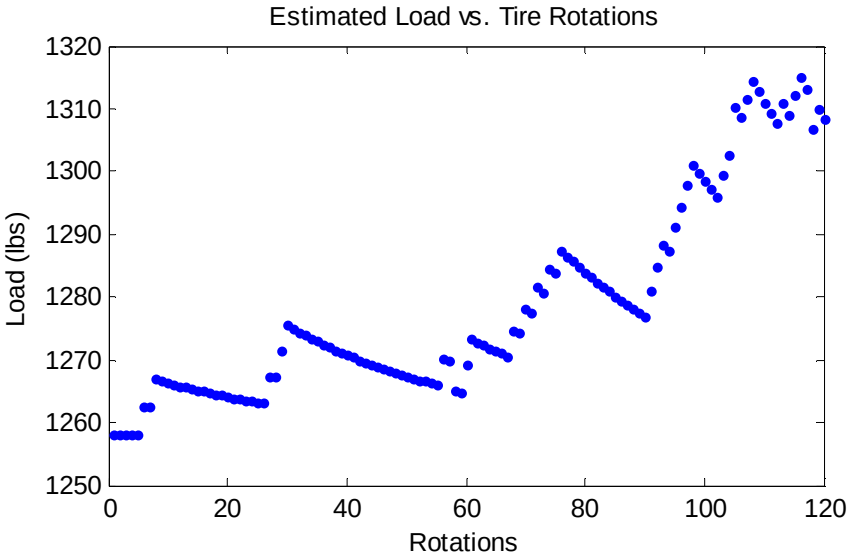

(b)

Figure 5.28. (a) Applied and **(b)** estimated loads at 32 psi inflation pressure for average applied load of about 1300 lbs and speed of 45 mph

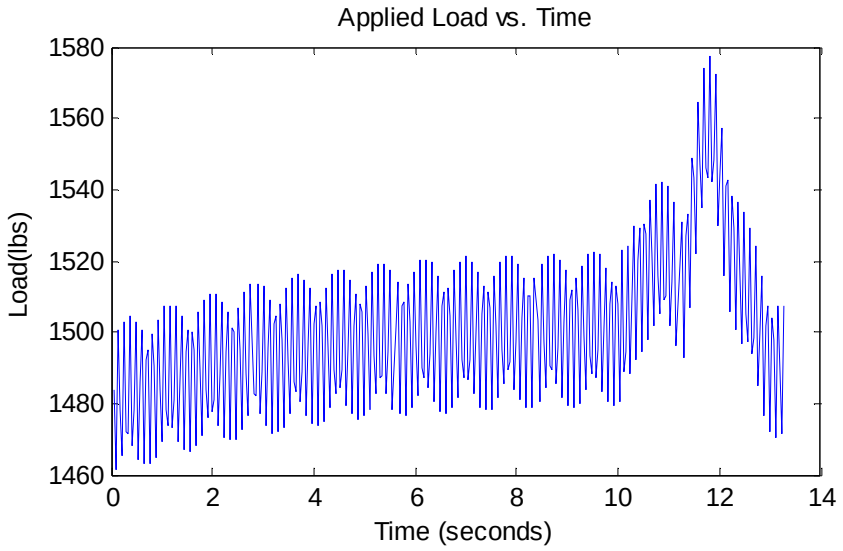

(a)

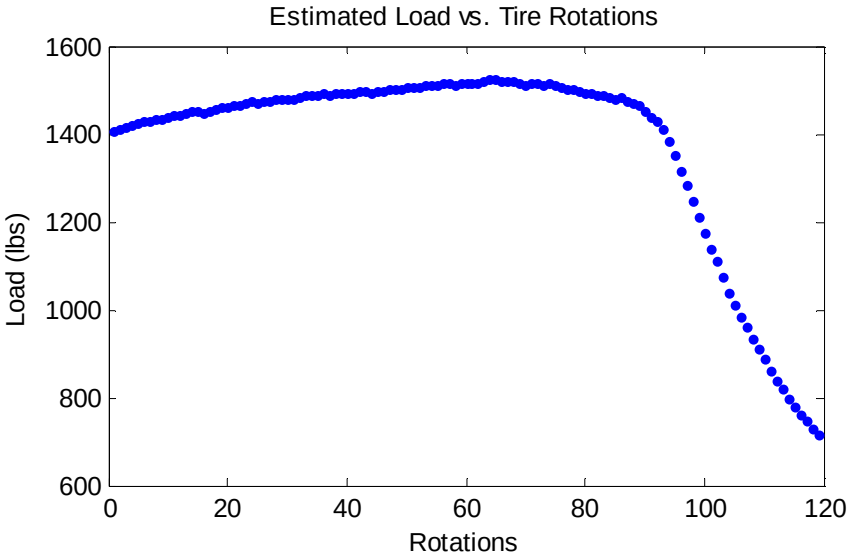

(b)

Figure 5.29. (a) Applied and **(b)** estimated loads at 32 psi inflation pressure for average applied load of about 1500 lbs and speed of 45 mph

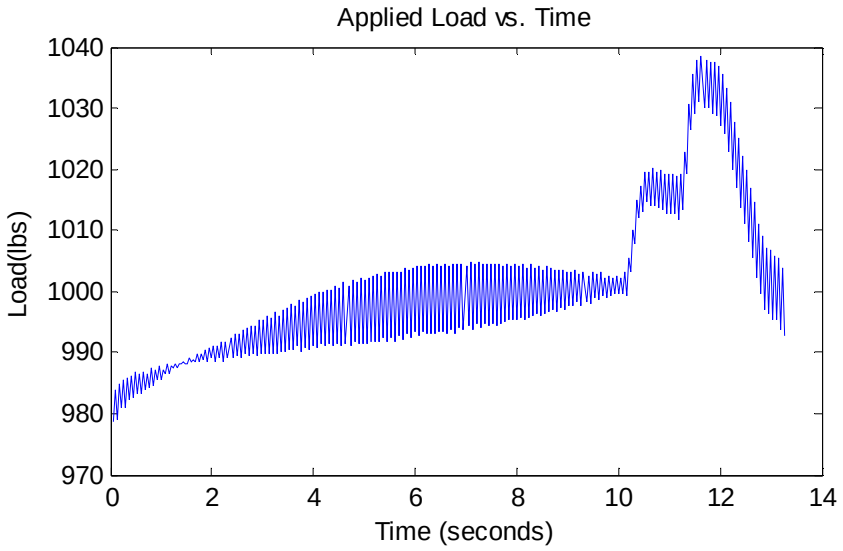

(a)

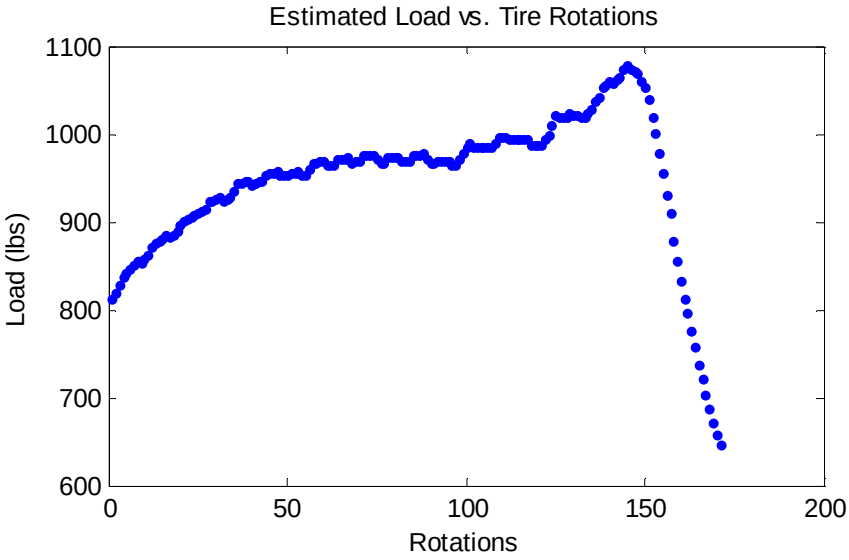

(b)

Figure 5.30. (a) Applied and **(b)** estimated loads at 32 psi inflation pressure for average applied load of about 1000 lbs and speed of 65 mph

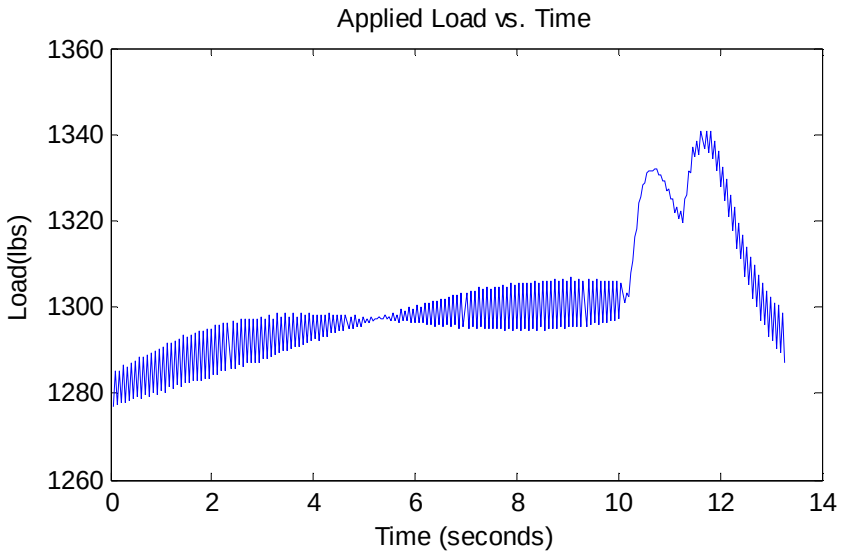

(a)

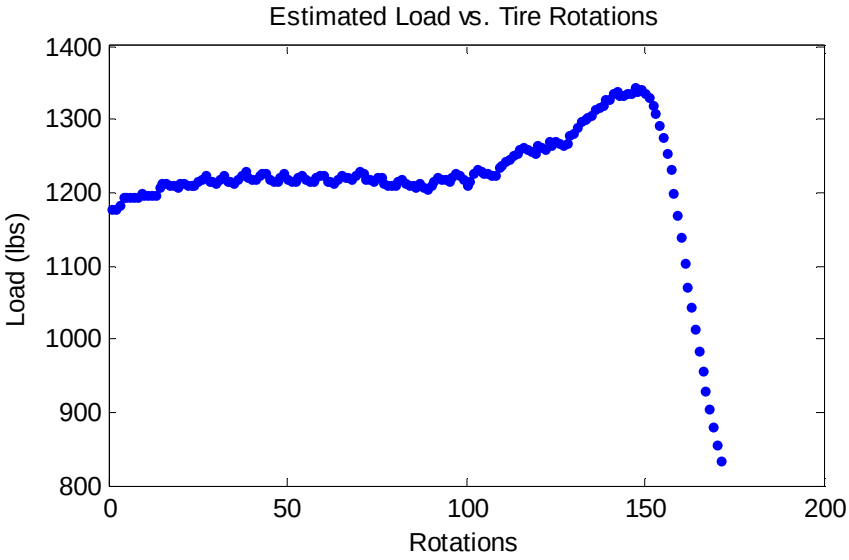

(b)

Figure 5.31. (a) Applied and **(b)** estimated loads at 32 psi inflation pressure for average applied load of about 1300 lbs and speed of 65 mph

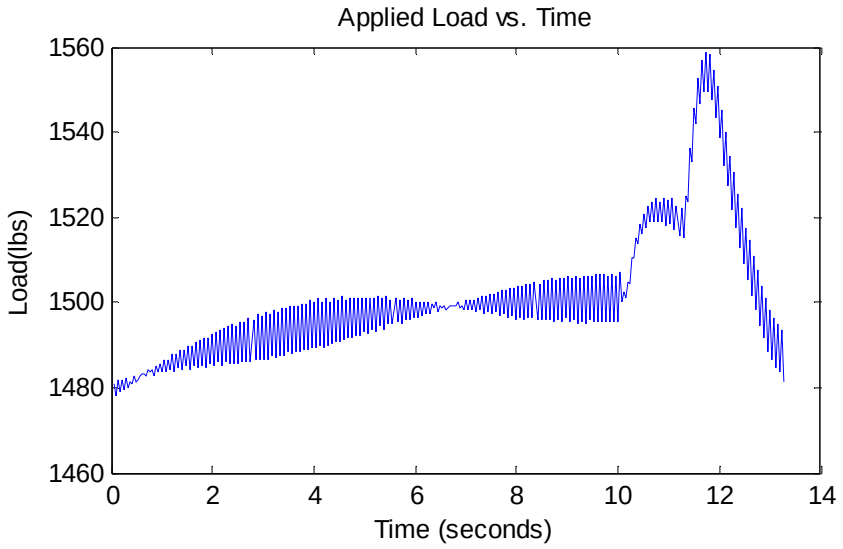

(a)

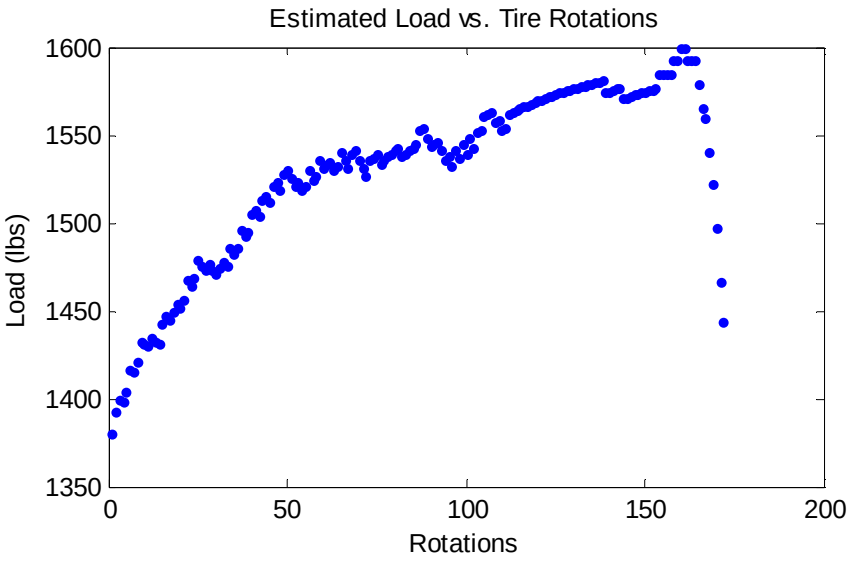

(b)

Figure 5.32. (a) Applied and **(b)** estimated loads at 32 psi inflation pressure for average applied load of about 1500 lbs and speed of 65 mph

5.6.3 Cambering

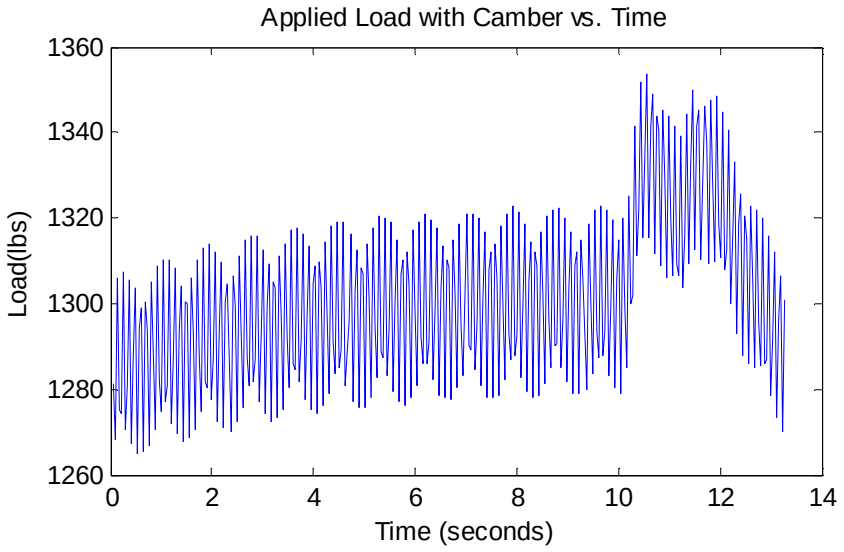

(a)

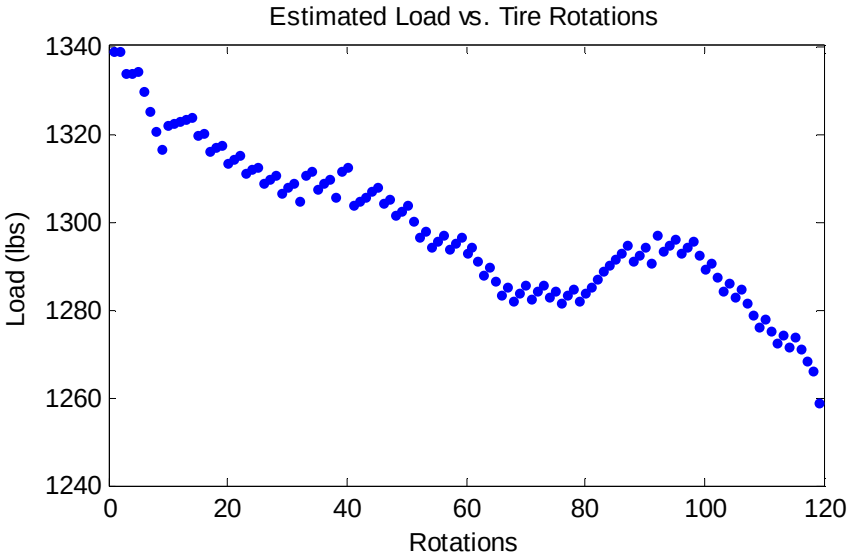

(b)

Figure 5.33. (a) Applied and **(b)** estimated loads at 35 psi inflation pressure for average applied load of about 1300 lbs and speed of 45 mph, with the wheel cambered at 2°

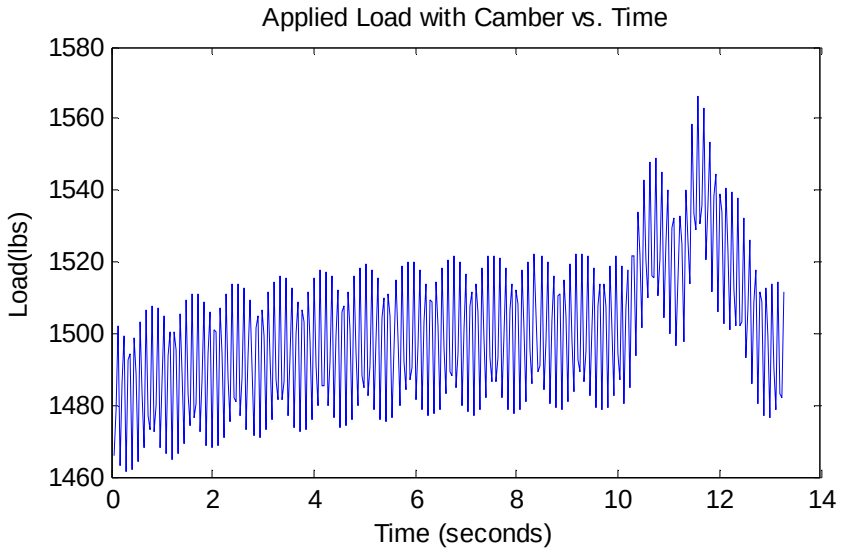

(a)

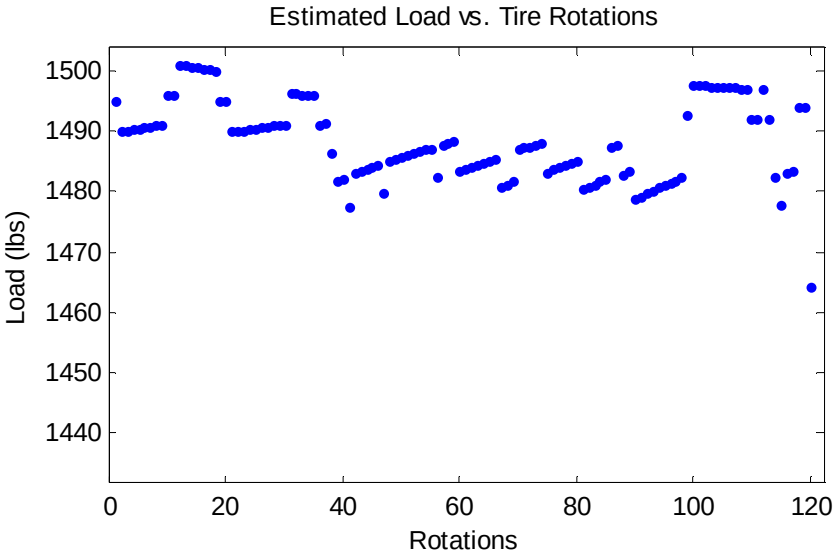

(b)

Figure 5.34. (a) Applied and **(b)** estimated loads at 35 psi inflation pressure for average applied load of about 1500 lbs and speed of 45 mph, with the wheel cambered at 2°

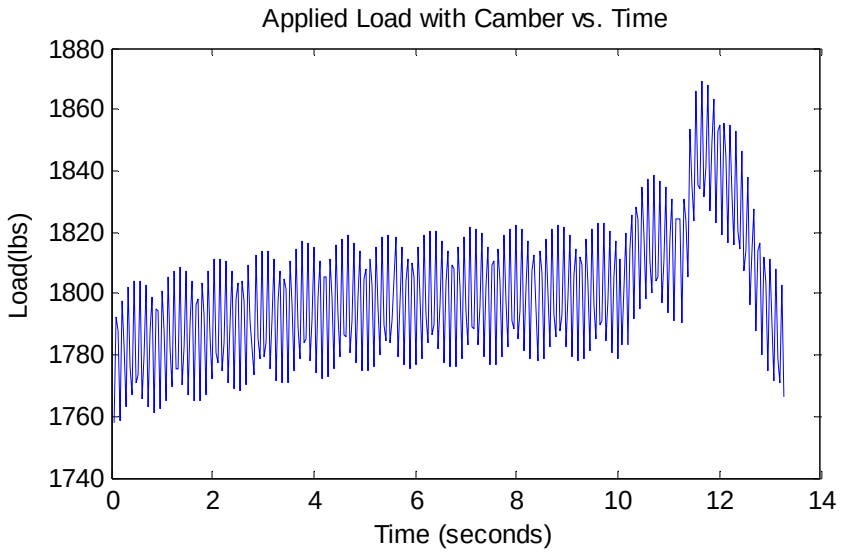

(a)

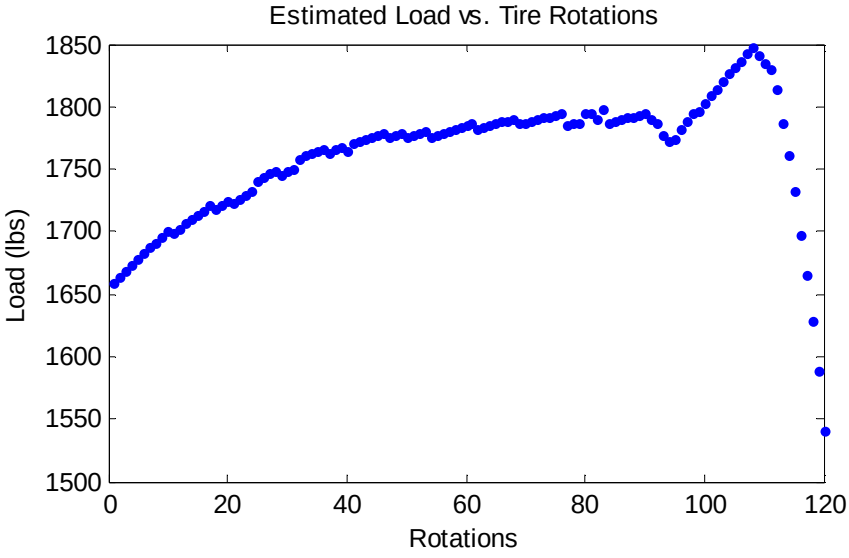

(b)

Figure 5.35. (a) Applied and **(b)** estimated loads at 35 psi inflation pressure for average applied load of about 1800 lbs and speed of 45 mph, with the wheel cambered at 2°

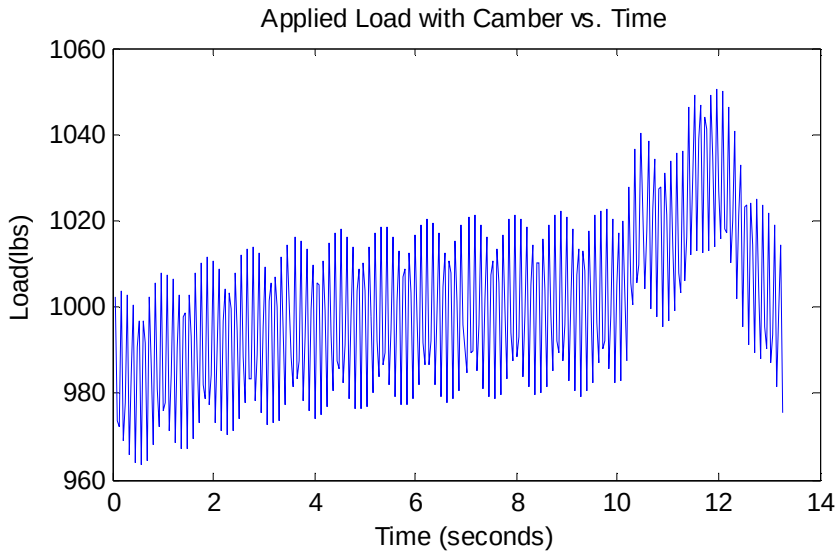

(a)

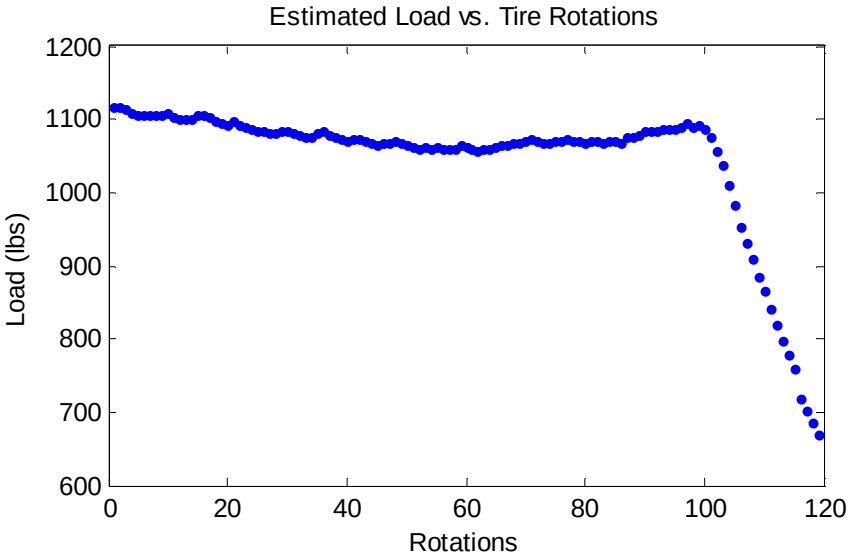

(b)

Figure 5.36. (a) Applied and **(b)** estimated loads at 32 psi inflation pressure for average applied load of about 1000 lbs and speed of 45 mph, with the wheel cambered at 2°

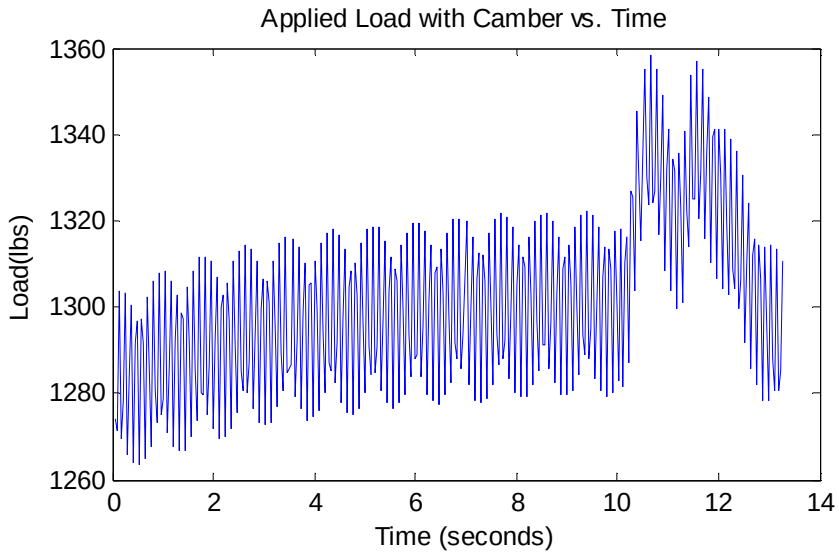

(a)

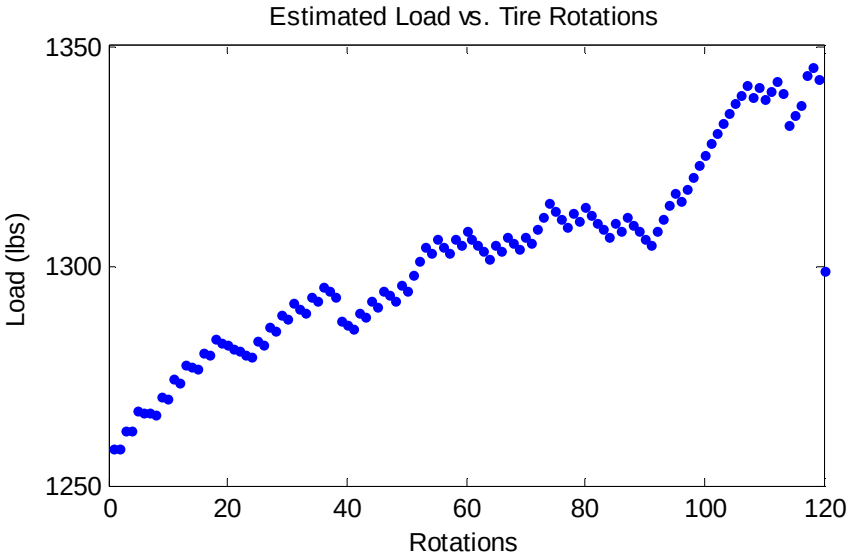

(b)

Figure 5.37. (a) Applied and **(b)** estimated loads at 32 psi inflation pressure for average applied load of about 1300 lbs and speed of 45 mph, with the wheel cambered at 2°

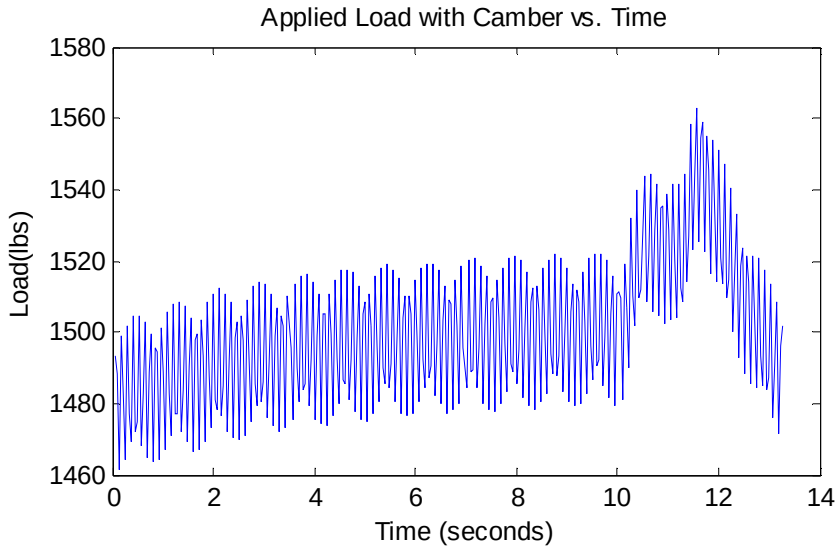

(a)

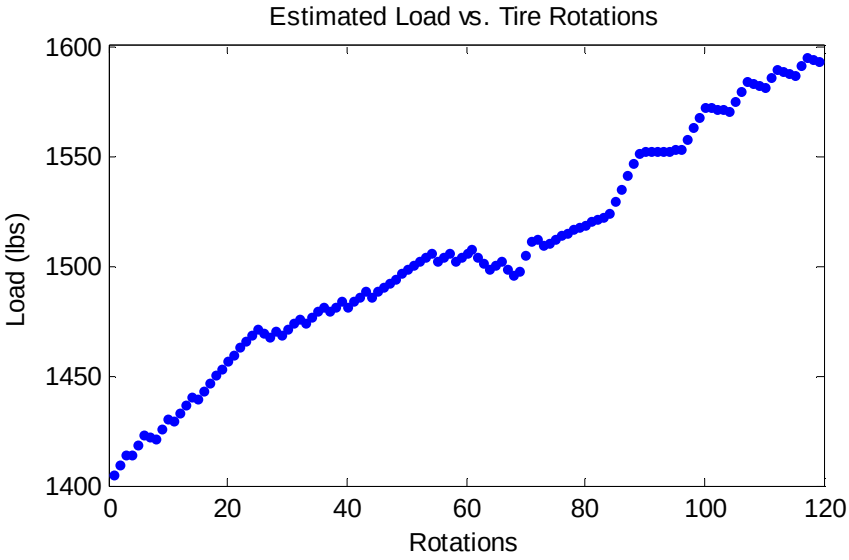

(b)

Figure 5.38. (a) Applied and **(b)** estimated loads at 32 psi inflation pressure for average applied load of about 1500 lbs and speed of 45 mph, with the wheel cambered at 2°

5.7 Summary

The methodology used to test the tire on a flat track machine at the Goodyear Innovation center was explained. This included a description of the loads, speeds, slip angles and the camber that the tire-wheel assembly was subjected to during the tests.

The algorithm developed in chapter 4 was used on the test data gathered on the flat track machine. The resulting estimates were found to be unsatisfactory, leading to modifications in the algorithm. An explanation for the estimates in load variation was provided and this led to the revised version of the algorithm that incorporated Kalman filtering to smooth the estimates. A linear filter cut-off frequency versus speed relationship was established. The filtered signal was used in detecting patch length, instead of using the raw signal as in chapter 4. A different equation was used to estimate load, as was a speed-dependent multiplicative factor *a*.

It was shown, by suitable plots, that the introduction of the Kalman filter has improved the estimates for the patch length, from the previous algorithm which did not use the filter. By properly weighting the estimate for a given cycle, based on the estimate from the previous cycle, the fluctuations have been smoothened out.

The process noise tolerance is low. It has been assumed that the noise variance is very low, of the order less than 0.01. This is a favorable assumption for a flat-track test where the surface on which the tire is running is fairly smooth. Experimenting on road will introduce more noise. More experiments have to be carried out to check what kind of changes need to be made.

6. Developing a Control Strategy

This chapter explains the development of a control algorithm that helps maintain a desired yaw rate for a vehicle.

6.1 Bicycle Model

As mentioned in section 2.3, the control strategy revolves around using a two degree of freedom 'bicycle' model to represent a vehicle and develop a control strategy based on the data from the tire. The model is restated here.

$$\begin{bmatrix} m & 0 \\ 0 & I_z \end{bmatrix} \begin{pmatrix} \dot{v} \\ \dot{r} \end{pmatrix} - \begin{bmatrix} -\dfrac{C_{\alpha f} + C_{\alpha r}}{u} & -mu + \dfrac{bC_{\alpha f} - aC_{\alpha r}}{u} \\ \dfrac{bC_{\alpha r} + aC_{\alpha f}}{u} & -\dfrac{b^2 C_{\alpha r} + a^2 C_{\alpha r}}{u} \end{bmatrix} \begin{pmatrix} v \\ r \end{pmatrix} - \begin{bmatrix} C_{\alpha f} \\ aC_{\alpha f} \end{bmatrix} (\delta_f) = 0 \qquad (6.1)$$

Most control algorithms rely on an estimate of the cornering stiffness [21] from a theoretical model to perform yaw rate control. The algorithm developed in section 5.5 shows how the load can be estimated; by using the Magic Tire Formula model, the lateral force can be calculated (equation 2.4). The values of the slip angles for front and rear tires calculated from equations 2.5 and 2.6 can be used in conjunction with the lateral force estimate to obtain the cornering stiffness (equations 2.8 and 2.9). Hence the vehicle stability control is based directly on the factors affecting a tire in motion i.e. the cornering stiffness values can be found from actual tire data and not from a model.

NOTE: The cornering stiffness values $C_{\alpha f}$ and $C_{\alpha r}$ will ideally be supplied by the load estimates from section 5.5. However, the values used in simulations in this chapter are not calculated from the loads shown in section 5.5, as the Pacejka coefficients required are not available for the particular tire under test. Also, there is no vehicle characteristics involved because only a single tire was tested. The values used in the simulations below are those supplied by the manufacturer.

6.2 Uncontrolled System

First, the uncontrolled system is simulated with parameters from an existing road going car.

m = 1418 Kg

I_z = 1819

$C_{\alpha f}$ = peak of 112000 N/deg

$C_{\alpha r}$ = peak of 84000 N/deg

u = 80 Km/h

l_f = 1.012 m

l_r = 1.568 m

It is assumed that the driver applies a steering input of 80° at the steering wheel; this translates to a steering input at the wheels of the car (with a steering ratio of 19.5) as δ_f = 4.1026 degrees/s. Simulating the system with these parameters, we get the plot of figure 6.1.

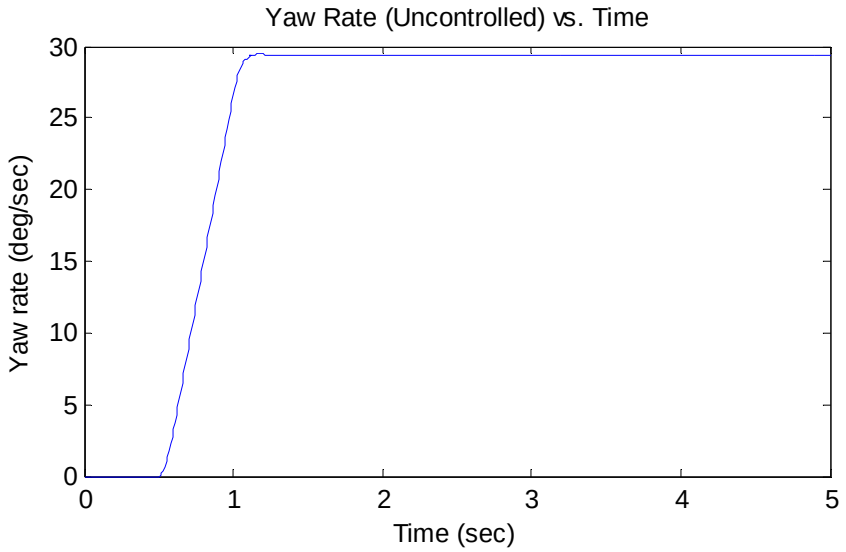

Figure 6.1. Uncontrolled yaw rate

The yaw rate shoots up to a large value (without feedback control). This is unacceptable as the vehicle will veer out of control at such a large yaw rate. We need to use feedback control to stabilize the vehicle.

6.3 Introducing a Controller

The steering input angle at the wheel (δ_f) is expressed as a sum of the driver steering input angle (δ_{fd}) and a controller steering input angle (δ_{fc}). δ_{fc} is the steering input at the wheels to be provided by the controller, in addition to the driver input.

$$\begin{bmatrix} m & 0 \\ 0 & I_z \end{bmatrix} \begin{pmatrix} \dot{v} \\ \dot{r} \end{pmatrix} - \begin{bmatrix} -\frac{C_{\alpha f} + C_{\alpha r}}{u} & -mu + \frac{bC_{\alpha f} - aC_{\alpha r}}{u} \\ \frac{bC_{\alpha r} + aC_{\alpha f}}{u} & -\frac{b^2 C_{\alpha r} + a^2 C_{\alpha r}}{u} \end{bmatrix} \begin{pmatrix} v \\ r \end{pmatrix} - \begin{bmatrix} C_{\alpha f} \\ aC_{\alpha f} \end{bmatrix} (\delta_{fd} + \delta_{fc}) = 0 \qquad (6.2)$$

In order to control the yaw rate, an additional term is introduced on the right hand side of the equation as shown. This reduces the system to being dependent on the controller input alone.

$$\begin{bmatrix} m & 0 \\ 0 & I_z \end{bmatrix} \begin{pmatrix} \dot{v} \\ \dot{r} \end{pmatrix} - \begin{bmatrix} -\frac{C_{\alpha f} + C_{\alpha r}}{u} & -mu + \frac{bC_{\alpha f} - aC_{\alpha r}}{u} \\ \frac{bC_{\alpha r} + aC_{\alpha f}}{u} & -\frac{b^2 C_{\alpha r} + a^2 C_{\alpha r}}{u} \end{bmatrix} \begin{pmatrix} v \\ r \end{pmatrix} - \begin{bmatrix} C_{\alpha f} \\ aC_{\alpha f} \end{bmatrix} (\delta_{fd} + \delta_{fc}) = - \begin{bmatrix} C_{\alpha f} \\ aC_{\alpha f} \end{bmatrix} (\delta_{fd})$$

..(6.3)

This can be rewritten as

$$\begin{bmatrix} m & 0 \\ 0 & I_z \end{bmatrix} \begin{pmatrix} \dot{v} \\ \dot{r} \end{pmatrix} - \begin{bmatrix} -\frac{C_{\alpha f} + C_{\alpha r}}{u} & -mu + \frac{bC_{\alpha f} - aC_{\alpha r}}{u} \\ \frac{bC_{\alpha r} + aC_{\alpha f}}{u} & -\frac{b^2 C_{\alpha r} + a^2 C_{\alpha r}}{u} \end{bmatrix} \begin{pmatrix} v \\ r \end{pmatrix} - \begin{bmatrix} C_{\alpha f} \\ aC_{\alpha f} \end{bmatrix} (\delta_{fc}) = 0 \qquad (6.4)$$

Rewriting the equation 6.3, we get the following.

$$\begin{pmatrix} \dot{v} \\ \dot{r} \end{pmatrix} = \begin{bmatrix} m & 0 \\ 0 & I_z \end{bmatrix}^{-1} \begin{bmatrix} -\frac{C_{\alpha f} + C_{\alpha r}}{u} & -mu + \frac{bC_{\alpha f} - aC_{\alpha r}}{u} \\ \frac{bC_{\alpha r} + aC_{\alpha f}}{u} & -\frac{b^2 C_{\alpha r} + a^2 C_{\alpha r}}{u} \end{bmatrix} \begin{pmatrix} v \\ r \end{pmatrix} + \begin{bmatrix} m & 0 \\ 0 & I_z \end{bmatrix}^{-1} \begin{bmatrix} C_{\alpha f} \\ aC_{\alpha f} \end{bmatrix} (\delta_{fc}) \qquad (6.5)$$

In the state space form, this is

$$\dot{x} = Ax + Bu \qquad (6.6)$$

Note: $\begin{bmatrix} m & 0 \\ 0 & I_z \end{bmatrix}$ is invertible because m and I_z are non-zero.

The problem has reduced to supplying a control input u (i.e. δ_{fc}) to maintain the yaw rate r at a desired value. For this thesis, the controller was designed to be a linear quadratic regulator (LQR). The problem is treated as a linear quadratic (LQ) optimal control problem where the state of the system has to follow a desired output, in this case the desired yaw rate.

6.4 Linear Quadratic Optimal Output tracking

According to [22] and [23], for a linear system represented by

$$\begin{aligned} \dot{x} &= Ax + Bu \\ y &= Cx \end{aligned} \tag{6.7}$$

that has to follow a desired output $y_d(t)$, a performance index of the following type can be considered.

$$\int_0^T (y - y_d)^T C^T Q_1 C(x - x_d) + \bar{x}^T Q_2 \bar{x} + u^T R u \, d\tau \tag{6.8}$$

C has full row rank. Q_1 and Q_2 are positive semi definite ($Q_1 \geq 0$, $Q_2 \geq 0$) and R is positive definite ($R > 0$).

$$\bar{x} = (1 - C^{\dagger}C)x \tag{6.9}$$

$C^{\dagger}$ is the Moore-Penrose pseudo inverse.

As shown in [22], the control law for this system is

$$u(t) = -R^{-1}B^T P(t)x(t) - R^{-1}B^T b(t) \tag{6.10}$$

where $b(t)$ is the solution to

$$\dot{b} = -(A - BR^{-1}B^T P)^T b + QC^{+}y_d, \qquad b(T) = 0 \tag{6.11}$$

This can be represented by the following block diagram:

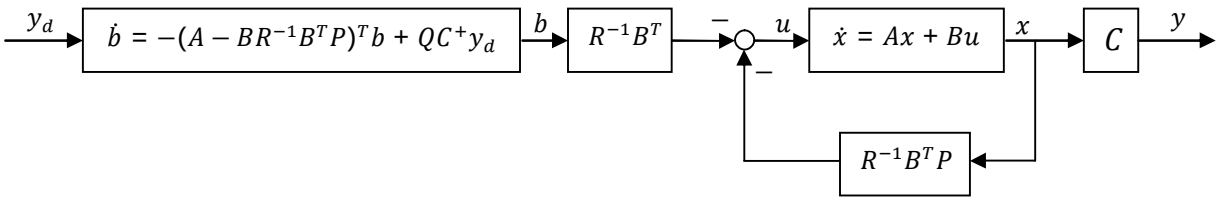

Figure 6.2. Output tracking block diagram

6.5 Practical Implementation

Assume the same system simulated in section 6.2, but this time, the controller is implemented using state feedback (with LQR). The first step is to determine the desired yaw rate. The driver input of 80 degrees at the steering wheel translates to a steering input at the wheel given by

$$\delta_f = \frac{\delta}{steering\ ratio} \tag{6.12}$$

Knowing this input at the wheel, the desired yaw rate is calculated according to equation 2.11. The yaw rate rises from zero to the maximum value in a finite time, assumed to be 0.5 seconds. This desired yaw rate is a reference input to the system (figure 6.3).

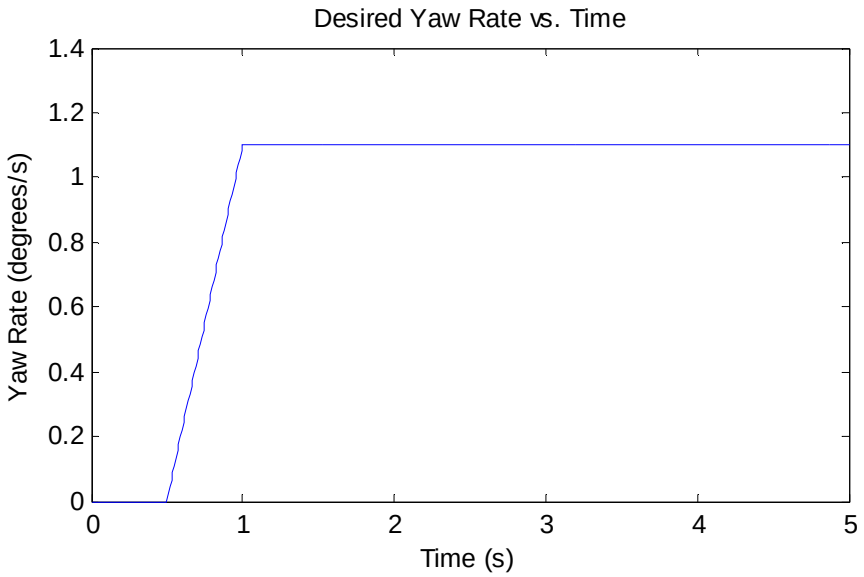

Figure 6.3. Desired yaw rate

As the yaw rate increases and levels off, so do the cornering stiffness values of the front and rear tires.

The penalty matrices Q_1 and R in equation 6.7 have to be chosen (Q_2 was taken to be 0). A trial and error approach was undertaken to settle on the values of Q_1 and R producing the most suitable response. The values of Q_1 and R were chosen to be 1 and 0.4 respectively.

The system was simulated using a combination of Matlab and Simulink. The following plots show how the desired and controlled yaw rates vary as the control input is applied.

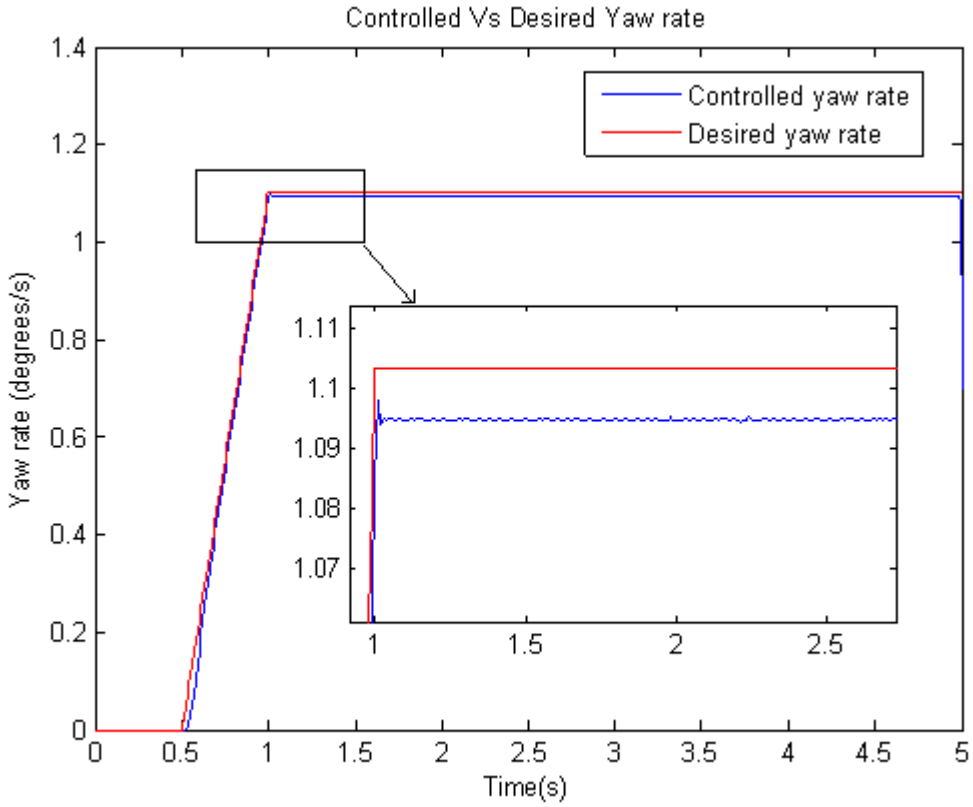

Figure 6.4. Variation of desired and controlled yaw rate with time

There is a small steady-state error between the controlled and desired yaw rate that is of the order of 0.01 degrees/s. However, the output yaw rate is in good agreement with the desired value, thus showing that the controller will work to prevent the vehicle from overturning.

Figure 6.5 shows the control input that is applied (in addition to the driver's input) by the controller, in terms of angle in degrees, to stabilize the vehicle at the particular desired yaw rate. The value of the control input is quite small (less than 0.2 degrees), showing that the controller does not rotate the wheels by a large amount to achieve the desired yaw rate. A large increase or decrease in the steering angle could be fatal to the passengers in the vehicle.

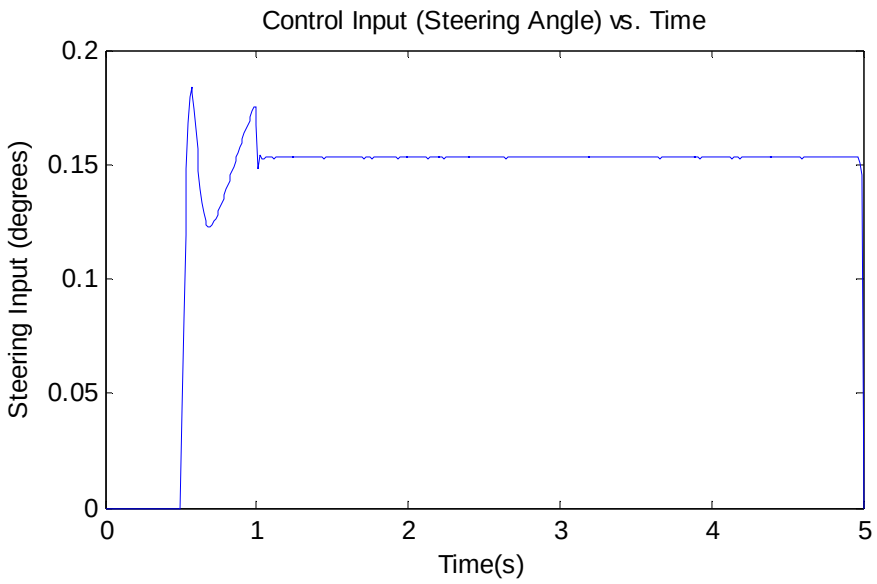

Figure 6.5. Variation of control input with time

The following plot (figure 6.6) shows the lateral velocity (*v*) of the vehicle. As can be seen, the lateral velocity has a very low value, less than 0.04 m/s in magnitude (less than 0.1 Km/h). The controller would not be a feasible option if the lateral velocity was also not controlled.

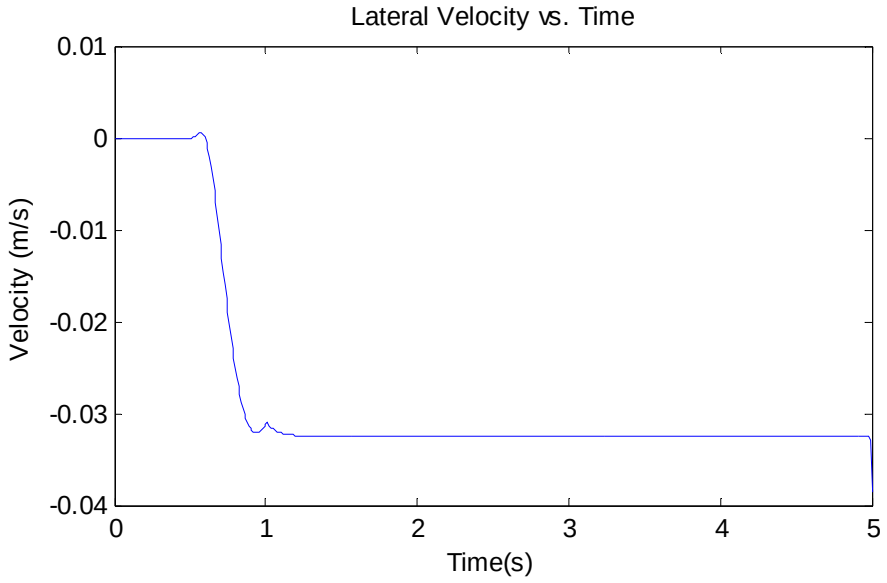

Figure 6.6. Variation of lateral velocity with time

Please note that the controller would work only if the vehicle is operating in the linear region of the lateral force versus slip angle curve [15]. For more violent maneuvers, such as the fish-hook maneuver [24], where the steering wheel input (delta) from the driver ranges between 300 degrees and -300 degrees, the system becomes non-linear and a different algorithm would be required.

6.6 Summary

The dynamic equation of a vehicle was examined with the help of a bicycle model. The relation between the load estimation of chapter 5 and the dynamic equations was explained in terms of the use of cornering stiffness that could be calculated from the load. The second order system was simulated with a typical input to show the uncontrolled nature of the output, in terms of yaw rate.

A control strategy was explained that would help maintain the yaw rate of a vehicle at a desired value based on the input from the driver. A linear quadratic regulator was developed by choosing the values of the penalty matrices Q_1 and R. The controlled system was simulated to show how the yaw rate of the vehicle followed a desired yaw rate. The control input and the lateral velocity were also shown to be within reasonable values, hence proving that the control system is a feasible option when the vehicle is operating in the linear region of the force versus slip curve of the tire.

7. Summary and Recommendations

This chapter provides a brief summary of the research carried out, followed by recommendations on how the work done can be improved.

7.1 Summary of Work Done

The problem provided was to develop a method to estimate the dynamic load on a tire. The research focused on accomplishing this through the use of accelerometers, knowing how the characteristic pattern of a signal from an accelerometer attached to the inner liner of a tire would appear.

An instrumented tire was developed with the associated electrical circuits. Uniaxial accelerometers were used in the instrumented tire. A data acquisition system was set up to capture data from the accelerometers. The tire was first tested on asphalt using a test rig to provide the data used to start the development of the algorithm. A method was found that could potentially detect patch length. However, it was subject to the data being constant for the time that the accelerometer is in the contact patch.

An appropriate equation was used to estimate the dynamic load from the patch length. The estimated load was compared to the applied load (read from the Kistler hub attached to the test rig). It was found that, although there seemed to be a correlation between the applied and estimated load, the tests conducted were not sufficient to arrive at an algorithm that could provide a good estimate of the load.

Tests were then conducted on a flat track machine on a tire instrumented with triaxial accelerometers. The algorithm developed earlier was tested on the new data. Although the estimates of load were in the region of the applied load, they were varying far too much to be of any practical significance.

It could be clearly seen that there was a need to bring the estimates closer to each other, with the estimate for one cycle of rotation being weighted by the data from the previous cycle of rotation.

This was achieved through the use of a Kalman filter. Some other modifications and additions were done to the algorithm, including a multiplicative factor dependent on speed and inflation pressure for load, a relation between filter cut-off frequency and speed et al. that helped in better estimation of the load. The results were repeatable for thirty test cases, hence showing that algorithm can be used in estimating the load quite successfully, at the very least within the conditions of testing.

Once the estimates of the load were found, it was shown how they can be used in controlling the yaw rate of a vehicle to stabilize it. A bicycle model was used in developing a control strategy that would keep the yaw rate down to the desired value, as opposed to an uncontrolled vehicle where the yaw rate shoots up.

7.2 Conclusions and Recommendations

It was shown that the algorithm developed during the course of the research could estimate the load on a moving tire with a small percentage of error. It is by no means conclusive proof of the working of the algorithm for all environments, only that it is at the very least suitable for the given conditions of testing. It might be worthwhile considering the use of linear interpolation as an alternative to the Kalman filter to smooth the variations in the estimates.

It is recommended that further tests be performed on an instrumented tire on the flat track to get even more data points so that the working of the algorithm can be tuned to work under the typical conditions that a tire is subjected to during everyday use. Since the conditions under which the tire is running can be controlled and observed easily on a flat track, this kind of testing would be the best way to develop the algorithm further. This would mean testing under extreme conditions of speed, load and slip that may happen during dangerous driving conditions like slippery roads, high-speed cornering or sudden braking.

Once the algorithm has been tuned to these different factors, it needs to be tested on a road going vehicle. Setting up the data acquisition system will not be an easy task; during the research, wires were used to obtain signals from the accelerometers which cannot be used in practical scenarios. Wireless systems need to be developed to get the data out of the tire.

8. Future Work

The work done in this research can be important to developing control systems that directly utilize tire data to control the movement of vehicles on the road. One aspect of this has already been discussed in chapter 6.

The data obtained during the course of the research can be an important tool in energy harvesting techniques. A feasibility study [25] has already been conducted using the vibration measurements in the data obtained from the instrumented tire. This will help both in powering the sensor and developing a wireless system to transmit the data from the tire to a receiver that is possibly attached to the processing unit of the car.

The data obtained from the testing process has also been studied to see if it can be used in the identification of the surface over which the tire is moving [26]. The frequency response obtained from the data can be studied to possibly characterize the terrain over which the vehicle is being driven and provide an appropriate feedback to the control system to maximize performance.

If the algorithm developed during this research is shown to work under different conditions, it may be possible to insert an application-specific integrated circuit (ASIC) that could process the signal and, with the appropriate Pacejka coefficients for the tire programmed in the chip, transmit the load information directly to the control unit. This IC could be powered by the use of energy harvesting techniques and could transmit data wirelessly. In addition, it could also process the signal to provide data that indicates the type of surface.

References

1. J.N. Dang, “Preliminary results analyzing the effectiveness of electronic stability control (ESC) systems,” National Highway Traffic Safety Administration, DOT HS 809 790, September 2004. [Online]. Available: http://www.nhtsa.gov
2. R. Matsuzaki and A. Todoroki, “Wireless monitoring of automobile tires for intelligent tires,” *Sensors*, 8(12), 8123-8138, doi: 10.3390/s8128123, 2008. [Online]. Available: Sensors, http://www.mdpi.com/journal/sensors
3. Office of Regulatory Analysis and Evaluation National Center for Statistics and Analysis, “Tire pressure monitoring system FMVSS No. 138,” National Highway Traffic Safety Administration, March 2005. [Online]. Available: http://www.nhtsa.gov
4. S. Velupillai and L. Güvenç, “Tire pressure monitoring,” IEEE Control Systems Magazine, pp. 22 -25, December 2007.
5. X. Zhang, F. Wang, Z. Wang, W. Li and D. He, “Intelligent tires based on wireless passive surface acoustic wave sensors,” in *2004 IEEE Intelligent Transportation Systems Conference*, 2004.
6. R. Matsuzaki and A. Todoroki, “Wireless strain monitoring of tires using electrical capacitance changes with an oscillating circuit,” Sensors and Actuators, A 119, pp. 323–331, 2005. [Online]. Available: http://www.sciencedirect.com
7. “Intelligent Tyre for Accident-free Traffic,” Technical Research Centre of Finland (VTT), Finland Tech. Rep. IST-2001-34372, 2005.
8. S.M. Savaresi, M. Tanelli, P. Langthaler and L. Del Re, “New regressors for the direct identification of tire deformation in road vehicles via “in-tire” accelerometers,” IEEE Trans. On Control Systems Technology, Vol. 16, No. 4, pp. 769-775, July 2008.

9. L. Fioravanti, “Method and system for monitoring the tire footprints of a motor vehicle, particularly for automatically optimizing the behavior of the motor vehicle,” U.S. Patent 5,247,831, September 28, 1993.
10. J.-F. Morand and J. Sirven, “Monitoring a tire by acceleration measurement,” U.S. Patent 6,538,566, March 25, 2003.
11. M. Brusarosco, A. P. Fioravanti, A. Taldo and F. Mancuso, “Method and system for monitoring instantaneous behavior of a tire in a rolling condition,” U.S. Patent 7,313,952, January 1, 2008.
12. F. Mancosu, M. Brusarosco and D. Arosio, “Method and System for determining a tire load during the running of a vehicle,” U.S. Patent 7,404,317, July 29, 2008.
13. R.F. Smiley and W.B. Horne, “Mechanical properties of pneumatic tires with special reference to modern aircraft tires,” National Advisory Committee for Aeronautics, Technical note 4110, p.13, January 1958.
14. S. Taheri, *Tire Mechanics Lecture Notes*, Virginia Tech, 2009.
15. H.B. Pacejka, *Tire and Vehicle Dynamics*, 2nd ed.: SAE International, 2006.
16. Rajesh Rajamani, *Vehicle Dynamics and Control*, Springer Science, c2006.
17. S. H. Tamaddoni and S. Taheri, “A new control algorithm for vehicle stability control,” in *Proceedings of the 10th International Conference on Advanced Vehicle and Tire Technologies*, 2008.
18. D. Karrnopp, *Vehicle Stability*. New York: Marcel Dekker, 2004, p.125.
19. J.G. Proakis and D.G. Manolakis, *Digital Signal Processing*, 3rd ed. Prentice-Hall of India, 1996, pp. 623-630.

20. Greg Welch and Gary Bishop, “An Introduction to the Kalman Filter,” July 24, 2006. [Online]. Available: http://www.cs.unc.edu/~welch/kalman/kalmanIntro.html
21. C. Sierra, E. Tseng, A. Jain and H. Peng, “Cornering stiffness estimation based on vehicle lateral dynamics,” *Vehicle System Dynamics*, Vol. 44 Supplement, pp. 24 — 27, 2006.
22. M. Farhood, *Linear Optimal Control Lecture Notes*, Virginia Tech, 2009.
23. P.N. Paraskevopoulous, Modern Control Engineering, New York: Marcel Dekker, 2002, pp. 502-508.
24. K. Weimert, “Fishhook Test,” Corrsys-Datron Sensorsysteme GmbH. [Online]. Available: http://www.corrsys-datron.com/Support/Applications/cds_r_fishhook_test.pdf
25. S. Taheri and K.B. Singh, “Energy Harvesting from Tires: Feasibility Study Using Tire Test Data from Accelerometers,” Intelligent Transportation Laboratory, Virginia Tech, 2009.
26. S. Taheri, K.B. Singh, “Real Time Terrain Classification System for Ground Vehicles Using Tire Vibration Pattern Analysis,” Intelligent Transportation Laboratory, Virginia Tech, 2009.
27. The Mathworks, “Matlab Help Files,” Cambridge MA, 2002.

Appendix A: Additional Results

As was shown in sections 5.2 and 5.3, the load estimated using the algorithm from chapter 4 had a large variation around the applied load. As a result, it was decided to modify the methodology used to obtain the patch length estimate. The following are some of the other plots that were generated (but not used) before moving on to the algorithm of section 5.5 and 5.6.

A.1. Cambering

The wheel was cambered at 2° and run at a speed of 45 mph (test cases 25- 30 in table 5-1) for the different inflation pressures. The following plots (figures A.1 (a) – (c)) show the estimated loads for test cases 25-27. As can be seen in the plots, the algorithm works in the same manner for the cambered wheel as the non-cambered wheel, with sometimes large variations in the estimated load.

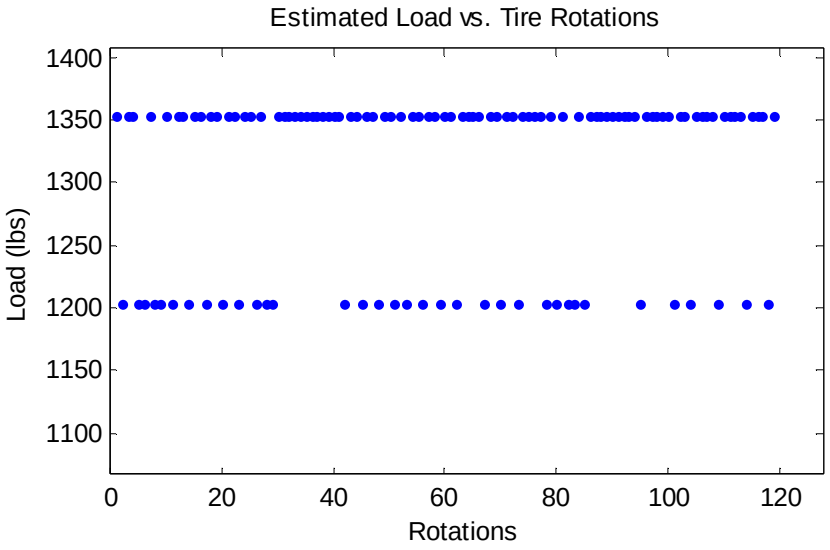

(a)

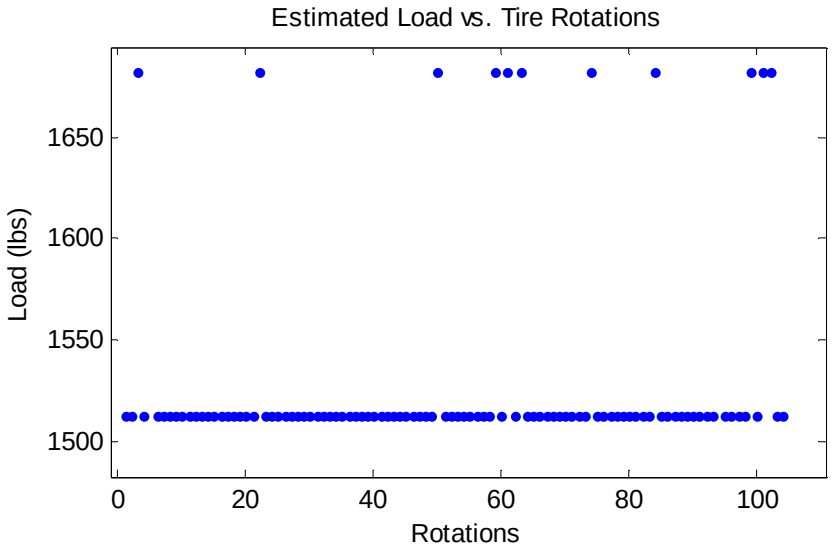

(b)

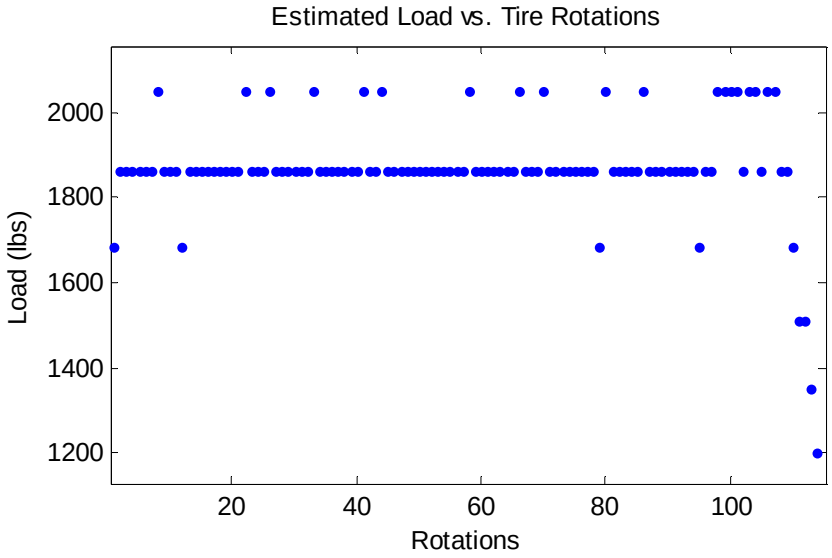

(c)

Figure A.1. Variation of estimated load with rotation for the tire run at 45 mph with the wheel cambered at 2° and applied loads of about **(a)**1300 lbs **(b)** 1500 lbs **(c)** 1800 lbs

A.2. Application of a Sweep Signal

We take a closer look at the load estimated during the application of sweep. As a sample, we can consider the applied load versus estimated load during the application of a sweep signal that

causes the tire to move through a slip angle of -2° to 2° through zero, for the case of the tire moving at 65 mph with an applied load of about 1800 lbs.

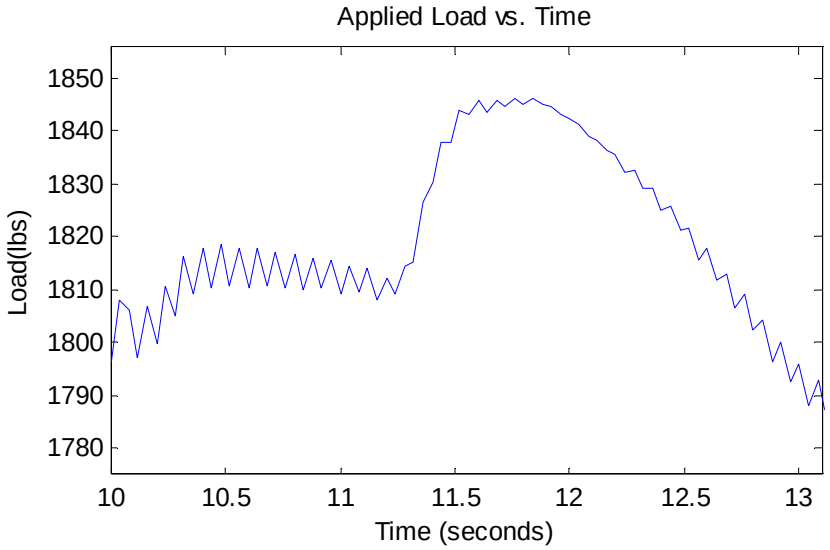

(a)

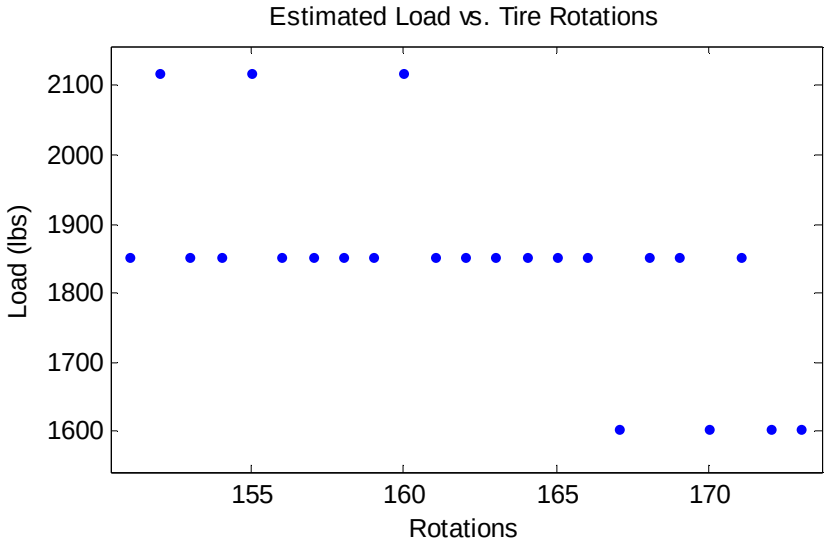

(b)

Figure A.2. (a) Applied and **(b)** estimated loads during application of sweep at inflation pressure of 35 psi and speed of 65 mph

The vertical load is not very different during the sweep signal as during the straight line run and hence the estimate is also similar to that during straight line run. It may be possible to calculate

other parameters (for example lateral force) by using the information from the other axes of the accelerometers. But development of algorithms based on those signals will require more research.

A.3. Load Estimation at Different Inflation Pressure

The tests conducted at an inflation pressure of 35 psi were repeated for an inflation pressure of 32 psi. The formula used to estimate the load from the patch length at 35 psi (equation 2.2) is used in this case too, except that the stiffness coefficient is now changed to reflect the change in pressure. The values of *a* at different speeds was the same as that used for 35 psi inflation pressure. The stiffness coefficient used is 1530 lbs/inch. The following plots (A.3 (a) - (c)) show the estimated load with an applied load of 1000 lbs, 1300 lbs and 1500 lbs, respectively, at 45 mph.

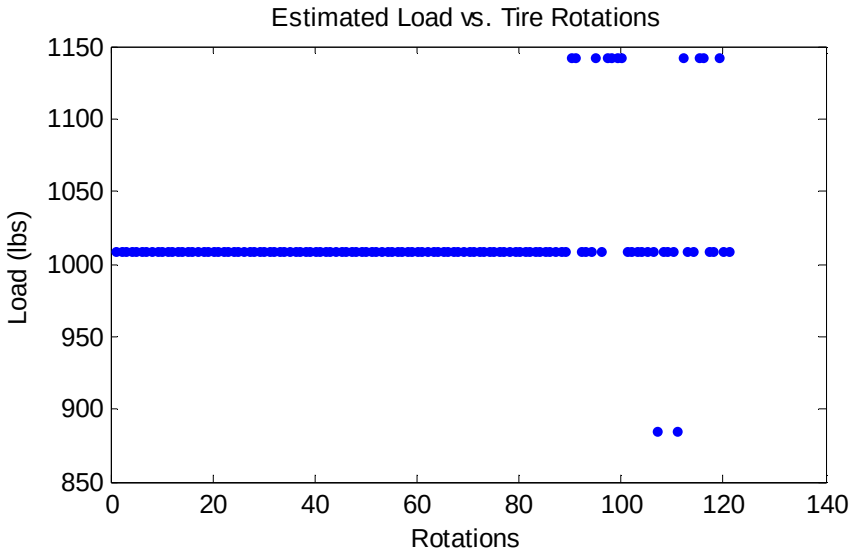

(a)

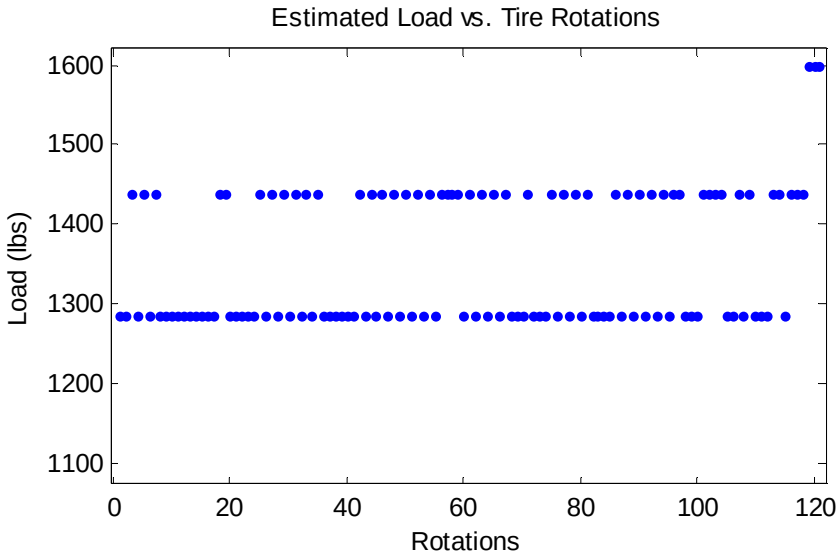

(b)

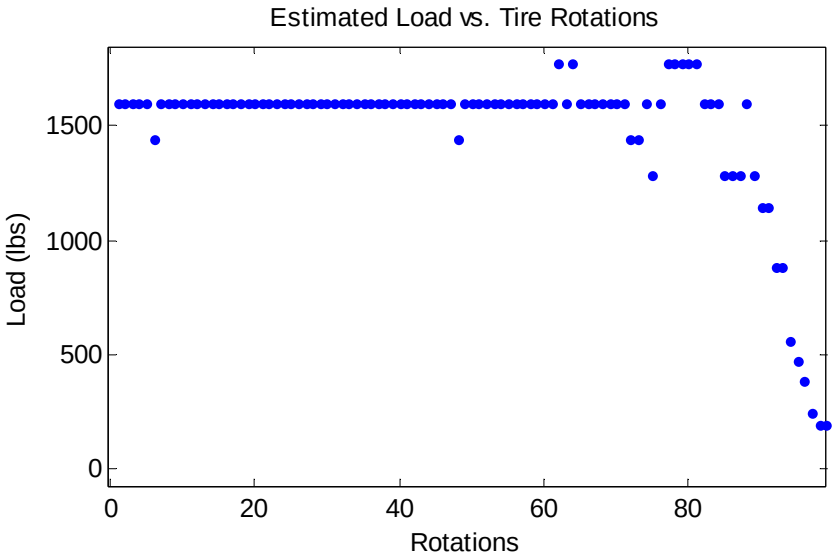

(c)

Figure A.3. Variation of estimated load with tire rotation at inflation pressure of 32 psi and speed of 45 mph, with applied loads of about **(a)** 1000 lbs **(b)** 1300 lbs **(c)** 1500 lbs

Again, the same kind of variations are seen here as in the case where inflation pressure is 35 psi. This seems to indicate that any changes that any changes introduced in better estimation of load for an inflation pressure of 35 psi may also improve the estimates at 32 psi. This can be seen in section 5.6.

Appendix B: Simulink Block Diagram

The Simulink block diagram used in simulating the control system (section 6.3) is shown in figure B.2. The parameters required for the simulation, including the various matrices, are run from a Matlab file and then the simulation (shown in figure B.1.) is run on Simulink. Plots are generated for the output yaw rate, the control input and the lateral velocity (figures 6.4 – 6.6).

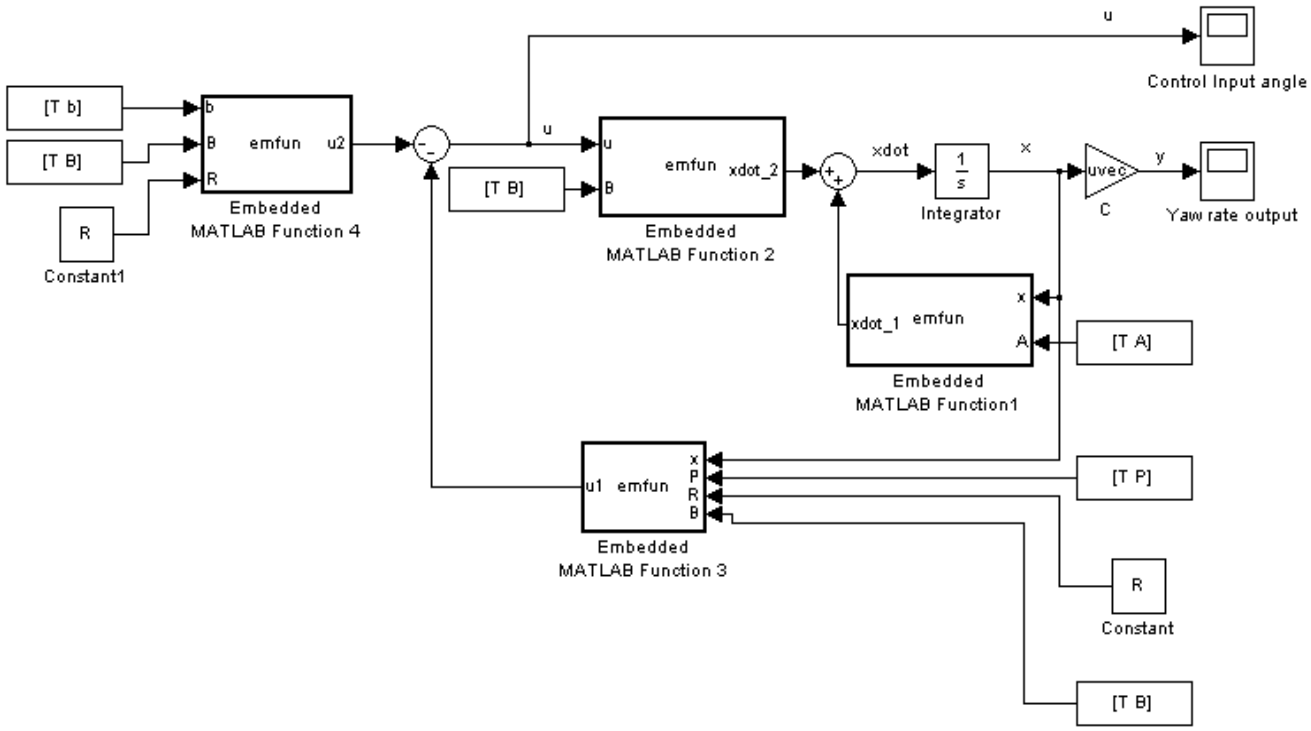

Figure B.1. Simulink block diagram of control system

The file implements the block diagram of figure 6.2. Embedded Matlab functions [26], (each labeled 'emfun' in the image and numbered 1 to 4) are used to implement equations 6.6 and 6.9. Outputs of the embedded Matlab function 1 and 2, *xdot_1* and *xdot_2* respectively, are combined to give *xdot* (equation 6.6), while outputs *u1* and *u2*, from embedded Matlab functions 3 and 4 respectively, are combined to give *u* (equation 6.9). *u* is the control input (figure 6.5) and *y* is the

desired output yaw rate (figure 6.4). The index *T* used in some of the blocks in figure B.1 shows the time varying nature of the system being simulated.